University of Southampton

Faculty of Natural and Environmental Sciences

Ocean and Earth Sciences

Coupling Nitrate Sensor Technology with Autonomous Gliders to Investigate Seasonal Controls on the Biogeochemical Cycle of Nitrate in a Temperate Shelf Sea

by

Alexander George Vincent

Thesis for the degree of Doctor of Philosophy

December 2018

University of Southampton

Abstract

Faculty of Natural and Environmental Sciences

Ocean and Earth Sciences

Thesis for the degree of Doctor of Philosophy

Coupling Nitrate Sensor Technology with Autonomous Gliders to Investigate Seasonal Controls on the Biogeochemical Cycle of Nitrate in a Temperate Shelf Sea

by

Alexander George Vincent

The oceans take up ~30 % of increasing atmospheric carbon dioxide (CO_2) concentrations. Shelf seas, though small (7 - 8 % of the total ocean area), play a significant role in the uptake and removal of this CO_2 by contributing 15 – 30 % of total oceanic primary production. Shelf seas are highly dynamic systems with seasonal cycles in nutrients, light, stratification and primary production. Two key stages in the seasonal cycles are the spring bloom and the summer formation of a sub-surface chlorophyll maximum (SCM). There is a growing need to increase spatial and temporal resolution of *in situ* measurements of nutrients and phytoplankton growth alongside the physical factors which drive their seasonal cycles as these measurements are needed to ground-truth and provide new data for biogeochemical models used to predict both contemporary and future changes in climate.

In this study, a novel wet-chemical microfluidic Lab-on-Chip nutrient sensor was deployed for the first time within an autonomous underwater glider where nitrate (NO_3^-) measurements were comparable to traditional ship-based methods (r^2=>0.98; n = 60). The Lab-on-Chip nutrient sensor was able to capture the large drawdown of NO_3^- within the surface mixed layer due to the onset of the spring bloom in the central Celtic Sea, where surface NO_3^- concentrations decreased from 5.74 µM to 1.42 µM, whilst bottom layer NO_3^- concentrations remained constant (6.86 ±0.16 µM).

Concurrent measurements of the dissipation of turbulent kinetic energy at the pycnocline resulted in a mean nitrate flux ($f\sum NO_x$ of~4.2 mmol m^{-2} d^{-1}) that is double that of previously reported estimates (~2 mmol m^{-2} d^{-1}) in the Celtic Sea. The mean $f\sum NO_x$ across the pycnocline was dominated by short mixing events that could potentially supply larger (> 15 mmol m^{-2} d^{-1}) intermittent fluxes of $\sum NO_x$ into the SCM. Using our spring and neap tide $f\sum NO_x$ estimates to represent the upper and lower limits, the contribution of new production estimated in this study, supported by the $f\sum NO_x$ into the SCM (58 (21-80) g C m^{-2}), could support all of the estimated annual new production (81.8 g C m^{-2}) in the Celtic Sea in the SCM alone during the summer period (120 days). If this under-estimation of the contribution of the summer SCM to the annual new production shown here in the Celtic Shelf Sea is indicative of all other continental shelf seas of the Northern Hemisphere, then their previously estimated ability to be net sinks of CO_2 (0.24 Pg C yr^{-1}; Laruelle *et al.*, 2010) could be underestimated.

Using bio-optical sensors (fluorescence and backscatter) deployed on a glider, bio-optical relationships were established between Chl-*a* and particulate backscatter that were used to derive values of particulate organic carbon (POC) and phytoplankton carbon. During the spring bloom this study showed a strong positive correlation between Chl-*a,* particulate backscatter and POC, which was decoupled during the summer SCM due to changing phytoplankton biomass and resuspended sedimentary material. This work has shown that using established empirical relationships the potential for bio-optical sensors on gliders to predict POC, and thus C_{phyto}, in a dynamic shelf seas environment.

This thesis demonstrated that autonomous platforms and novel *in situ* biogeochemical sensors are an invaluable tool for the observation of the changing marine environment and are well placed to provide new insight into biogeochemical, physical and bio-optical fields as well as to augment, with complimentary high-resolution datasets, moorings, ships and satellites methodologies.

Table of Contents

List of Tables

List of Figures

Research Thesis: Declaration of Authorship

Print name:	Alexander George Vincent

Title of thesis:	Coupling Nitrate Sensor Technology with Autonomous Gliders to Investigate Seasonal Controls on the Biogeochemical Cycle of Nitrate in A Temperate Shelf Sea

I declare that this thesis and the work presented in it are my own and has been generated by me as the result of my own original research.

I confirm that:

1. This work was done wholly or mainly while in candidature for a research degree at this University;
2. Where any part of this thesis has previously been submitted for a degree or any other qualification at this University or any other institution, this has been clearly stated;
3. Where I have consulted the published work of others, this is always clearly attributed;
4. Where I have quoted from the work of others, the source is always given. With the exception of such quotations, this thesis is entirely my own work;
5. I have acknowledged all main sources of help;
6. Where the thesis is based on work done by myself jointly with others, I have made clear exactly what was done by others and what I have contributed myself;
7. Parts of this work have been published as:
   Vincent, A.G., *et al.,* (2018), Nitrate drawdown during a shelf sea spring bloom revealed using a novel microfluidic in-situ chemical sensor deployed within an autonomous underwater glider, *Mar. Chem.* https://doi.org/10.1016/j.marchem.2018.07.005.

Signature:		Date:	

Acknowledgements

I would like to firstly thank my supervisor Maeve Lohan, for giving me the opportunity to undertake a PhD and you're continued support and guidance through this challenging experience. To undertake this research would have taken twice as long if it wasn't for the help Alex Nimmo-Smith gave me early on learning to code, so thank you very much. I would also like to thank my academic panel Duncan Purdie and Douglas Connelly.

Thank you to Robin Pascal, Alex Beaton and Adrian Nightingale for all your help and knowledge with all things Lab-on-Chip, and Matthew Palmer, Jo Hopkins and Charlotte Williams for their support and sharing their knowledge on turbulence and gliders.

I will be forever grateful to Andy Rees for giving me my first opportunity in marine research and to Lisa Al-Moosawi for making it so enjoyable.

I wish to acknowledge all the crew and scientists on-board the *R.R.S Discovery* and colleagues within the Marine Autonomous and Robotic Systems and Ocean Technology and Engineering groups at the National Oceanographic Centre, Southampton.

I am very grateful for the time I spent with friends and colleagues as part of the Biogeochemical research groups at the University of Plymouth and then the University of Southampton and National Oceanographic Centre.

Finally, thank you to my friends, loved ones and parents. I couldn't have done it without you all.

Abbreviations

AUV autonomous underwater vehicle

BML bottom mixed layer

b_{bp} particulate backscattering coefficient

CCS Celtic shelf sea sampling site

Chl-*a* chlorophyll-*a*

CO_2 carbon dioxide

C_{phyto} phytoplankton carbon biomass

CTD conductivity, temperature and depth profiler

ε dissipation of turbulent kinetic energy

$\sum NO_x$ nitrite + nitrate

$f\sum NO_x$ flux of $\sum NO_x$

K_z vertical eddy diffusivity

LoC lab-on-chip

MLD mixed layer depth

NO_2^- nitrite

NO_3^- nitrate

OMG ocean microstructure glider

PAR photosynthetically available radiation

POC particulate organic carbon

SCM sub-surface chlorophyll maximum

SML surface mixed layer

SOG sensors on gliders

Chapter 1: Introduction

The shelf seas are situated between the continental landmasses and the open oceans, and therefore, play an important role as a conduit of macronutrients and buffer linking the terrestrial and marine ecosystems. At the boundaries of the of shelf seas, the dynamic interactions of chemical, biological and physical elements across these boundaries play a vital role and influence globally significant biogeochemical cycles and, thus, the earth's climate.

A large percentage of the global population lives in proximity to the shelf seas which have been estimated to be the most valuable biome on Earth, and thus, are of substantial socio-economic importance. As a result of anthropogenic activities there is a high potential for considerable change, consequently it is imperative to create a baseline and understand how climate change could affect these vital physical and ecosystem processes in the shelf seas.

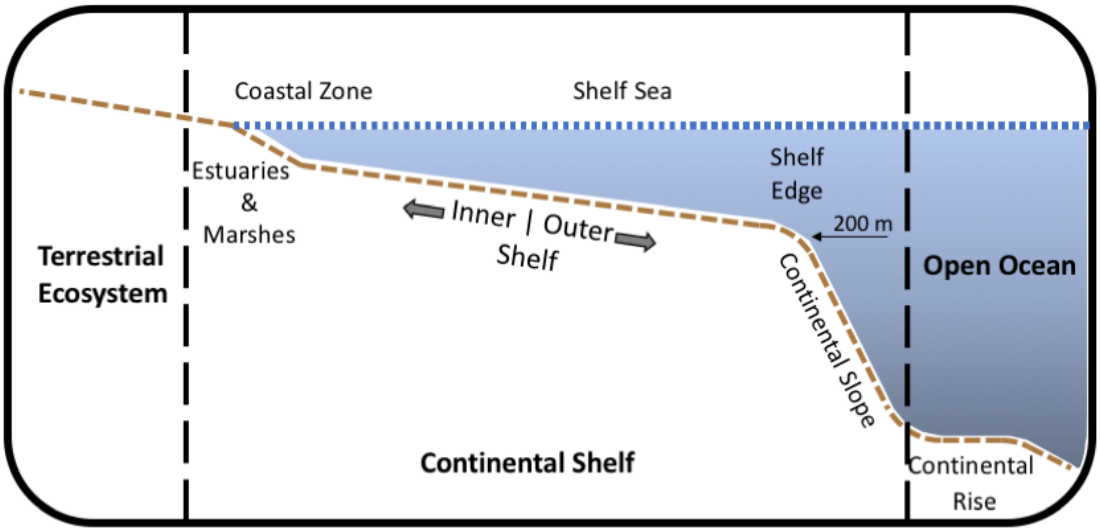

Figure 1.1: Schematic locating the shelf sea between the terrestrial and oceanic ecosystems.

1.1 Primary Production in temperate shelf seas

Primary production is the formation of new complex organic compounds through the harnessing of solar energy by Photoautotrophs (known as marine microflora called phytoplankton) in a process called Photosynthesis to provide the chemical energy needed to fix inorganic carbon (dissolved carbon dioxide; Falkowski and Raven, 1997) and convert this to organic matter:

$$CO_2 + H_2O \xrightarrow{light} CH_2O + O_2 \quad (1.1)$$

Solar energy is absorbed by the chloroplasts within phytoplankton cells and converted into biological energy in two stages (known as the 'light-dependent' and 'light-independent') and stored in the form of organic compounds. In the first stage, light is absorbed by pigments (e.g. chlorophyll-*a*) within the chloroplasts and used to make adenosine triphosphate (ATP) and reduced nicotinamide adenine dinucleotide phosphate (NADPH). Within the next stage, ATP and NADPH are used, as park of the Calvin-Benson cycle, to reduce dissolved inorganic carbon (DIC) into products such as carbohydrates, amino acids and lipids. Further details regarding the process of photosynthesis can be found in Falkowski & Raven (1997) & Kirk *et al.* (1994).

Phytoplankton are unicellular and live in a pelagic environment with a cell diameter ranging from 1µM to ~ 70µM (Lehman, 2000). Phytoplankton require sufficient solar irradiance and macronutrients (e.g. nitrogen, phosphorus, silicon) and micronutrients (e.g. iron) in order to photosynthesise and produce enzymes, carbohydrates, lipids and DNA/RNA, with nitrogen (N) being a principal nutrient in most biosynthetic reactions (Falkowski and Raven 1997). Photosynthesis by phytoplankton strongly links the assimilation of nutrients and the fixation of carbon (C) as these elements are needed to build living organic tissue, with Redfield, Ketchum and Richards (1963) proposing phytoplankton have a relatively fixed cell quota and so assimilate different elements in an approximate fixed ratio known as the Redfield ratio:

$$106CO_2 + 16NO_3^- + HPO_4^{2-} + 78H_2O + 18H^+ \Rightarrow C_{106}H_{175}O_{42}N_{16}P + 150O_2 \quad (1.2)$$

where $C_{106}H_{175}O_{42}N_{16}P$ is the average composition of organic matter in phytoplankton according to the Redfield ratio. This ratio matches to a certain extent the average ratio of dissolved inorganic N and P in seawater (Geider and La Roche, 2002) as these proportions are fixed into particulate organic material that eventually is remineralised via bacterial mediation returning the elements back into the water column in their inorganic forms becoming again available for assimilation (Raymont, 1980), which is known as '*nutrient stoichiometry*'. However, there is considerable variability in the stoichiometric ratios within phytoplankton cells. The main reason for the deviation from fixed stoichiometric ratios is that these are not only set by the nutrient requirements of different species of phytoplankton but also by the nutrient availability in seawater (Arrigo, 2005). While the consistency of the Redfield ratio is useful for calculating relationships, the variability can be used to interrogate the balancing of cycling processes for a single element (Chester and Jickells, 2012).

The oceans are an important buffer for atmospheric carbon dioxide (CO_2) and absorb a quarter of annual anthropogenic CO_2 emissions (Le Quere, 2015). The world's oceans cover 72% of the planet, and of this, shelf seas only make up 7 - 8 % of the total area and less than 0.5 % of the volume. Despite their relatively small size, shelf seas generate 15 – 30 % of total oceanic

primary production (Gattuso, Frankignoulle and Wollast, 1998; Simpson and Sharples, 2012), with some studies of new primary production estimating open ocean values of 2.9 Pg C y^{-1} and shelf seas at 3.7 Pg C y^{-1} (Walsh, 1991; Liu *et al.*, 2000) The levels of carbon dioxide (CO_2) in the atmospheric is steadily increasing (IPCC, 2014), and the shelf seas have an average carbon fixation rate per unit area up to 3 times greater than the open ocean and are therefore vital regions for the fixation and sequestration of CO_2 (Jahnke, 2010; Simpson and Sharples, 2012). Shelf seas, particularly those located in higher latitudes (Frankignoulle and Borges, 2001; Thomas *et al.*, 2004), act as globally important carbon sinks through mechanisms known as the '*biological pump*' and '*continental shelf pump'* (Tsunogai *et al.*, 1999; Thomas *et al.*, 2004). Within the oceans carbon is drawn out of the surface waters down below the thermocline as either dissolved inorganic carbon (DIC), particulate organic carbon (POC) after being fixed during photosynthesis, or as dissolved organic carbon (DOC; Fennel, 2010). In mid to higher latitude shelf seas DIC is drawn into the surface from the atmosphere by either the solubility increasing due to cooler water temperatures or by DIC being assimilated by phytoplankton, leading to the near-surface partial pressure of CO_2 decreasing causing the gradient in CO_2 concentrations between the atmosphere and sea surface to increase, thus, driving an air-sea flux of CO_2 (Millero, 1996; Behrenfeld *et al.*, 2006). Carbon, depending on its type (i.e. particular or dissolved) can then be transported off the shelf through horizontal advection or isopycnal mixing, where the associated carbon will be exported to the deep ocean or locked away through burial on continental shelves and the adjacent slope (Tsunogai, Watanabe and Sato, 1999; Thomas *et al.*, 2004; Takahashi *et al.*, 2009; Jahnke, 2010). Thomas *et al.* (2004) reported that the North Sea is a highly efficient *'continental shelf pump'* and is capable of exporting ≈ 93% of the CO_2 taken up from the atmosphere, this was due to the fact the northern North Sea was estimated to be undersaturated and that the subsurface layer is subjected to major exchange circulation with the North Atlantic Ocean (8.5×10^{12} g C yr^{-1}).

1.1.1 Seasonal dynamics in Celtic Sea

The Celtic Sea is a shallow (100 to 200 m) temperate shelf sea located in the North West European shelf surrounded by land on three sides (the Republic of Ireland, United Kingdom and France), with links to the English Channel and Irish Sea (Figure 1.2). The Celtic Sea is a seasonally stratifying shelf sea that is strongly influenced by the balance of solar heating and tidally generated mixing (Simpson and Hunter, 1974). It is a tidally dynamic region with tidal speeds ranging from ~ 0.25–1.5 m s^{-1} (Pingree *et al.,* 1976) and has an estimated water residence time of 1-2 years (Hydes *et al.,* 2004). This makes it ideal to investigate the seasonal cycle of nitrate and its role in primary production.

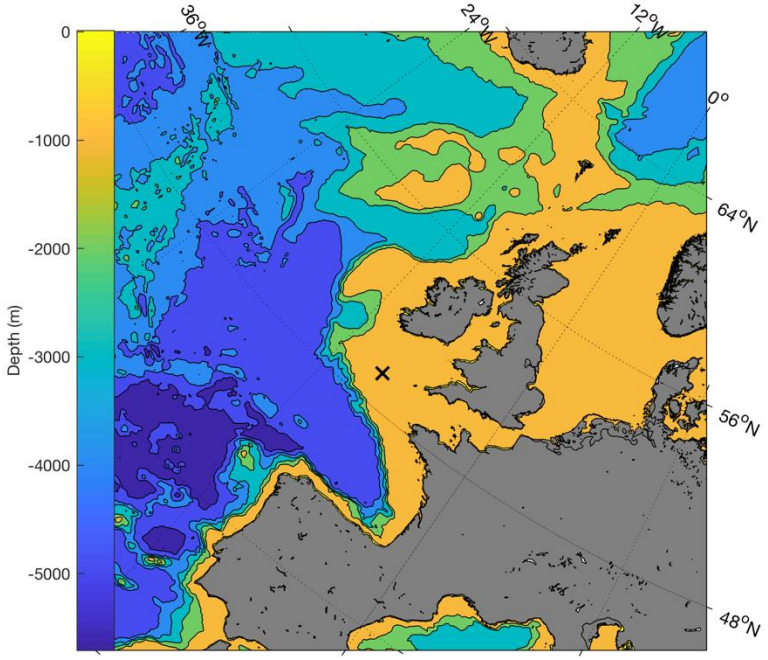

Figure 1.2: Map of the Northwest European shelf. The black cross denotes the Celtic sea and the central Celtic Sea (CCS) sampling site (49° 24’ N, 8° 36’ W), ~150 m depth. Data provided by the National Geophysical Data Centre (1995).

During the winter months the water column of the Celtic Sea is fully mixed due to net heat loss and convective overturning controlling vertical structure, with observed nitrate concentrations ranging from 6.5-8.5 µM (Rees, Joint and Donald, 1999; Hydes *et al.*, 2001, 2004). Even though the whole water column is homogenous with available nitrate, phytoplankton growth is limited by low levels of irradiance as it is turbulently mixed throughout the water column away from higher levels of irradiance at the surface. Photosynthesis has been shown to decreases with depth in proportion to the exponentially decay of irradiance with depth due to being attenuated by water, scattered and absorbed by suspended particles (Sverdrup, 1952; Kirk, 1994). The depth at which PAR becomes 1 % of surface values defines the base of the euphotic

zone and within the Celtic sea this has been shown to be at depths > 50 meters (Poulton *et al.*, 2018). The critical depth argument, proposed by Sverdrup (1952), states that once phytoplankton are mixed below this depth phytoplankton spend too much time in the dark and respiration exceeds photosynthesis and light limits phytoplankton growth.

The nitrate budget for the following spring and summer period, is setup by winter mixing and nutrient recycling/remineralization processes and the convection of water onto the shelf that occur leading up to the start of spring (Simpson and Sharples, 2012; Birchill *et al.,* 2017). In the Celtic sea, the onset of stratification during spring occurs in April (Fasham *et al.*, 1983), when increasing solar heating overcomes the destabilising mixing energy from tidal and wind inputs (Simpson and Sharples, 2012). The water column is stratified and divided into two vertical layers: the wind-mixed surface layer and the barotropic-tidally mixed bottom layer (BML), which are separated by a sharp gradient in temperature (known as the thermocline). The thermocline acts as a physical barrier, restricting the exchange of properties (e.g. nutrients and phytoplankton cells) between the BML and upper euphotic zone (Sharples *et al.,* 2001). Phytoplankton cells are retained within the euphotic zone, where high nitrate concentrations and levels of irradiance trigger a rapid growth, resulting in an event known as the spring bloom (Sverdrup, 1952). The spring bloom is a recurring seasonal event which is fundamental to primary production in the Celtic Sea, making up ~ 50 % of the annual new primary production (Hickman *et al.*, 2012; Sharples *et al.*, 2013). It causes a rapid drawdown of macronutrients in the euphotic zone to concentrations below the limit of detection (< 0.1 µM). This results in a vastly reduced rate of primary production due to the limited availability of nitrate (Dugdale and Goering, 1967), which has been observed in previous studies in the Celtic Sea (e.g. Pingree *et al.*, 1976a; Sharples *et al.*, 2001; Sharples and Moore, 2009; Hickman *et al.*, 2012; C. Williams *et al.*, 2013) and is the case throughout the oceans (~75% of the ocean is limited by inorganic nitrogen availability (Gruber, 2008)).

Following the spring bloom, primary production in the euphotic zone is sustained by a limited supply of regenerated nitrogen (Sharples *et al.,* 2007; Hickman *et al.,* 2012; Davidson *et al.,* 2013), whilst the bottom-mixed layer remains relatively stable with observed nitrate concentrations ranging between ~7.3-12 µM (Hydes *et al.,* 2004; Davidson *et al.,* 2013; Tweddle *et al.,* 2013), where regeneration of organic material increases these nitrate levels (Pingree, Holligan and Mardell, 1978) compared to what was observed in winter (6.5-8.5 µM; Rees, Joint and Donald, 1999; Hydes *et al.*, 2004). However, within the seasonal thermocline is a layer of increased concentrations of phytoplankton that is routinely observed and is ubiquitous in stratified waters; this feature is ecologically significant with observed concentrations of >10 mg Chl-*a* m^{-3} and is known as the *'subsurface chlorophyll maximum'* (SCM; Pingree *et al.,* 1978;

Holligan *et al.*, 1984; Sharples *et al.*, 2001; Cullen, 2015). The formation and location of the SCM is generally controlled by biological-chemical-physical interactions on vertical scales between one and ~10 meters and is strongly coupled to the nitracline which is located within the pycnocline (Holligan *et al.,* 1984; Sharples *et al.,* 2001).

New production within the SCM is controlled by vertical mixing across the seasonal thermocline of nitrate from the replete bottom water up into the SCM, which maintains summertime production and sets the limit on new production at the SCM (Pingree, Mardell and Cartwright, 1981; Sharples *et al.*, 2001, 2007; Rippeth *et al.*, 2009). While the seasonal thermocline acts to suppress the mixing of water characteristics, it is not until current shear is sufficient to overcome the tendency of the water column to remain stratified allowing for the transfer of water properties across the thermocline (Thorpe, 2007). The energy needed for internal mixing and instability creation at the thermocline can be supplied through shear generated by a variety of sources. These include the barotropic tide (Simpson *et al.*, 1996; Sharples *et al.*, 2001), the baroclinic tide (Moum and Nash, 2000; Rippeth and Inall, 2002; Sharples *et al.*, 2007), and episodic increases in wind forcing and sudden changes in wind direction (Rippeth and Inall, 2002; Rippeth e*t al*., 2005; Charlotte Williams *et al.*, 2013). All of these processes aid in the supply of nitrate into the base of pycnocline, and enable the formation of the SCM. Recent studies suggest that summer new production (~ 120 days) is comparable to the spring bloom, which is estimated to produce around ~50% of annual new production (Tweddle, 2007; Hickman *et al.*, 2012)

During the late summer/autumn the net atmosphere-ocean heat flux reverses so that the sea surface progressively cools and mixing energy from wind inputs increase. The result is a gradual weakening of the seasonal stratification over several months until full winter overturning is achieved (Simpson and Sharples, 2012). The weakening stratification permits increased vertical transport of nitrate that alleviates the oligotrophic conditions that prevail during the summer resulting in an autumn bloom of phytoplankton (Pingree *et al.*, 1976b; Wihsgott, 2018).

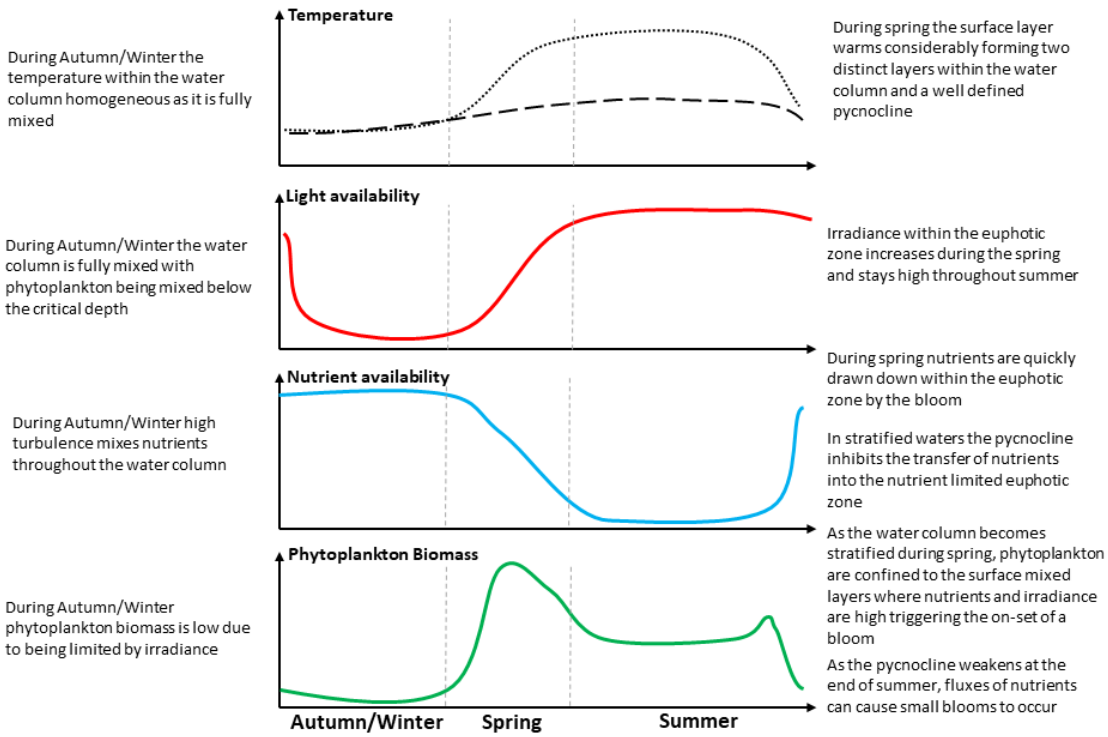

1.1.2 Mixing and Fluxes

Within the seasonally stratifying shelf seas the thermocline is a vital interface separating the differing water characteristics of the SML and BML and therefore influences nutrient availability and hence biogeochemical cycles. The seasonal thermocline acts to suppress the mixing of water characteristics between the SML and BML, it is not until current shear is sufficient to overcome the tendency of the water column to remain stratified allowing for the transfer of water properties across the thermocline (Thorpe, 2007). The energy needed for internal mixing and instability creation at the thermocline can be supplied through shear generated by a variety of sources. These include: (1) the barotropic tide which creates bed generated shear with increasing current velocities approaching spring tides, this drives turbulence higher into the water column along with sharpening and moving the pycnocline closer to the surface (Simpson *et al.,* 1996; Sharples *et al.*, 2001), (2) the baroclinic tide and other internal waves (Moum and Nash,

2000; Rippeth and Inall, 2002; Sharples *et al.*, 2007), and (3) inertial oscillations, produced by episodic increases in wind forcing and sudden changes in wind direction, which cause shear at the pycnocline and shear instabilities (Rippeth *et al.,* 2002; Rippeth *et al.,* 2005; Williams *et al.,* 2013). The vertical flux of nutrients into the euphotic zone is controlled by physical processes that drive turbulence, by understanding the variably in turbulence and its control on the vertical flux of nutrients we can determine the variability in new production in the shelf seas during the summer stratified period (Simpson and Sharples, 2012).

With the removal of any physical mixing, the transfer of fluid properties across an interface can be achieved through molecular diffusion as described by Fick's Law (1855):

$$J = -D\frac{\delta C}{\delta \chi} \quad (1.3)$$

J is the diffusion flux (mol m^{-2} s^{-1}), D is the diffusion coefficient (m2 s^{-1}), C is the concentration (mol m^{-3}) and χ is position (m). It suggests a flux will transfer from a region of high concentration to low, with the magnitude proportional to the concentration gradient. In comparison to molecular diffusivity, turbulent diffusivity (K) describes a rate a scalar property (e.g. heat or solutes) is dispersed, due to the influence of energetic eddying state of motion resulting in the generation of relatively large gradients in velocity at small scales, typically 1 mm to 1 cm, that mix solutes at rates higher than those of molecular processes (Thorpe 2007). This is described by the equation of Tennekes & Lumley (1972):

$$\frac{\delta \mathrm{C}}{\delta t} = K\frac{\delta C}{\delta z} \quad (1.4)$$

C is the scalar property, t is time and z is depth. Further details regarding turbulence in the open ocean or shelf seas can be found in Thorpe (2007) and Simpson and Sharples (2012) respectively. Turbulence is generated wherever there is a gradient in currents and is referred to as current shear. Shear can be generated when fluid moves along a fixed boundary such as the seabed or when wind induced flows, inertial oscillations and internal waves which propagate along a density discontinuity (SIMPSON and HUNTER, 1974; Thorpe, 2007; Simpson and Sharples, 2012).diapycnaldiapycnal,by point single integrated value,s

1.2 Biogeochemical observations: Macronutrients

Biogeochemical variables, such as macronutrients, have been traditionally determined by colourimetric methods either at sea or on land (Wurl, 2009; Hydes *et al.*, 2010). Discrete water samples are collected, and if required for analysis, filtered to remove particulates and/or cease biological activity. Using either a CTD rosette system or a pumped underway system results in either vertical profiles or a horizontal surface dataset, where measurement resolution is governed by the number of rosette bottles or the ships transect and pumping characteristics, respectively. These measurements are restricted by the length of the cruise and cannot sample continuously at a higher frequency (~1Hz) over extended temporal periods (e.g. tidal cycle to multiyear). Similarly, due to the platform it is impractical to sample in challenging locations (e.g. under ice, hydrothermal vents) or with adverse weather conditions (e.g. winter storms), and therefore limits the opportunity to fully observe the variations in biogeochemical parameters. Therefore, capturing macronutrient distributions over temporal and spatial scales and in a highly dynamic shelf system is challenging. It is essential to be able to determine macronutrients in shelf systems in order to examine fluxes across the pycnocline to assess the contribution of SCM to global primary production.

The marine environment is under increasing pressure from anthropogenic influences and climate change with fundamental changes in biogeochemistry already underway that are predicted to become more profound in the near future (Gruber and Galloway, 2008; Gruber, 2011; Gattuso *et al.*, 2015). Currently repeating biogeochemical observations use single locations or transects and are undertaken infrequently in shelf systems, and even less frequently in oceanic settings, and are not suitable to form a well-defined baseline of knowledge of the complex marine environment to enable an assessment of how biogeochemical processes and budgets will change in the future at regional to basin scales. To understand current processes and budgets, and more importantly how they could change, numerical models have been used to simulate 3D biogeochemical cycling across different spatial and temporal scales (Wild-Allen and Rayner, 2014). Numerical models (e.g. Friedrichs *et al.*, 2007; Butenschon *et al.*, 2016; Holt *et al.*, 2017) have provided valuable insights on climate change and ecosystem health, informing policy and management, while the novel use of neural networks (Sauzède *et al.*, 2017) have the potential to support the initialization and validation of biogeochemical models which presently crucially lack reference data. However, the validation and assessment of the skill of each model is currently limited due to the limited availability of observations and limited ranges of observed parameters (Vichi *et al.*, 2011; Wild-Allen and Rayner, 2014; Holt *et al.*, 2017). By removing the bottleneck caused by under sampling at multiple spatial and temporal scales, the potential of using complex

computer-based tools to understand our dynamic oceans in the present and look further ahead could be fully unlocked. The use of permanent *in situ* sensors and sensor-on-mobile platforms within networks have been identified as a solution to under-sampling of the marine environment on varying temporal and spatial scales (Mowlem, 2008; Gallager and Whelan, 2003; Johnson, 2003; Johnson *et al.*, 2007, 2009; Adornato *et al.*, 2010).

The ability of instruments to easily observe physical parameters in high resolution has been vital to obtaining our current understanding of the physical processes within the oceans and their interactions with other earth systems and cycles. Unfortunately, the instruments and methods used within the marine biogeochemical field to measure macronutrients and bio-optical properties have only recently started to catch up and produce sufficiently high-resolution datasets. The first significant step forward can be said to have been Lorenzen's 1966 fluorometric determination method, allowing measurements of phytoplankton biomass on vertical resolutions of <1m (Cullen, 2015). Current CTD deployable versions of fluorometric sensors are able to go beyond these basic observations and interrogate the photosystem II for phytoplankton and also produce a rate of carbon fixation (Kolber and Falkowski, 1993; Smyth, 2004). In contrast to physical sensors, biogeochemical sensors are in their infancy and are dominated by large macro (~0.5 m^3), expensive (£10-100k) one-off devices requiring expert operation and intervention (Kendra L Daly *et al.*, 2004; Statham *et al.*, 2005).

To date a small number of biogeochemical sensors have become commercially available and these measure *in situ* nitrite and nitrate using direct ultra-violet (UV) absorption methods, and more recently wet chemical systems are starting to become more widely used. Nitrate sensors based on the UV absorption methods (e.g. SUNA & ISUS) have been successfully used for time series and autonomous and lagrangian platforms and have shown an ability to combat the under sampling of our oceans and be a staple sensors in future global sensor networks (K. L. Daly *et al.*, 2004; Johnson *et al.*, 2009; Sakamoto, Johnson and Coletti, 2009; Lomas *et al.*, 2013; Pasqueron De Fommervault *et al.*, 2015; Olsen *et al.*, 2016). .With *in situ* measurement methods, accuracy and lifetime of resources, such as battery and reagents, are key issues and the advantages and disadvantages of these methods revolve around these topics. Direct ultra-violet (UV) absorption methods have also been widely used *in situ* (e.g. ISUS, Johnson and Coletti, 2002 and ProPS, Zielinski *et al.,* 2007) and provide high frequency data (1 Hz) without the need for reagents. When compared to wet chemical systems, UV systems suffer from a lower performance (ISUS V3 precision ±0.5 µM; accuracy ±2 µM; Satlantic Incorporated, 2010), interferences (Sakamoto *et al.,* 2009), drift (P. Christensen and Melling, 2009) and high-power consumption (6.5 W for ISUS V3). However, they can easily detect increases in nitrate into surface waters (Fig. 1.4).

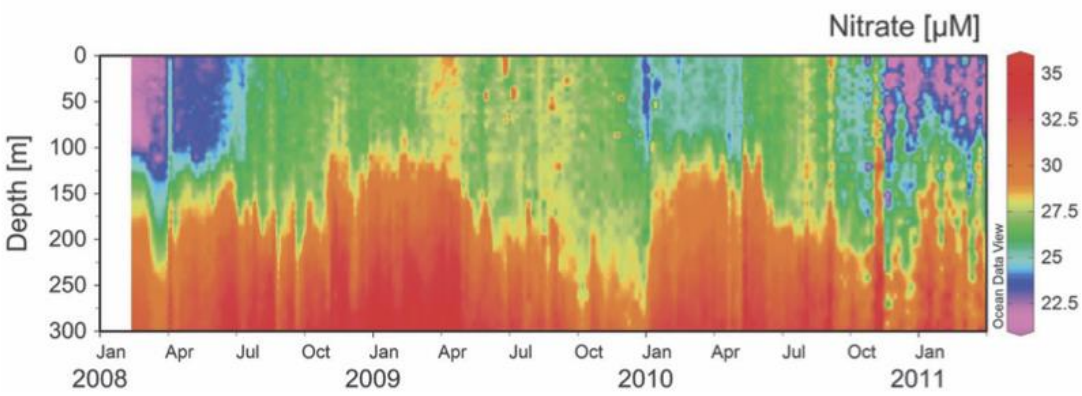

Figure 1.5: An example of timeseries profiles of nitrate collected by an ISUS sensors deployed on an APEX profiling float (Teledyne Webb Research) in the Indian sector of the Southern Ocean (Johnson *et al.*, 2013).

Wet chemical systems using colorimetry have been shown to be well suited to both *in situ* observations and mobile platforms (Nightingale *et al.,* 2015), due to their basis in a well-understood chemical method (Dutt and Davis, 2002) and strong analytical performance (e.g. Beaton *et al.,* 2011). To increase resource lifetime, *in situ* sensors use microfluidics to drastically decrease reagent use by using 150 µm wide channels within the chip, and also reduce energy use when moving fluid around due to less power being needed by the pump (Jokerst, Emory and Henry, 2012; Nightingale, Beaton and Mowlem, 2015). There have been examples of *in situ* chemical sensors, based on wet-chemical microfluidic systems, being deployed on underwater vehicles, such as Remotely Operated Vehicles and AUV's, but they have so far been limited to deployments of less than 24 hours, not time series, and on platforms where power is not critical (e.g. Le Bris *et al.*, 2000; Statham *et al.*, 2005; Provin *et al.*, 2013). By deploying biogeochemical sensors based on novel wet chemical microfluidic systems on long endurance autonomous platforms (e.g. AUVs) the problem of sparse observation scales and limited ranges of observed parameters can be greatly alleviated and our understanding of globally key biogeochemical cycles and budgets increased.

1.3 Autonomous Underwater Vehicles: Increasing marine observations

Over the last three decades a profound increase in global basin scale oceanic observations has been achieved (Olsen *et al.*, 2016). This is due to the success of projects based on repeating ship transects (e.g. Mawji *et al.*, 2014; Rees *et al.*, 2015; Talley *et al.*, 2016), international projects such as CLIVAR, GEOTRACES, WOCE and time-series moorings (Harris, 2010; Lomas *et al.*, 2013; Karl and Church, 2014). As technology advances and becomes increasingly available to marine research it opens new capabilities and provides insightful contributions to previously established fields. A prime example of this technology was the introduction of remote sensing platforms such as satellites (Yoder and Kennelly, 2006; Yang *et al.*, 2013; Le Traon *et al.*, 2015). The success of satellite observations can be said to be down to their unique ability to undertake continuous monitoring over large spatial scales, which has produced an exponential amount of novel data that just wasn't possible or feasible with mooring or ship based platforms (Esaias *et al.*, 1998; Gregg and Casey, 2004).

While satellite remote sensing has increased our ability to observe the surface of the ocean, ship-based platforms have been the staple observational platform to understand the spatial and temporal variability of the whole water column. They can investigate and track particular areas and features of scientific interest with high levels of mission flexibility but struggle to resolve mesoscale or high frequency processes for extended periods of time. While time-series occupations, mostly done through the use of moorings or chains, do not have the spatial coverage of satellites or ship-based sampling, they are well suited to provide continuous long-term and high-resolution observations of specific features of interest while having a lower resource footprint (Church *et al.,* 2013). In the 1970s to increase the spatial and temporal resolution of marine observations and move away from bottle-based sampling, specifically biogeochemical and bio-optical observations, Aiken *et al.* (1977) used a towed vehicle sensor platform. Using a towed vehicle has provided an opportunity to improved ship-based observational capabilities, allowing for higher resolution biogeochemical observations within the surface layer (Hales, *et al.,* 2004). However, this method still suffers from the disadvantages of boat-based platforms.

The most significant improvement to oceanographic observational capabilities to date has been through the introduction of autonomous underwater vehicles (AUVs) to marine research. In their relatively short deployment history, AUVs have been able to observe the oceans at a temporal and spatial scale previously thought un-attainable and have already opened up new research possibilities (Roemmich *et al.*, 2001; Rudnick *et al.*, 2004; Roemmich and Steering Team, 2009; Rudnick, 2016). Unlike previous platforms, AUVs can operate in harsh environments (e.g. under sea-ice and winter storms), have the capacity to sample at a higher resolution to observe

time sensitive processes and events and provide a long term low cost monitoring platform (e.g. Davis *et al.,* 2008; Queste *et al.,* 2012; Thomalla *et al.,* 2015).

The Array for Real-time Geostrophic Oceanography (ARGO) program is the most established and successful global observations project using an autonomous underwater vehicle (Roemmich *et al.*, 2001). Currently there are over 3900 active profiling floats (http://www.jcommops.org) and it has become one of the biggest marine observation systems, with floats providing temperature and salinity data every ~ 10 days of the upper 2000 m, equating to over ~ 8000 profiles each month (Gould *et al.*, 2004; Roemmich and Steering Team, 2009). The profiling float has no control over its direction of movement and travels by drifting at a set 'parking depth' (optimally at 1000m). It is therefore unable to provide observations in areas such as divergences or shallow seas, and is also unable to repeat transects or track mobile features (Kamenkovich *et al.*, 2009; Riser *et al.*, 2016).

The ability to position instruments within three-dimensional space within our oceans and continuously collect high resolution data autonomously, is where underwater gliders come to the fore. Three variations of underwater gliders have been developed and used widely within oceanographic research. These consist of the Spray, developed by Woods Hole Oceanographic Institute and Scripps Institute of Oceanography (Sherman *et al.*, 2001), the Slocum, developed by Webb Research (Webb, Simonetti and Jones, 2001; Schofield *et al.*, 2007), and the Seaglider, which was developed by the University of Washington (Eriksen *et al.,* 2001).

Gliders have been deployed with a suite of sensors to observe an array of physical and biogeochemical parameters. What makes up a gliders standard suite of sensors along with their capacity to carry extra sensors internally or mount externally varies between the models produced by different manufacturers (e.g. Kongsberg, Teledyne, Woods Hole Oceanographic Institute, Bluefin Robotics and Alseamar). Gliders were originally developed to mainly undertake physical oceanographic research with the standard deployment of physical sensor consisting of un-pumped, now pumped, Conductivity Temperature Depth (CTD) packages (e.g. Sea-Bird SBE13 CT Sail, Seabird Electronics). Recently microstructure profiler packages (Rockland Scientific International; Palmer *et al.,* 2015) and Acoustic Doppler Current Profiler (ADCP; Nortek Aquadopp; Baumgartner & Fratantoni, 2008) have become more common. With regards to biogeochemical observations, active optical sensors measuring inherent optical properties and fluorescence to observe phytoplankton biomass, coloured dissolved organic matter, turbidity and dissolved and particulate organic carbon have been developed (e.g. WET Labs ECO Puck). Sensors measuring Photosynthetically Available Radiation (PAR; Hemsley *et al.,* 2015; Biospherical Instruments) and oxygen concentrations (Aanderaa 4330F Optode; Queste *et al.*, 2016) are now

regularly deployed on gliders. The calibration of deployed physical or optical sensor is vital to be able to compare to data collected on other platforms or to understand the impacts of drift or fouling that occurs over long-term deployments (e.g. Cetinić *et al.*, 2009). While manufacturer calibration of instruments is common, sensors need to be calibrated pre and post deployment against *in situ* data to be more representative of the natural variability observed during the deployment but also to account for effects of drift, standard degradation or biofouling can have during longer deployments.

The addition of autonomous underwater gliders to the ever-expanding toolbox for marine research has already significantly added to the previously limited density of oceanographic observations and has secured a defined role as a dynamic instrument platform. Whether used alone with a single defined research task, or as part of a suite of observation platforms undertaking extended/continuous environmental monitoring, gliders have become part of the expanding global observation network that acquires simultaneous physical and biogeochemical parameters affected at a complex range of temporal and spatial scales. For a more detailed review of glider technology, deployment results and future of the vision see Meyer (2016), Testor *et al.* (2010), Wood & Mierzwam (2013) and Rudnick (2016).

1.4 Bio-optical observations

Different optical components of the marine environment (e.g. absorbance, fluorescence and scattering) can be separated from remotely sensed ocean optical data. These components can be used to estimate key bio-optical variables within the surface water column at basin and global scales (at a 1km resolution from daily to monthly time scales) through empirical relationships, algorithms and semi-analytical models (McClain, 2009). Such bio-optical components have been reported to show a relationship with water column characteristics and constituents, such as, particulate load and characteristics (e.g. suspended organic matter; Babin *et al.*, 2003) and phytoplankton biomass (e.g. Chlorophyll-*a* fluorescence; Gordon *et al.*, 1983). As the field of remote sensing moves forward and new empirical relationships are validated, a next-generation of products are being introduced grouped around primary production and carbon (Balch *et al.*, 2018). For example, backscattering can be used to estimate POC concentration, phytoplankton carbon biomass, coccolithophores and particulate inorganic carbon (Balch *et al.*, 2007; Olmo *et al.*, 2015), while the ratio of chlorophyll-*a* to light scattering can be used as an optical index of phytoplankton physiology (Behrenfeld and Boss, 2003).

These satellite derived products have now become an indispensable tool for increasing our understanding of globally scale primary production/ocean colour (Blondeau-Patissier *et al.*, 2014), sea surface temperature (Kawai and Wada, 2007), and mesoscale variability (Pascual *et al.*, 2006). However, these observations are not capable of observing optical parameters below 60 m from the surface and therefore, miss critical phenomena such as the deep chlorophyll maximum (DCM). The vertical structure is generally estimated using statistical relationships between the satellite-derived values and vertical profiles from *in situ* observations (Loisel *et al.*, 2013). Validation of remotely sensed data and the algorithms used are vital as the uncertainties produced by distinct regional differences in optical characteristics make it complex to quantitively characterise the global ocean (Strutton *et al.*, 2013). Moreover, coastal areas are optically complex and satellite observations struggle to derive accurate observations. The optical characteristics of coastal waters are highly variable and show extreme spatial heterogeneity (Loisel *et al.*, 2013).

Gliders and profiling floats equipped with optical instrumentation are well placed to improve bio-optical products and address the areas above highlighted for improvement. Such platforms have been able to provide both complimentary and calibration datasets for remotely sensed products and observe the vertical structure and characteristics of the water column (e.g. fluorescence, backscatter, radiance, irradiance) that remote sensing currently cannot directly observe (Schofield *et al.*, 2007; Boss and Behrenfeld, 2010; Strutton *et al.*, 2013). This has allowed for the validation of satellite products and improved bio-optical algorithms, global primary production estimates and estimates of particulate organic carbon (Loisel *et al.*, 2013; Thomalla *et al.*, 2017, 2018). Additionally, studies using both satellite and glider platforms have shown by using both platforms you can unlock a new insight into local event driven processes in optically complex coastal waters, such as river plumes (Many *et al.*, 2018). Both remote sensing and AUV's provide observations that intersect in complimentary spatio-temporal domains, thus allowing vital insight in seasonal variations in biogeochemistry and mesoscale oceanic processes, which are fundamental to improve our understanding of our current and quickly changing marine ecosystem (National Research Council, 2011).

1.5 Aims and Objectives

The main aim of this thesis was to investigate the biogeochemical cycle of nitrate + nitrite ($\sum NO_x$) and the fluxes across the pycnocline within the central Celtic sea in unprecedented detail into biogeochemical cycle + nitrite ($\sum NO_x$).using autonomous gliders and wet chemical sensors. In addition, bio-optical sensors deployed on autonomous gliders were used to determine if established empirical relationships from open ocean waters are valid in a seasonally stratifying shelf system. By deploying for the first time a novel wet chemical microfluidic Lab-on-chip nutrient sensor (LoC; NOCS, OTE), within an autonomous underwater glider (Kongsberg Seaglider), alongside bio-optical sensors and a second Slocum glider (Teledyne Webb research) with a Microrider microstructure package (Rockland Scientific International), the following objectives were achieved:

- To accurately determine $\sum NO_x$ concentrations ship-based within the water column by successfully deploying a novel Lab-on-chip nutrient sensor within an autonomous Seaglider

- To investigate the availability of $\sum NO_x$ for primary production within the central Celtic Sea by quantifying the $\sum NO_x$ flux across the pycnocline

- To determine if established empirical relationships from bio-optical sensors deployed on a Seaglider to estimate Particulate Organic Carbon (POC) and phytoplankton carbon are valid in dynamic shelf systems by comparing with discrete seawater samples

Chapter 2: Methods

2.1 The Shelf Seas Biogeochemistry program

The Shelf Seas Biogeochemistry program (SSB) was funded by the National Environmental Research Council (NERC). The main aims were to increase the understanding of the sources, sinks and cycling of nutrients and carbon around the Celtic Shelf Sea (North West Europe), and the importance of processes within temperate shelf seas to global climate and biogeochemical cycles (http://www.uk-ssb.org/). Using the data collected over a yearlong field campaign SSB also seeks to greatly improve predictive marine biogeochemical and ecosystems models.

For this thesis, the data presented consists of biogeochemical and physical datasets that were collected during the SSB program using two autonomous underwater gliders, which were a Seaglider (Kongsberg) and Slocom (Teledyne Marine), in addition to traditional ship-based data from the *R.S.S. Discovery*. Auxiliary data, such as tidal (Juliane Wihsgott: University of Liverpool) and meteorological data (Joanne Hopkins: National Oceanographic Centre, Liverpool), were collected from both mooring and seabed frame deployments. The location for this study was at the Central Celtic Sea sampling site (CCS; 49°24'N, 8°36'W), located ~ 145 miles off the South West coast of the United Kingdom in a max water depth of ~ 140 meters (Figure 2.1). Datasets were collected from two cruises; the first took place from the 1st of April to 30th April 2015 (DY029), and the second from the 11th of July to 2nd of August 2015 (DY033).2.1

2.2 Auxiliary Data: CTD rosette, Buoys and Landers

A stainless-steel rosette and CTD package, consisting of a CTD (Seabird 911+), optical backscatter (WET Labs, ECO BB), fluorimeter (Chelsea Technologies Group, Aquatracka MKIII) and Niskin bottle system (24 x 20 L) was deployed from the *R.S.S. Discovery* for both cruises at CCS. Conductivity, temperature and pressure were measured by the CTD system, with discrete seawater samples collected for Chl-*a* and nutrient analysis following the GO-SHIP sampling and handling procedures (Hydes *et al.*, 2010). Salinity (calculated from conductivity and temperature) and Chl-*a* (fluorescence, 682 nm) measurements obtained from CTD casts were calibrated daily on-board against discrete seawater samples. Salinity samples were analysed on an Autosal 8400B salinometer (Guildline). Chl-*a* samples were filtered through 0.7 µm glass microfiber filters (Whatman GF/F) and extracted in 90% acetone overnight, before being measured on a pre-calibrated (spinach Chlorophyll-*a* standard, Sigma) fluorimeter (Turner Design Trilogy; Holm-Hansen *et al.,* 1965). Nitrate (measured as NO_2^- + NO_3^-) was analysed on-board within ~ 3 hours of CTD recovery, using a five channel segmented-flow autoanalyzer (Bran & Luebbe) following the colorimetric procedures of Woodward and Rees (2001) and Brewer & Riley (1965). A certified reference material (http://www.kanso.co.jp/eng/production/) was analysed daily as part of the quality control protocols and to ensure reproducibility of results. Precision was between 2% and 3% and the limits of detection of 0.02 µM and 0.01 µM for nitrate and nitrite respectively.

Tidal data (horizontal velocity) was collected at CCS using an Acoustic Doppler Current Profiler (ADCP) mounted to a frame on the seabed at 145 m (49 º 24'N, 8 º35'W). The upward facing ADCP (RDI 150 kHz workhorse) measured current magnitude (m s^{-1}) and direction (degrees from north) at a vertical resolution of 2 meters every 2.5 minutes (Wihsgott *pers. comm.,* 2017). Meteorology was provided at CCS by the deployment of a Met Office buoy. The Ocean Data Acquisition System (ODAS) buoy provided hourly averages of wind speed (m s^{-1}; including maximum gust speeds) and direction (degrees from north) 3 meters above sea level. Neutral wind stress was calculated following Large and Pond (1981).

2.3 Autonomous Underwater Vehicle: Gliders

In April and July 2015, two different gliders were deployed to sample in a circular holding pattern around CCS (e.g. Figure 2.1c) and coincided with two SSB research cruises DY029 (April) and DY033 (July). The first was a Kongsberg Seaglider (Ogive fairing) with a Lab-on-Chip nutrient sensor (Ocean and technology and Engineering Group, National Oceanography Centre, Southampton, UK) which measured nitrite + nitrate (defined as $\sum NO_x$). The second was a Slocum

glider (Teledyne Webb research, USA) with a Microrider microstructure package (Rockland Scientific International, USA) which measured turbulence.

The Seaglider was deployed at CCS between the 4th to 25th April and 13th to 30th of July (decimal days 94.2 to 114.6 and 194.2 to 211.5), collecting 1547 and 1128 profiles (total number of profiles = descending + ascending) to a depth of ~ 120 meters along a saw-tooth trajectory at typical vertical speeds of 0.1 m s^{-1} (Rudnick *et al.*, 2004). Two-way communication through an Iridium satellite connection allowed for the transmission of data packets containing the 'status' of the Seaglider and information from on-board scientific sensors. The relay of scientific data after each dive not only mitigated against the accidental loss of the Seaglider but also allows for the review of scientific measurements to adapt the current sampling strategy.

2.3.1 Sensors, Calibration and Corrections

For both the April and July deployments the LoC glider was equipped with an un-pumped SBE13 Conductivity and Temperature Sail (CT sail; Seabird Electronics, USA), Paine pressure sensor (Paine Electronics, USA) and Triplet ECOPuck (WetLabs, USA) measuring fluorescence (excited at 470 nm and measured at 682 nm), Coloured Dissolved Organic Matter (CDOM; excited at 370 nm and measured at 460 nm), and particulate optical backscatter (650 nm).

The processing of the vast amounts of scientific data produced by sensors on-board the Seaglider and the Slocum gliders is extensive, with sensors requiring extended post-processing, calibration and corrections. The manufacturers of the glider platforms and the sensors deployed on/within them currently do not provide a processing methodology (including software suites) that is comprehensive enough to enable simple processing of this data. Therefore, there are many steps involved in the processing to ensure all data is quality controlled. At present, the '*glider community*' consists of many national facilities, individual research institutes and well-funded research groups, each with their own processing tools and guidelines (Heslop *et al.*, 2015). The extraction, processing, corrections, calibration, visualisation and analysis of the Seaglider and LoC nutrient sensor data for this thesis was done using MatLab^{TM} (MathWorks). For the LoC sensor custom scripts were provided by the Ocean and Technology and Engineering Group (National Oceanography Centre, Southampton) and modified for this work. A Seaglider toolbox, http://bitbucket.org/bastienqueste/uea-seaglider-toolbox, provided by Bastien Queste (University of East Anglia), was used to extract and perform the initial quality control. In addition, further custom scripts were provided by the Marine Physics and Marine Climate group (Joanne Hopkins: National Oceanography Centre, Liverpool) and modified for the quality control, calibration and gridding of the CT sail and ECOPuck data.

2.3.1.1 Conductivity and Temperature

The Seaglider runs a single threaded processor and is unable to run the guidance and control processes whilst also simultaneously polling each scientific sensor at the same time. The time stamp for each round of polling for the scientific sensors therefore had to be corrected as the time taken to record a measurement is the cumulative value of the sampling duration of the previous sensors and each of their varying warm up times. Custom scripts within the UEA Seaglider toolbox automatically correct for this and are described in Queste *et al.* (2012). Following this, raw measurements from the CT sail were checked for bounds, spikes and anomalies, and then measurements of temperature and conductivity were calibrated using manufacturer-supplied coefficients. Further processing was undertaken to correct for thermal lag and thermal inertia, as physical separation and disparity in response time between the temperature and conductivity sensors must be accounted for when deriving salinity and density (Garau *et al.*, 2011; Palmer *et al.*, 2015).

Thermal lag is caused by the slow response of the temperature probe to equalize to the changing water temperature around the Seaglider. A correction for first order thermal lag was applied to the raw temperature as a function of the thermal gradient encountered by the instrument described as:

$$T_{real} = T_{obs} + \tau \frac{\delta T_{obs}}{\delta t} \quad (2.1)$$

where τ is a time constant of 0.6 seconds, t is time and T_{real} and T_{obs} are real and observed times respectively (Garau *et al.,* 2011). This correction is done by the UEA Toolbox and is vital when there is a steep thermocline, as often observed in seasonally stratified shelf seas.

Thermal inertia due to a temporal and spatial mismatch between temperature and conductivity measurements results in inaccurate calculations of salinity. As temperature is measured outside of the conductivity cell, the temperature reported by thermistor is different from the actual temperature inside the conductivity cell. The conductivity cell has a thermal mass which influences the temperature of the water flowing through the conductivity cell, thus affecting the measurement of conductivity. To correct for thermal inertia, the approach by Garau *et al.* (2011), built on the work by Lueck and Picklo (1990) and Morison *et al.* (1994) was used and calculated using the following equation:

$$T_T(n) = -bT_T(n-1) + a[T(n) - T(n-1)] \quad (2.2)$$

T is the temperature measured outside of the cell and the coefficients *a* and *b* are calculated as described in (Garau *et al.,* 2011). A key parameter needed for the calculation of coefficients *a* and *b* is the flow speed through the CT sail conductivity cell, which is not measured directly (Morison *et al.,* 1994). The flow speed was calculated using a hydrodynamic flight model of the Seaglider, and is run iteratively to optimise the hydrodynamic parameters used to calculate the Seaglider's velocity (Frajka-Williams *et al.,* 2011).

Glider-derived temperature and salinity profiles were calibrated against CTD cast data taken at the Central Celtic Sea CCS site (Hopkins *pers. comm.,* 2017). Only CTD casts taken within 2.6 km of the glider were used for the calibration. Four (CTD013, CTD049, CTD121, CTD122) and three (CTD1 CTD76 CTD78) CTD casts were used for calibration from the DY029 (April) and DY033 (July) respectively. Based on the mean CTD temperature and salinity of the water between 80 m and 105 m, a constant offset of 0.0277 ºC and 0.0024 PSU and 0.0618 ºC and - 0.0173 PSU for the DY029 and DY033 cruises, respectively, was applied and density recalculated.

2.3.1.2 Chlorophyll-*a*

The initial calibration of the fluorescence counts (also colored dissolved organic matter (CDOM) and backscatter) from the WetLabs Triplet consists of applying the manufacturer-supplied coefficients, subtracting the instrument blank (Sea-Bird Scientific, 2017), and applying a scaling factor (0.0122). Calibration to convert fluorescence counts to Chl-*a* concentrations is based on the fluorometers (WetLabs) response to the cultured diatom, *Thalassiosira weissflogii,* at a known Chl-*a* concentration (Wetlabs, 2017).

During periods of higher surface irradiance, commonly around midday, there is a marked reduction of *in vivo* fluorescence that is uncorrelated to Chl-*a* concentrations, and this leads to an underestimation of Chl-*a* within the euphotic zone (Falkowski and Kolber, 1995). This was corrected for using the methodology described in Sackmann, Perry and Eriksen (2008) and Hopkins *et al.* (in prep). By using the ratio of Chl-*a* fluorescence to optical backscattering (F:bb), the depth to which quenching was occurring and the temporal extent to which it persisted was identified, and the depth of the maximum Chl-*a* concentration was then extrapolated to the surface. During the July cruises a well-defined SCM was present, with average surface Chl-*a* concentrations substantially lower (0.31 mg m^{-3}) than during the April cruise (3.06 mg m^{-3}). There was also only a small difference in surface Chl-*a* concentrations between night and day profiles (< 3 mg m^{-3}), and so quenching corrections were not undertaken.

A visual comparison between calibrated Chl-*a* profiles from the Seaglider and calibrated CTD bottle-samples was done to facilitate quality control. Profiles of Chl-*a* were compared and

showed no large systematic variation between the datasets; the small-scale variability between Seaglider and calibrated CTD collected data was likely due to the variation between the datasets as a product of a greater number of Seaglider profiles (CTD profiles = <25, Seaglider profiles = >1100), lateral distance and the period of time between compared profiles. The relative 'patchy' characteristics of phytoplankton communities in dynamic systems will also fundamentally affect separately sourced Chl-*a* data (Holligan, 1978).

2.4 A Microfluidic Lab-on-Chip Nutrient Sensor

The Lab-on-Chip (LoC) sensor is based on microfluidic principles (Sieben *et al.*, 2010) and is a miniaturised wet-chemical sensor designed and built by the Ocean Technology and Engineering Group (National Oceanographic Centre, UK). The LoC system is a platform capable of measuring a range of analytes, facilitated by modifications to the LoC structure and chemical assays used (Beaton *et al.*, 2011; Rérolle *et al.*, 2013; Grand *et al.*, 2017). The LoC platform with a Nitrite (NO_2^-) and/or Nitrate (NO_3^-) sensor has been successfully tested (Beaton *et al.*, 2012). The LoC $\sum NO_x$ sensor was deployed on a benthic lander in the Mauritian oxygen minimum zone to examine cross-shelf transport of NO_3^- rich waters (Yücel *et al.*, 2015), and in glacial meltwaters rivers draining the Greenland Ice Sheet (Beaton *et al.*, 2017).

LoC nitrate (NO_3^-) + nitrite (NO_2^-), hereafter defined as $\sum NO_x$ uses the Griess assay (Griess, 1879), where NO_3^- is reduced to NO_2^- using a custom off-chip Copper-activated Cadmium tube (SEAL analytical, UK; Moorcroft, Davis and Compton, 2001). The LoC $\sum NO_x$ sensor had three different length measurement cells, each suited to a different range of $\sum NO_x$ due to non-linearity of the Beer-Lambert law at higher absorbance values. The cell lengths were 25 mm, 2.2 mm, and 0.8mm and were each suitable for measuring $\sum NO_x$ in ranges between 0.025 – 35 µM, ~35 - 350 µM, and up to 1000 µm respectively (Beaton *et al.*, 2012). In this study the longest channel (25 mm) was chosen as its analytical range (0.025 – 35 µM) was most suited to the range of $\sum NO_x$ concentrations predicted to be observed during the April and July deployments (0.2 to < 10 µM).

A LoC $\sum NO_x$ sensor, without housing, is 119 x 120 mm (diameter x height) in dimension and consists of a microfluidic chip/platform, fluid control components, optical measurement components, and electrical components for the overall control of the sensor and data handling (Beaton *et al.*, 2011, 2012). These elements, and the internal fluidic layout, are highlighted in Figure 2.3 The LoC is composed of three layers of poly(methyl methacrylate) (PMMA) with harbored precision-milled micro-channels (150 µm wide, 300 µm deep). A 460 mm long

serpentine mixing channel aids in the mixing of analyte sample and reagents. Optical components consisted of four LED (525 nm, Avago Technologies, USA) and photodiode (TAOS) pairs. A stepper motor linked to three glass barrel syringes (70 µL) and 15 microinert solenoid valves (Lee Products Ltd., UK) controls the movement of fluid into and around the chip. When deployed, the LoC sensor was encased in a mineral oil-filled housing (PVC, 12 cm diameter, 30 cm height) with an internally fitted pressure-compensating bladder, and samples were filtered through a 0.45 µm MILLEX-HP filter unit (Millipore, Ireland) that is connected to the sensor using polytetrafluoroethylene (PTFE; IN = 0.5 mm) tubing and ¼ 28'' connectors. All Griess reagents, standards (NO_3^-) and blank (artificial seawater) solutions were stored in externally attached gas impermeable 150 mL Flexboy bags (Sartorius, UK) and the waste collected into a 500 ml Flexboy bag (Figure 2.2).

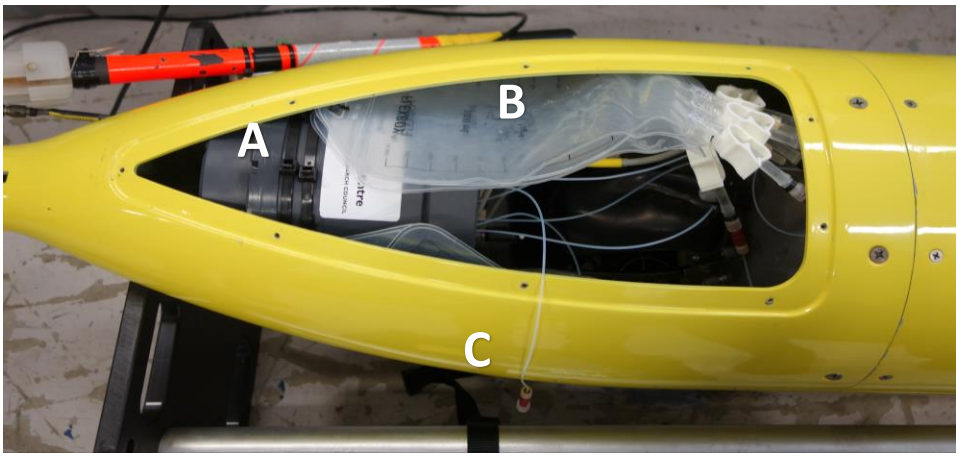

Figure 2.2: A LoC nutrient sensor deployed within the wet bay of a Seaglider (Ogive Profile). The annotated components are (a), the LoC is in an oil-filled housing (b), multiple blood bags used to store reagents, blanks and standards and (c), an 0.45 µm MILLEX-HP filter unit (Millipore) that is attached to the cover of the bay before deployment.

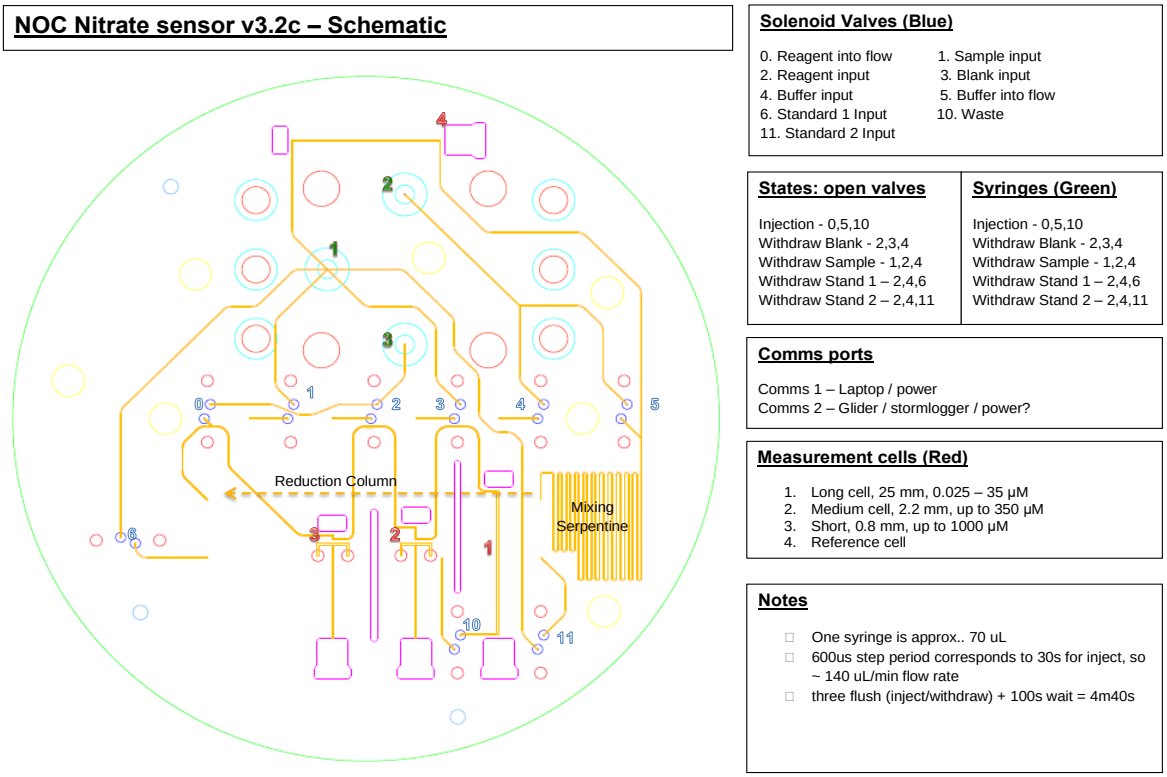

Figure 2.3: Annotated schematic of a LoC nutrient sensor (NOC, UK; version 3.2c). This version of the LoC sensor measures nitrite plus nitrate and uses a reduction column mounted on the outside of the chip. Information regarding the annotations is provided (left side) along with valve operation combinations.

2.4.1 Chemical preparation: Griess Reagents

All glassware and plastic flasks (HDPE; Nalgene, UK) used were cleaned using nutrient-free detergent (10% Decon, Neutracon for 24 hours), followed by soaking in hydrochloric acid (10 %) for 24 hours and rinsed three times with MilliQ (Millipore).

The Griess reagent was made by dissolving 0.5 g of sulfanilamide (Fisher Scientific, UK) in ~ 100 mL of Milli-Q water and 5 mL of concentrated hydrochloric acid (Sigma- Aldrich, UK) in a 500 mL volumetric flask. Once dissolved, 0.05 g of N-(1-Naphthyl)ethylenediamine hydrochloride (Sigma-Aldrich, UK) was added with Milli-Q to make a final volume of 500 mL. The imidazole buffer solution was made by adding 3.4 g of imidazole (Fisher Scientific, UK) and 1 mL of 10 mM copper sulphate solution to 1000 mL of Milli-Q water, and the pH adjusted to 7.8 with concentrated hydrochloric acid. Artificial seawater was prepared by dissolving 35 g of sodium chloride (Fisher Scientific, UK) and 0.5 g of sodium hydrogen carbonate (Fisher Scientific, UK) in

approximately 900 mL of Milli-Q water and made up to 1 L. A NO_3^- stock solution (100 mM) was prepared by dissolving 10.11 g of potassium nitrate (Fisher Scientific, UK) in 1000 mL of artificial seawater. Serial dilution with artificial seawater was performed to make the various working standards, and 0.1% chloroform (Fisher Scientific, UK) was added to preserve the standards.

2.4.2 Control and Operation

The LoC $\sum NO_x$ sensor is controlled by a custom design electronic control package. Within the package, a micro-controller runs low level operations and the programmable arbitrary state machine. A state machine is a timed series of control events in a defined sequence controlling the functionality of elements of the sensor. A state machine is uploaded to the LoC over a RS232 serial connection and is initiated with the powering on of the LoC sensor. Below is a brief explanation of a basic state machine performing a stop-flow protocol for a repeating a measurement cycle.

The repeated measurement cycle consists of the analysis of a blank (Milli-Q or artificial seawater) sample (filtered when deployed) and associated standard(s). Between each measurement the whole chip was flushed with the next analyte solution. Solenoid valves, controlling the flow and input of solutions into and around the chip, are actuated, enabling the Griess reagent, buffer and analyte solutions (blank, sample or standards) to be drawn simultaneously into the three glass barrel syringes (Figure 2.3). The solenoid valve configuration then changes (valves are closed and opened) and fluid was pushed/injected through the chip, forcing the previous fluid within the chip out of the waste port. The analyte solution and buffer solution are then injected into the mixing serpentine before passing through the out-board cadmium reduction column. After the cadmium reduction column, the Griess reagent is injected into the channel containing the mixed analyte and buffer solution, before passing into the three measurement cells. All solutions are injected at a 1:1:1 ratio by volume. The control system then waits for a set period (100-120 seconds), allowing for diffuse mixing and the azo dye colour to develop, which is proportional to the nitrate concentration. After this time, the transmission values from the photodiodes output voltage during the final 5 seconds are averaged. The 'flushing' cycle is then repeated 3 to 7 times to flush the whole chip between analyte measurements (Figure 2.4). Increased flushing was used to prevent carryover due to the increased dead space added by a filter and extended sampling tube.

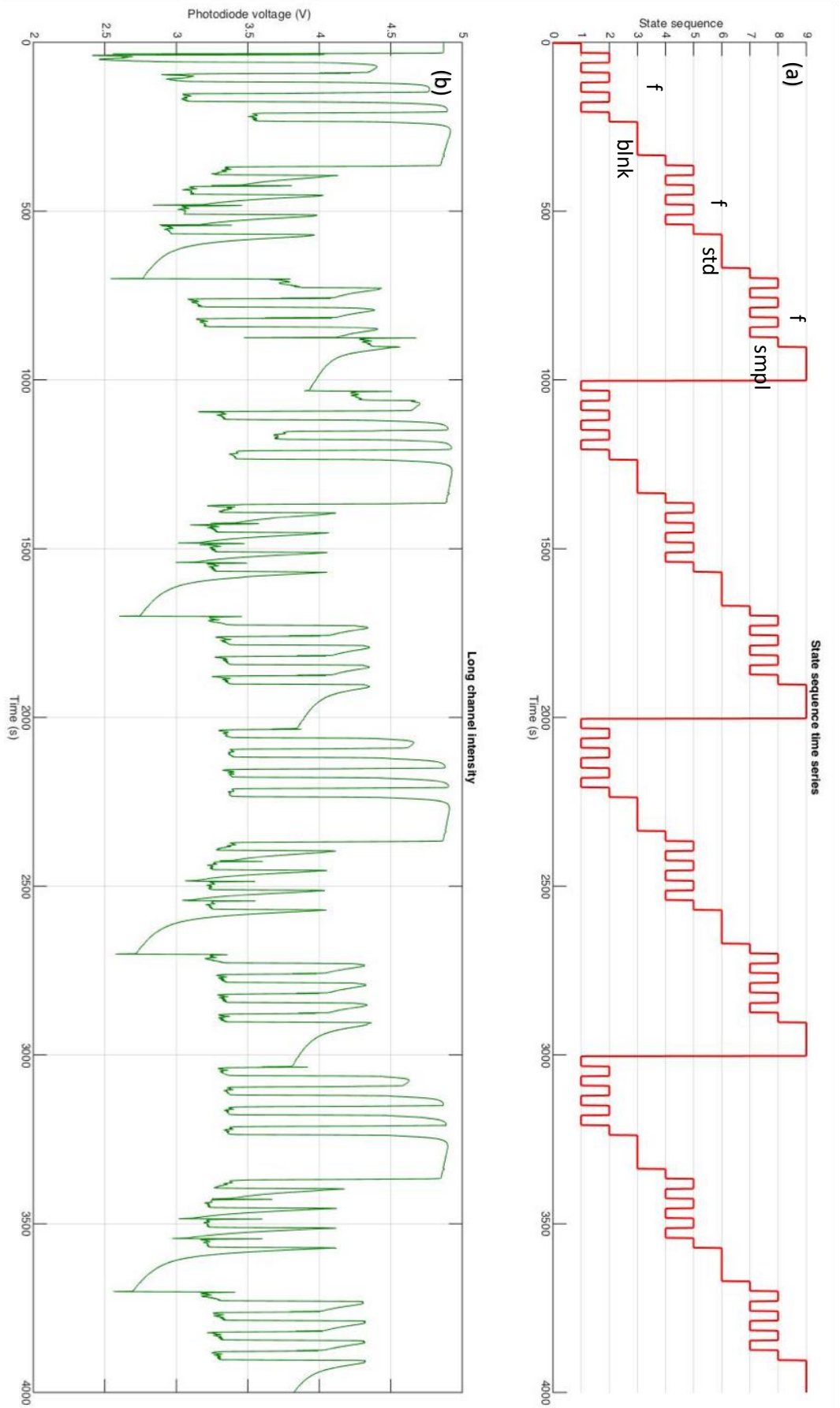

Figure 2.4: An example of LoC data outputs consisting of (a), a time series of the state machine instruction sequence with four flushes (f) each followed by the colour development period (100 seconds) of a blank (blnk), standard (std) and sample (smpl), and (b), the long channel photodiode voltage output.

Once the LoC $\sum NO_x$ sensor is deployed and/or initiated, the pre-existing state machine code cannot be directly modified by external means. Variations to the running order of the state machine can be achieved by triggers that initialise pre-coded variations; these consists of counts (do task x times), timings (wait x hrs/days) and external (if parameter x is y do task z). The following examples are based on the interactions between the LoC sensor and Seaglider when deployed at sea and show variations to the state machine running order and decision opportunities:

- The LoC sensors micro-controller is able to receive live depth values from the Seaglider. A conditional statement returns True or False depending upon if the received depth value is smaller or greater than a pre-set value, causing the micro-controller to continue on the current state machine routine or change to a pre-coded variation (i.e. IF depth < 5m DO Plan A, ELSE, DO Plan B)
- The micro-controller is able to count in defined iterations. Whilst the Seaglider is descending to the pre-set maximum depth, the micro-controller will undertake a minimum of two blank and standard measurements. Once completed, if the maximum depths have not been reached, additional measurements will be done until a maximum amount or depth is reached
- By using the on-board clock, the micro-controller can use the completion of a wait period to re-start the state machine or initialise a pre-coded variation. If the Seaglider is at the surface for an extended period, the micro-controller can initialise the measurement of extra standards/blanks

2.4.3 Lab-on-Chip Deployments on Seaglider and CTD

During both deployments (April and July 2015) a single LoC nutrient sensor, measuring $\sum NO_x$, was deployed in the wet payload bay within the Ogive fairing of a Seaglider (Kongsberg; see Figure 2.2). This combination of LoC $\sum NO_x$ sensor deployed within a Seaglider will hereafter be defined as the LoC glider. During the July deployment and cruise, a second LoC nutrient sensor, measuring $\sum NO_x$, was mounted on a stainless steel CTD rosette, in the place of a Niskin bottle, to

enable the direct comparison of $\sum NO_x$ concentrations from both methodologies collected *in situ* at the same depth and time at CCS.

For deployments on the stainless steel CTD rosette, the LoC $\sum NO_x$ sensor was encased in a mineral oil-filled housing (PVC, 12 cm diameter, 30 cm height) with an internally fitted pressure-compensating bladder. The LoC $\sum NO_x$ sensor, along with its battery, reagents, standard (3µM NO_3^-), blank (ASW) and waste (all stored in blood bags) was mounted on a custom frame. This complete package was of a similar size to a 20 L Niskin bottle and its mounting mechanism was the same (Figure 2.5). When the CTD rosette was deployed and reached a depth of 5 m a pressure sensor on the battery of the LoC $\sum NO_x$ sensor powered the sensor on. Once the CTD ascended back to 5m the pressure sensor powered the sensor off.

Figure 2.5: A LoC nutrient sensor within a custom frame mounted on a CTD rosette system in place of a single Niskin bottle. The LoC sensor and battery are located within the bottom grey section, while the blood bags for the reagents, nitrate standard and waste are located in the top section. The 0.45 µm MILLEX-HP filter unit can been seen located between both the top and bottom sections.

When deployed on the CTD rosette, the LoC $\sum NO_x$ sensor state machine was programmed to undertake a repeating measurement sequence of artificial seawater blank, discrete seawater sample and standard (3 µM NO_3^-). Seawater samples were drawn into the sensor through a 0.45 µm MILLEX-HP filter unit (Millipore, USA). Between each measurement the LoC $\sum NO_x$ sensor was flushed 7 times to minimize carryover. This resulted in one blank-corrected seawater sample measurement and standard (3 µM NO_3^-) every 17 minutes during the CTD cast. The CTD rosette was held at three depths (45, 50 & 90 meters) for > 90 minutes to allow for triplicate LoC $\sum NO_x$ sensor seawater measurements at the prescribed depth, each bracketed by a blank and standard measurement. During this time period two Niskin bottles were fired, one within 5 minutes of the first LoC $\sum NO_x$ sensor measurement and the second within 5 minutes of the last LoC $\sum NO_x$ sensor measurement.

The deployment of the LoC $\sum NO_x$ sensor on an autonomous underwater glider is discussed in Chapter 3 of this thesis.

2.4.4 Data processing

The retrieval of data from the LoC $\sum NO_x$ sensor was achieved by two methods: (1) a 'snapshot' of measurement data was transmitted at the end of each dive as part of the Seaglider's communication to the base station via Iridium, and (2) the complete raw dataset stored internally (SD card) which was retrieved after the recovery of the Seaglider. The transmitted data consisted of a 5 second average of the photodiode output voltage for every measurement (blank, standard, and seawater sample), from the end of the colour development period, along with their respective depths and state machine instruction number (used to identify between the types of measurements; Appendix B.1). The raw dataset consisted of the full output from the polling of all sensors within the LoC $\sum NO_x$ at 1Hz. This consisted of (a) the voltage output of the photodiode in each measurement cell (reference, small, medium and large), (b) time and depth parameters received from the Seaglider, and (c) multiple parameters from the LoC $\sum NO_x$ sensor for diagnostic use (i.e. temperature of the electronics, power supply and Hall effect sensors; Appendix B.2). All LoC $\sum NO_x$ sensor data was processed and analysed using custom MatLab™ (MathWorks) scripts.

For all deployments of the LoC $\sum NO_x$ sensor for this thesis, only a single NO_3^- standard (µM) was deployed, and the processing routine done to convert the photodiode output voltages (V) into NO_3^- concentrations (µM) is described below. The $\sum NO_x$ concentration of the discrete sample was calculated by multiplying the deployed on-board standard concentration (Conc; µM) by the ratio of the absorbance (Abs; AU) of the discrete seawater sample and standard. The absorbance value for each standard and discrete sample was calculated as follows:

$$Absorbance = -1\ x \log 10 \left(\frac{Trans_{Standard}}{Trans_{Blank}}\right) \quad (2.3)$$

where $Trans_{Standard}$ and $Trans_{Blank}$ are the mean voltages of the photodiodes in the measurement cells during a 5 second period at the end of each colour development period.

$$Concentration = Conc_{Standard}\ x \left(\frac{Abs_{Sample}}{Abs_{Standard}}\right) \quad (2.4)$$

All discrete seawater samples were calculated on a dive-by-dive basis with the associated blank and standard from that dive, and if there was more than one blank or standard an average of the two transmission values was used.

2.4.4.1 Post-processing - Quality Control & Analytical assessment

A drift between the start timestamp of each dive in the Seaglider and LoC $\sum NO_x$ sensor data occurred during the deployments. Both devices are on two separate clocks that cannot be actively synced *in situ*. Due to the previously described Seaglider timing issues (Section 2.3.1.1) the LoC $\sum NO_x$ sensor data, which is collected at 1 Hz, will not have a parallel data point from the Seaglider dataset. A correction was carried out to align the start timestamp for each LoC $\sum NO_x$ sensor and Seaglider dive file, with all timing data converted to a Unix time stamp. By correcting the start timestamps and using the same timing format complimentary Seaglider data (CTD and bio-optical) can be acquired for each time a discrete sample drawn into the LoC $\sum NO_x$ sensor.

Anomalous standard and blank transmission values can drastically affect final concentrations calculations (e.g. ± 0.005 absorbance can result in ~ 0.7 µM $\sum NO_x$ difference). As most dives only had a single standard and blank value to calculate the discrete concentrations, flagging these anomalous transmission values was vital and was undertaken manually or automatically by comparison to a moving window average. When a dive had multiple blank/standard measurements, a value would be flagged 'bad' if its relative standard deviation was >5 %, for a single blank/standard measurement this would be calculated against the moving window average. Where dives had a flagged blank or standard transmission value, the moving window average value was used to calculate the absorbance values.

The on-board standard (µM NO_3^-) is vital to be able to calculate (Equation 2.4) the concentration of discrete seawater samples, and therefore knowing the precise concentration when deployed and any variation during the deployment is paramount. Variation of the concentration of the on-board standard could occur through contamination and degradation. Contamination could occur during the making of the standards and degradation can occur due to non-ideal working and storage environment over long-term deployments (e.g. longer than one week). To account for this, all deployed standards and blanks were analysed for $\sum NO_x$ (µM) using a Quattro high performance segmented flow analysis (SFA) system (SEAL Analytical Ltd., UK) both pre and post deployment, with any contamination or degradation factored into calculations (Table 2.).

Table 2.2: Pre and post cruise $\sum NO_x$ (µM) concentrations of the blanks (artificial seawater) and standards (NO_3^-) deployed with the LoC sensors on the CTD rosette and Seaglider for both cruises (2015) at CCS.

CRUISE	BLANK: PRE	STANDARD: PRE	BLANK: POST	STANDARD: POST
APRIL	<0.01 µM	Seaglider: 6.48 µM	Seaglider: <0.01 µM	Seaglider: 6.65 µM
JULY	0.51 µM	3.22 µM	CTD: 0.58 µM	CTD: 3.44 µM
			Seaglider: 0.51 µM	Seaglider: 3.36 µM

The limit of detection (LOD) is the lowest concentration that can be reliably detected by a method and is defined as three times the standard deviation of the blank measurement (Long and Winefordner, 1983). For the LoC $\sum NO_x$ sensor LOD is regulated by the point-to-point variations of the absorbance value of the deployed standard (Beaton *et al.*, 2012). When the LoC is used in a continuous protocol, consisting of a repeated measurement routine of a sample bracketed by a blank and standard(s), each sample and standard has an associated blank used to calculate absorbance. The LOD is then taken as three times the standard deviation of these standard absorbance measurements from the back-to-back measurements. Within a laboratory setting a detection limit of 20 nM has been demonstrated (Beaton *et al.,* 2012). When the LoC $\sum NO_x$ sensor was deployed on a Seaglider, the sampling routine (Section 3.2) was only able to complete 1 or 2 blank and standard measurements per dive that were > 40 minutes apart. Therefore, considering the inherent uncertainties of a > 20-day deployment with degrading standards and cadmium column, the estimated analytical uncertainty of LoC $\sum NO_x$ sensor was calculated to understand the analytical uncertainty of the LoC $\sum NO_x$ sensor over the deployments. The estimated analytical uncertainty was calculated from two times the standard deviation of the standard absorbance values; for all deployments for this thesis the estimated analytical uncertainty was <0.2 µM (n = 193).

Chapter 3: The First Deployment of a Lab-on-Chip Nitrite + Nitrate sensor in an Autonomous Underwater Glider

The research presented in this chapter has been published in *Marine Chemistry*.

Vincent, A.G., Pascal, R.W., Beaton, A., Walk, J., Hopkins, J.E., Woodward, E.M.S., Mowlem, M. and Lohan, M.C. (2018), Nitrate drawdown during a shelf sea spring bloom revealed using a novel microfluidic in-situ chemical sensor deployed within an autonomous underwater glider, *Mar. Chem.* https://doi.org/10.1016/j.marchem.2018.07.005.

Alex Vincent [A] analysed all the data from the Seaglider and wrote the manuscript

Maeve Lohan [A], assisted with the editing of the manuscript and deployed the sensor at sea

Robin Pascal [B], Alexander Beaton [B], John Walk [B] and Matthew Mowlem [B] contributed to the development, deployment and programming of the LoC and its deployment within a Seaglider.

[C-] Joanne Hopkins contributed with the initial processing of the Seaglider data

[D] E. Malcolm Woodward contributed the CTD rosette nutrient data

[A] Ocean and Earth Science, University of Southampton, Southampton SO14 3ZH, UK

[B] Ocean Technology and Engineering Group, National Oceanography Centre, Southampton SO14 3ZH, UK

[C] National Oceanography Centre, Joseph Proudman Building, Liverpool L3 5DA, UK

[D] Plymouth Marine Laboratory, Prospect Place, Plymouth PL1. 3DH, UK

3.1 Introduction

Seasonally stratified, temperate shelf seas act as important global carbon sinks through the continental shelf pump mechanism (Tsunogai, Watanabe and Sato, 1999; Thomas *et al.*, 2004; Takahashi *et al.*, 2009). Despite the shelf seas' relatively small size (8% of global ocean area), they actually account for 15–30% of total oceanic primary production (Tweddle *et al.*, 2013) and have an average carbon fixation rate per unit area ~2.5 times greater than the open ocean (Simpson and Sharples, 2012). The interplay between light, nutrients and mixing are key drivers of primary production. A well-studied temperate shelf system, the Celtic Sea, shows a clear seasonal cycle whereby initial light and nutrient conditions are ideally suited to support the onset of the spring bloom (Fasham, Holligan and Pugh, 1983). This results in the rapid drawdown of nitrate (NO_3^-) from ~ 6-8 µM to below the limit of detection (<0.1 µM) (e.g. Hickman *et al.*, 2012; Davidson *et al.*, 2013). Post-bloom, new primary production is limited to the sub-surface chlorophyll maximum (SCM) where fluxes of NO_3^- into the thermocline fuels new production (Hickman *et al.*, 2009).

In the central Celtic Sea, shear generated turbulence (Sharples *et al.*, 2001, 2007; Rippeth *et al.*, 2009) and wind-driven oscillations (Tom P. Rippeth, 2005) are the central mechanisms in driving diapycnal mixing of NO_3^- up into the nutrient deplete surface mixed layer. Wind-driven shear occurs in episodic short-lived spikes (0.5-1 hr) and has the potential to have a large impact on NO_3^- fluxes, with observations indicating that this flux can be up to 4 times greater than when no shear was observed (Sharples *et al.*, 2001; Palmer, Rippeth and Simpson, 2008; Rippeth *et al.*, 2009).

At present, it is difficult to effectively sample nitrate at the high resolution required to observe these key short-term mixing events (Sharples *et al.*, 2007; Charlotte Williams *et al.*, 2013). Combined with limited winter data, this can lead to incorrect seasonal estimates of NO_3^- fluxes that are key to primary production and carbon fixation. Chemical *in-situ* sensors can provide the high-resolution data necessary to resolve biogeochemical processes occurring in shelf seas (Prien, 2007; Adornato *et al.*, 2010). Wet-chemical analysers, centred on microfluidic Lab-on-Chip (LoC) technology, are at the leading edge of advancements for chemical *in-situ* nutrient measurements (Nightingale, Beaton and Mowlem, 2015). Due to their compactness, low resource use and analytical performance comparable to laboratory-based methods, LoC nutrient sensors are well suited to high-resolution float, glider and mooring deployments. Autonomous underwater vehicles, such as gliders, have already been shown to provide an economic and efficient observation platform to resolve mesoscale and submesoscale structures, allowing for high-resolution sampling of biogeochemical parameters, such as NO_3^- using an *in situ* ultraviolet spectrophotometer (Johnson *et al.,* 2009,2017; Rudnick, 2016).

Here we demonstrate the power of coupling the LoC nutrient sensor into a Seaglider to obtain continuous *in-situ* high temporal and spatial resolution nitrite + nitrate (NO_3^-+NO_2^- hereafter defined as $\sum NO_x$) measurements over the duration of the spring bloom in April 2015. This enabled short-term mixing events key to establishing the spring bloom and its subsequent decline to be observed.

3.2 Experimental

A single LoC $\sum NO_x$ sensor (Ocean Technology and Engineering Group, National Oceanography Centre, Southampton, UK) was integrated within the science bay of a Kongsberg Seaglider (Ogive fairing) and deployed from the *R.S.S Discovery* in the Celtic Sea, as part of the NERC funded Shelf Sea Biogeochemistry program in April 2015. In addition, a second LoC $\sum NO_x$ sensor was mounted on a Conductivity-Temperature-Depth (CTD; Seabird 911 plus) rosette to enable direct comparison of its measurements to concentrations of $\sum NO_x$ from seawater samples collected *in-situ* at the same depth and time in July 2015.

Both LoC deployments by Seaglider and discrete ship-based CTD rosette samples were collected from the Central Celtic Sea site (CCS; Figure 2.1) located ~137 miles off the Cornish coast, UK (49°24.134'N, 8°36.248'W), with a water column depth of ~ 145 meters. The Seaglider with integrated LoC $\sum NO_x$ sensor was deployed for 21 days (4th-25th April 2015) and completed 776 dives within 10 km of the CCS station. A total of 24 CTD casts within < 22 km of CCS were also conducted, allowing for comparison between discrete water samples and the LoC $\sum NO_x$ sensor. The rosette package consisted of a Seabird 911 plus CTD and 24 bottle Niskin system, which was used to collected discrete seawater samples. Chlorophyll *a (*hereafter Chl-*a*) was measured on a pre-calibrated (spinach extract, Sigma Aldrich) fluorometer (Turner Design Trilogy). Water samples collected from the Niskin bottles were analysed onboard for NO_3^-+NO_2^- using a segmented-flow autoanalyzer (Bran & Luebbe) following the colorimetric procedures of Woodward and Rees (2001).

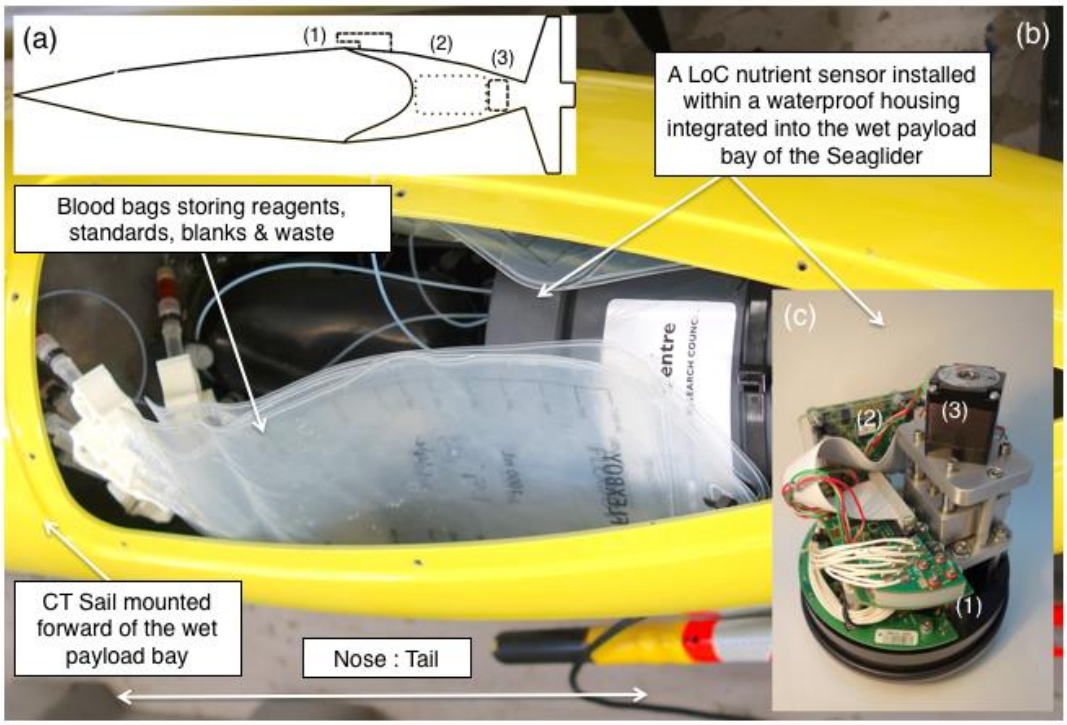

Figure 3.1: (a) Diagram of the locations of sensors deployed on the Seaglider (Kongsberg; Not to scale): (1) CT sail, (2) LoC, and (3) ECOPuck. (b) A LoC ∑NOx Sensor deployed with housing within the sensor payload bay of a Seaglider (Ogive Profile). (c) A LoC ∑NOx sensor consisting of (1) microfluidic chip, (2) custom electronics, and (3) syringe pump assembly.

The LoC $\sum NO_x$ sensor was integrated into the payload bay of the Seaglider (Figure 3.1b and connected by cable directly into one of the glider serial ports. The inlet tube with filter is located on the surface of the payload bay cover ~30 cm behind the CT sail (Seabird Electronics). The Seaglider software uses a CNF file that contains the configuration for each on-board instrument and a CMD file that provides mission parameters. The CNF file enables communication between the Seaglider and the LoC $\sum NO_x$ sensor. The LoC $\sum NO_x$ sensor is set to 'logger' in the CNF file, which enables the glider to send several commands. These commands allow the Seaglider to send and receive data to and from the sensor. Some of the key commands are 'clock-set', used only at the start of each dive but enables the sensor to store any time offset between glider and LoC $\sum NO_x$ sensor, 'status' which sends the sensor depth every 5 seconds along with 3 trigger values and 'download' sent at the end of each dive requesting the sensor to send both ascent and descent data files of processed $\sum NO_x$ values. During deployments the CMD file is typically transmitted to the Seaglider by satellite and includes three trigger values that can be passed to the LoC $\sum NO_x$ sensor using the 'status' command. These triggers are used to modify sensor behaviour at different depths. Primarily these are used to ensure the LoC $\sum NO_x$ sensor does not

take samples on the surface and risk the intake of air, and to aid with additional blank and standard measurements.

For deployments in the Seaglider, the LoC $\sum NO_x$ sensor was encased in a mineral oil-filled housing with an internally fitted pressure-compensating bladder, and along with the reagents, standard (6.5 µM NO_3^-), blank (ASW) and waste (all stored in blood bags), secured into the wet payload bay of the Seaglider. Power and communication between the LoC $\sum NO_x$ sensor and Seaglider was facilitated by a RS232 cable directly connected into one of the Seaglider's serial ports.

The LoC $\sum NO_x$ sensor's state machine was programmed to obtain a minimum of one blank (ASW) and one standard measurement (µM NO_3^-) at the beginning and end of each Seaglider dive. After the first measurements of blanks and standards, the LoC $\sum NO_x$ sensor undertook continuous measurements of seawater samples on both the descent and ascent. Continuous measurements of seawater samples were undertaken until the Seaglider informed that the LoC $\sum NO_x$ sensor was at a depth of 10 m. Seawater samples were drawn through a 0.45 µm MILLEX-HP filter unit (Millipore) into the sensor within the payload bay. Over the period of sampling (21 days), this resulted in 312 and 199 artificial seawater blanks and standards respectively, which was sufficient to determine both the $\sum NO_x$ concentration and any drift associated with either the artificial seawater blank and/or the NO_3^- standard.

The Seaglider is a buoyancy driven autonomous underwater vehicle, capable of multi-month deployments collecting high-resolution profiles of physical and biogeochemical parameters to 1000 m with a maximum travel range of 4,600 km (Rudnick *et al.*, 2004). Bilateral communication between the Seaglider and base station, through an Iridium satellite connection, allowed dive configurations to be modified once deployed. Data was transmitted back to shore during deployments to assess the performance of the LoC $\sum NO_x$ sensor. In addition to the LoC $\sum NO_x$ sensor within the science bay, the Seaglider measured conductivity & temperature (non-pumped Sea-Bird SBE13 CT Sail, Seabird Electronics), pressure (Pain Electronics) and fluorescence, turbidity and optical backscatter (Triplet ECOPuck, Wet Labs). Conductivity, temperature and pressure were collected at a frequency of 1 Hz during deployment with all dive profiles lying within 4 km of CCS (Figure 2.1c). Temperature and conductivity were extracted and processed using the UEA Glider Toolbox (Queste, 2013). These routines apply manufacturer calibrations correct for thermal inertia following the methods of Garau *et al.* (2011) remove spikes and anomalous data, and draw upon a flight model similar to that described by Frajka-Williams *et al*. (2011). Four CTD casts, taken within 1.6 km of the glider, were used to calibrate the temperature and salinity. Manufacturer calibrations were initially applied to data from the WetLabs Triplet for coloured dissolved organic matter (CDOM), backscatter and fluorescence by subtracting the

instrument blank and applying a scaling factor. Calibration to convert fluorescence to Chl-*a* is based on the sensor's response to a cultured diatom, *Thalassiosira weissflogii* at a known Chl-*a* concentration (Hemsley *et al.*, 2015; Sea-Bird Scientific, 2017).

3.3 Results and Discussion

3.3.1 Assessing the accuracy of LoC $\sum NO_x$ sensor using discrete water samples

The ability of the LoC $\sum NO_x$ sensor to accurately determine $\sum NO_x$ was assessed in two ways: (i) by comparison of the LoC $\sum NO_x$ sensor mounted on the stainless-steel rosette with discrete water samples collected using Niskin bottles at the same time and (ii) by comparing profiles obtained from the LoC $\sum NO_x$ sensor deployed within the glider with discrete water samples collected from the CTD on the same day at CCS. The LoC $\sum NO_x$ sensor, along with battery and reagents, was a similar size to the 20L Niskin bottle and was mounted in place of a single Niskin bottle on the frame. Once below 5 meters, a pressure sensor on the battery activated the power to the LoC $\sum NO_x$ sensor. The CTD rosette was held at three depths (45, 50 & 90 meters) for at least 90 minutes to allow for triplicate LoC $\sum NO_x$ sensor measurements at the prescribed depth, each bracketed by a blank and standard measurement. During this time period, two Niskin bottles were fired, one within 5 minutes of the first LoC $\sum NO_x$ sensor measurement and the second within 5 minutes of the last LoC $\sum NO_x$ sensor measurement. Water was collected from these discrete bottle firings for determination of NO_3^-+NO_2^- concentrations using the segmented flow autoanalyzer in the ship-based laboratory. Figure 3.2a indicates the excellent agreement between sensor measurements and analysis of discrete water samples with a correlation of r^2 = >0.99 (n = 9; p = <0.001). The estimated analytical uncertainty of the LoC $\sum NO_x$ sensor was calculated from two times the standard deviation of the absorbance value of the deployed standard over the three deployments and was 0.14 µM (n = 10). This analytical uncertainty is higher than reported values for traditional segmented flow autoanalyzer analysis of $\sum NO_x$ (0.03-0.07 µM; Dafner, 2015) but lower than previous LoC $\sum NO_x$ deployments (0.4-1 µM; Yücel *et al.*, 2015).

LoC $\sum NO_x$ data, collected from within the glider, was compared with NO_3^- + NO_2^- values from 24 CTD profiles collected at CCS throughout the 21-day deployment. Unlike the previous assessment of analytical uncertainty, data from the CTD profiles were not collected at the same time (1 – 10 hr window) or depth range (±3 meters) and all samples were collected in a dynamic shelf sea system. Figure 3.2b, however, shows the excellent agreement the LOC $\sum NO_x$ data and the discrete water sample measurements over the 21-day period, with a correlation of r^2 = >0.98 (n = 51; p = <0.001). The average

estimated analytical uncertainty for the LoC $\sum NO_x$ sensor during this period was 0.19 µM (n = 142) similar to the 0.14 µM (n = 10) for the CTD NO_3^- profiles.l

Initial Seaglider dives (4th to 9th of April) were configured in a standard flight mode, whereby the Seaglider adjusts its pitch and buoyancy to maintain a uniform glide slope and decent and ascent speed (Eriksen *et al.*, 2001). The LoC $\sum NO_x$ sensor was switched on at the beginning of each dive and completed a blank and standard measurement followed by continuous measurements. The LoC $\sum NO_x$ sensor acquired depth information directly from the Seaglider, and using a depth trigger at 10 meters, the sensor recognized the Seaglider was diving and after completing its current blank or standard measurement would undertake continuous sample measurements. Triggers were also used to take advantage of extra time at the beginning, apogee and end of dives to undertake extra blank and standard measurements.

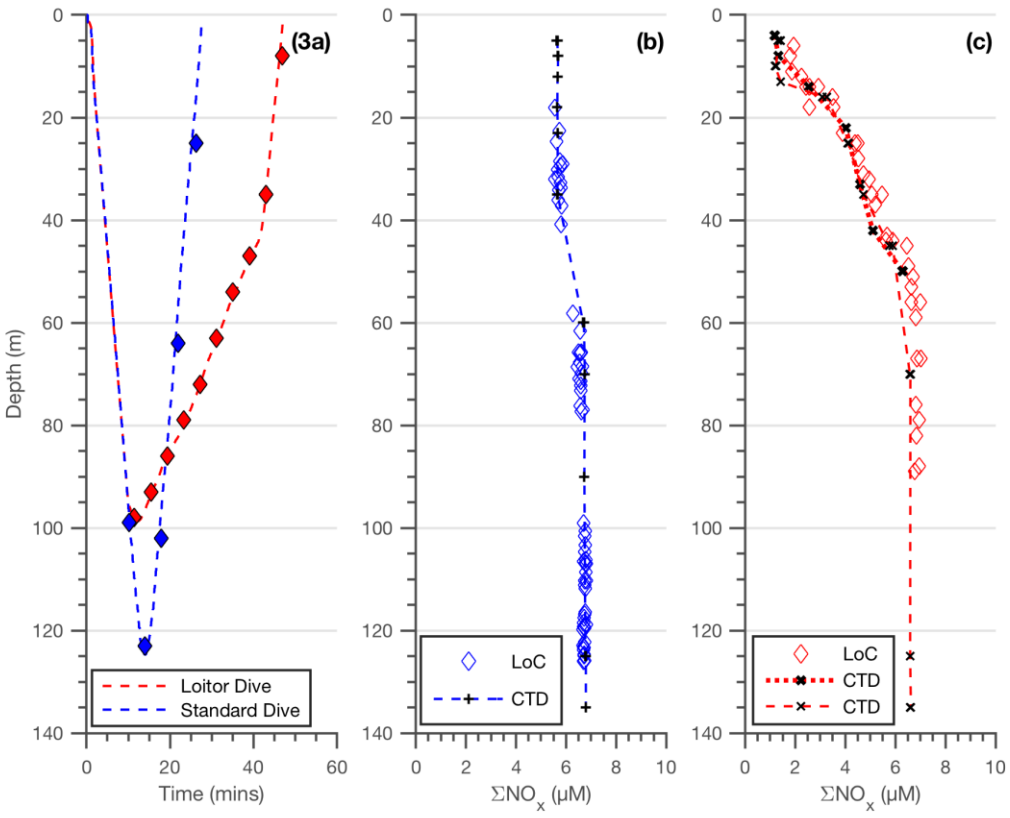

Figure : (a) Comparison of the two different dives used in this study. Blue and red diamonds indicate where ∑NOx measurements were obtained. (b) ∑NOx measurements from one CTD cast (02:06 am; dashed line) and sixteen standard dives (00:18 to 09:25 am; diamonds) from the 6th April 2015. (c) ∑NOx measurements from two CTD cast (02:06 and 08:22 am; dashed lines) and seven 'loiter' dives (11:19 am to 16:25 pm; diamonds) from the 16th April 2015.

Figure 3.3 (a) shows that when the Seaglider was operated in the standard dive mode, the LoC $\sum NO_x$ sensor carried out 5 sample measurements per 120 m dive with a total dive time of 30 ± 8 minutes. Moreover, these measurements were always in the same depth ranges within the water column due to the relatively shallow water column (~145 meters) and sensor operation timings. Figure 3.3b) shows the excellent agreement between the LoC $\sum NO_x$ sensor and traditional CTD segmented flow autoanalyzer measurements, for one single CTD cast at 02:06 am and sixteen dives by the Seaglider from 00:18 to 09:25 am on the 6th of April 2015. However, the temporal and spatial resolution of $\sum NO_x$ data (over the period of the day within the surface layer and across boundaries such as the nitracline) would not be sufficient to investigate the depletion of $\sum NO_x$ as the spring bloom develops. As the glider can be controlled remotely to increase the distribution of measurements by the LoC $\sum NO_x$ sensor throughout the water column, in particular across the nitracline, a second dive methodology - termed a 'loiter' dive - was employed. After the Seaglider

has reached its maximum depth for that particular dive and started its ascent, for 30 mins the ascent angle was lowered and the glider 'loitered', thus increasing the resolution of measurements within the water column (Figure 3.3a). Selected maximum target depths (90, 60, 40 and 25 meters) were used to control the maximum dive depth and ensured a higher number of measurements in areas of interest (Figure 3.3c). Loiter dives to 90 meters doubled the amount of measurements made compared to the previous standard dives. Figure 3.3c shows a comparison between $\sum NO_x$ concentrations from two CTD casts at 02:06 and 08:22 am and LoC $\sum NO_x$ concentrations from seven 'loiter' dives from 11:19 am to 16:25 pm on the 15th of April 2015. Once more, good agreement between the LoC $\sum NO_x$ sensor and traditional segmented flow autoanalyzer measurements of CTD discrete samples was observed throughout the whole water column during this 14-hour period. To ascertain the ability of the LoC $\sum NO_x$ sensor to make comparable measurements to the segmented flow autoanalyzer, over an extended time period (4^{th} to 25^{th} April, 2015), we compared the measurements within the bottom layer at 60 -120 m where little changes in $\sum NO_x$ were observed. Excellent agreement between both the segmented flow autoanalyzer (6.86 ± 0.09 µM; n = 22) and LoC $\sum NO_x$ sensor (6.86 ± 0.16 µM; n = 120) was observed. We have demonstrated the $\sum NO_x$ concentrations measured from the LoC $\sum NO_x$ sensor are comparable to those of the shipboard measurements analysed on a segment flow autoanalyzer. Moreover, this shows that accurate measurements can be obtained from the LoC $\sum NO_x$ wet chemical sensor over 21 days in a dynamic shelf environment.

On-board calibration with artificial seawater blanks and NO_3^- standard for each dive enables both the monitoring of instrument performance and stability over long-term deployments. To ensure maximum efficiency of the cadmium column, where NO_3^- is reduced to NO_2, a flow rate of 150 µl/min was chosen (Beaton *et al.*, 2012). However, it is important to monitor any drift in the efficiency of the cadmium column over time as this may impact on the $\sum NO_x$ concentrations. In this study, a decrease in absorbance values was observed, likely due to the gradual reduction in efficiency of the cadmium column over time. As sample concentrations are calculated from their associated blank and standard measurements, where the ratio of the absorbance of the sample and standard are determined, any drift caused by the decreasing reduction efficiency of the cadmium column is compensated for. Our results demonstrate that any decrease in absorbance values observed did not impact on the accurate determination of $\sum NO_x$ from the LoC as shown by the excellent agreement with traditional autoanalyzer $\sum NO_x$ method from discrete water samples collected throughout the 21-day deployment.

3.3.2 Biogeochemical cycling of Nitrate during the Spring bloom in the Celtic Sea

The data set presented here was collected during the spring phytoplankton bloom, a period during which integrated net productivity becomes greater than integrated losses and phytoplankton biomass accumulates in surface waters (Sverdrup, 1952). Over the 21-day deployment the LoC ΣNOx sensor was able to accurately capture the large drawdown of ΣNOx within the surface layer due to the onset of the spring bloom (Figure 3.4). Concentrations decreased from 5.74 µM (4th) to 1.42 µM (25th), whilst bottom layer NO_3^- concentrations remained constant (6.86 ±0.16 µM), as observed in previous studies within the Celtic Sea (Tweedle, 2007; Williams, 2013).

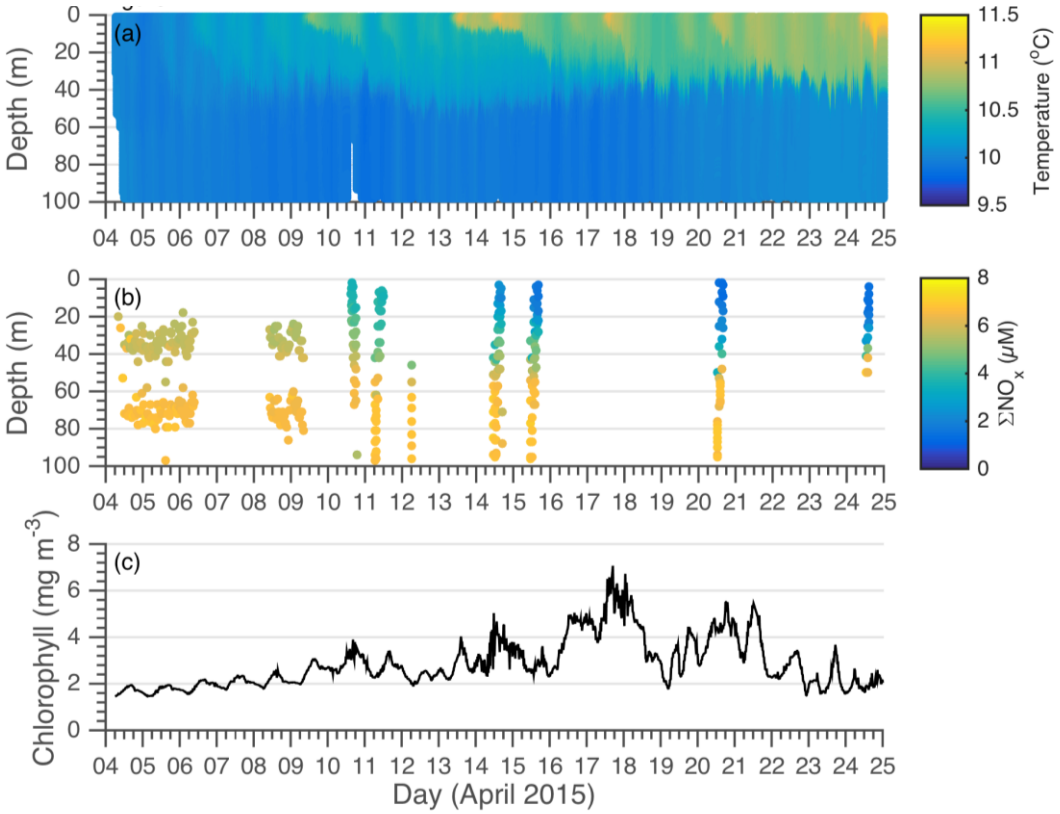

Figure 3.4: (a) temperature (˚C), (b) LoC ∑NO_x (µM) and (c) mean surface (< 20 m) Chlorophyll-a measurements obtained from one Seaglider deployment from the 4th to 25th April 2015.

At the start of the deployment (4th–6th April 2015), a small 0.8 µM difference between near surface (20-40 m) and bottom water (60-80m) ∑NO_x concentrations was observed. During this time, surface Chl-*a* concentrations were relatively low (1.8 mg m^{-3}) but much higher (by 1.5 mg m^{-3}) than those typically observed during the winter in the area (Pingree *et al.*, 1976; Smyth *et al.*, 2010). This suggests that some phytoplankton growth had already occurred prior to deployment of the glider.

Between the 4th and 6th April, the $\sum NO_x$ concentration between 20-40 m remained constant. Any changes in the near surface (<20 m) water, however, where you might expect the largest draw down in NO_3^-, were not resolved since the standard dive pattern used during this early period did not result in near surface LoC $\sum NO_x$ measurements being made. Nevertheless, it is clear from Figure 3.4 that a large drawdown of 3 µM $\sum NO_x$ occurred between the 4th and 11th of April 2015 (<40 m) as stratification of the water column initialized. This corresponds to the observed increase in surface water Chl-*a,* from 1.8 mg m^{-3} to 3.7 mg m^{-3}, indicative of phytoplankton growth, and thus nutrient drawdown, during the onset of the spring bloom. Changing the dive configuration to 'loiter' dives on the 11th of April increased the resolution of ∑NOx surface data.

Just as the temperature sensor resolves the gradual deepening and warming of the surface mixed layer, the LoC ∑NOx sensor resolves the coincident deepening of the nitracline and draw down of ∑NOx above it. Between the 4th and 25th April surface waters warmed by >1°C and a 40 m deep thermocline is established. During this time there is a 4.2 µM drawdown of ∑NOx and an increase in Chl-a from a background of 1.8 mg m^{-3} to 4-6.8 mg m^{-3}.

By the end of the Seaglider deployment (25th), a two-layer water column had developed with a warm, nutrient depleted, 40 m surface layer overlying colder, nutrient-rich bottom waters. Previous studies suggest that phytoplankton growth starts to become $\sum NO_x$ limited when concentrations fall below 1 µM (Eppley, Rogers and Mccarthy, 1969). The low surface water $\sum NO_x$ concentrations (1.4 µM) measured during the end of the deployment suggest that this was close to happening. This is supported by a coinciding decrease in Chl-*a* (to <2 mg m^{-3}) towards the end of the deployment. Ship-based observations show that it was not until the 28th that surface water concentrations were below the limit of detection of 0.1 µM (Birchill *et al.*, 2017).

3.3.3 Future use of a LoC $\sum NO_x$ sensor on long term AUV deployments

This study has demonstrated for the first time that it is possible to accurately measure $\sum NO_x$ over long-term deployments using a wet chemical nutrient sensor deployed within a glider. Our study provides a novel methodology of differing operational characteristics to current high-resolution capable methodology (Johnson *et al.*, 2013), enabling an increase in observations of $\sum NO_x$ dynamics in temperate shelf seas during key transitional events (e.g. the onset of stratification and the spring bloom, convective overturning and the autumn bloom) and across fine-scale vertical and horizontal features (e.g. tidal mixing fronts, sub-surface chlorophyll maximum). At present, wet chemical biogeochemical sensors do not have the vertical resolution capabilities of the commonly used physical and optical sensors such as temperature, fluorescence

or established ultraviolet spectrophotometer nitrate sensors (Johnson and Coletti, 2002). This resolution could be further improved by decreasing the time taken between measurements. By increasing flow rate, decreasing colour development time, decreasing the number of flushes and increasing N.E.D (naphthylethylenediamine dihydrochloride) concentration and reaction temperature, an increased measurement resolution could be achieved, but at the expense of measurement sensitivity (Pai, Yang and P. Riley, 1990; Beaton *et al.*, 2012).

For long-term deployment of wet chemical sensors, reduced resource consumption (power and reagents) and compact size are the main advantages of microfluidic systems. Deployment of sensors on moorings, where solar and wind power are available, negates power constraints. However, for autonomous underwater vehicles power becomes the greatest limiting resource (Dickey *et al.*, 2008). During the 21-day deployment, the LoC $\sum NO_x$ sensor (version 3.2) had a low power consumption of 1.5 W. This was only marginally higher than the other standard sensor packages on the Seaglider (0.9 W and 0.25 W for the WetLabs ECO Triplet and SBE pumped payload CTD respectively), but lower than other wet chemical and UV absorption systems (e.g. ISUS V3, Satlantic, USA; NitraVis, YSI, USA; SubChemPak, SubChem Systems, USA). A single dive of the LoC $\sum NO_x$ sensor consumed 2.5 mL of Griess reagent, 2.5 mL of buffer solution and 0.21 mL of standard and blank solution, achieving 1 blank and standard measurement and ~ 10 samples on a dive to 120 meters. This would enable a total of 400 dives to be made and 4000 sample measurements. During this study, the LoC was only active during periods when the *R.S.S Discovery* was also sampling at CCS to enable a direct comparison between the two types of measurements over a long-term deployment of the LoC. This resulted in accurate LoC $\sum NO_x$ determined over 21 days. With a sampling strategy focused on achieving the maximum amount of measurements, a profile consisting of 10 sample measurements could be undertaken every ~ 40 minutes, allowing for increased observations of episodic and transient events unable to be observed by discrete sampling.

3.4 Conclusions

The temporal and spatial variability of biogeochemical processes has been successfully measured through the use of remote sensing, time series moorings and ship-based methods, but these, to an extent, fall short in resolving the dynamic temporal and spatial elements with long-term endurance in a low-cost package. From this, there has been a strong call for the development of biogeochemical sensors to be deployed on stationary and mobile platforms, to provide *in situ* measurements as part of sensor networks aimed at providing long term monitoring within a low cost package (Johnson *et al.*, 2009; Adornato *et al.*, 2010). The LoC $\sum NO_x$ sensor deployed within the Seaglider in this study clearly demonstrates that nitrate & nitrite can be accurately determined over monthly timescales due to the sensor's low resource use, small size and *in situ* calibration abilities. Moreover, deployed within a glider with other physical and biochemical data (e.g. CTD and the WetLabs Triplet sensor measurements), it provided a powerful tool for resolving dynamic biogeochemical processes within a dynamic shelf system.

Chapter 4: Measuring vertical $\sum NO_x$ fluxes using a Lab-on-Chip nutrient sensor and Microstructure profiler

This research within this chapter will be submitted to *Geophysical Research Letters.*

4.1 Introduction

Shelf seas are globally key transition regions between terrestrial, atmospheric and oceanic environments that play a vital role in global carbon, macronutrient cycling and fisheries (Gattuso, Frankignoulle and Wollast, 1998; Pauly *et al.,* 2002). This is due to the significant levels of new production from shelf seas (~3.7 Pg C y^{-1}; Liu *et al.,* 2000; Jahnke, 2010), estimated to be responsible for 10-20% of ocean carbon sequestration (Muller-Karger, 2005). Moreover, shelf seas have been identified as net sinks of atmospheric CO_2 (Frankignoulle and Borges, 2001; Borges, Delille and Frankignoulle, 2005; Chen and Borges, 2009). Despite their relatively small size, temperate and high latitude shelf seas have a significant impact on the air-sea carbon flux and the storage and export of carbon to the seafloor and deep ocean (Tsunogai *et al.*, 1999; Thomas *et al.*, 2004; Jahnke, 2010).

Temperate shelf seas are dynamic environments with well-defined seasonal cycles and in primary production with a spring and autumn bloom and summer sub-surface chlorophyll maximum (SCM; Sverdrup, 1952; Pingree *et al.*, 1976; Simpson and Sharples, 2012). The onset of stratification in spring confines phytoplankton to within the euphotic zone, resulting in a rapid increase in biomass, known as the spring bloom, which causes a subsequent large drawdown of nitrate (Pingree *et al.*, 1976; Fasham, Holligan and Pugh, 1983). The seasonal pycnocline inhibits the vertical diapycnal transfer of nitrate into the euphotic zone, and phytoplankton are then limited to regenerated sources of bio-available nitrogen (e.g. ammonium) or external sources of 'new' nitrate introduced from outside the local system (e.g. atmospheric deposition and riverine inputs; Dugdale and Goering, 1967). The spring bloom is a key annual production event that is estimated to produce around ~50% of annual new production (Richardson *et al.,* 2000; Hickman *et al.*, 2007). Studues, have observed that rates of new production SCMthat into the base of the pycnolice) are eqivilent to 10 to 19 g C m^{-2} over the whole summer period (~ 120 days) are comparable (Sharples, 2008; Hickman *et al.*, 2012), and could even surpass spring bloom new primary production values (Richardson *et al.,* 2000; Weston *et al.*, 2018)seasonally.

During summer, new production in the Celtic shelf sea occurs at the tidal mixing fronts (Holligan *et al.*, 1984; Horne *et al.*, 1996), the shelf edge, due to vertical transport of nutrient rich water by internal tides (Joint *et al.*, 2001; Sharples and Moore, 2009), and within the sub-surface chlorophyll-*a* maximum across the shelf, due to diapycnal fluxes (Richardson *et al.,* 2000; Sharples *et al.,* 2001). Within the SCM and the surface mixed layer (SML), nitrate is depleted and therefore new production is controlled by the flux of nitrate from the bottom mixed layer (BML) through the pycnocline into availablethe SCM (Sharples *et al.,* 2001). Bottom boundary layer generated

turbulence, arising from barotropic tidal current interactions with the sea floor, powers the mixing of nitrate into the base of the pycnocline and SCM

To fully capture and understand the variability in nitrate fluxes and their effects on phytoplankton biomass dynamics, an increase in observational resolution and endurance is required. The background diapycnal $\sum NO_x$ fluxes for the Celtic shelf sea has been estimated at 1-2 mM m^{-2} day^{-1} (Sharples *et al.,* 2001; Tweddle, 2007; Hickman *et al.,* 2009; Rippeth *et al.,* 2009; Hickman *et al.,* 2012; Williams *et al.,* 2013). These studies also highlighted that short-term mixing events, caused by one or a combination of spring tides and internal waves (Sharples *et al.,* 2001, 2007), lee waves breaking over a bank (Tweedle *et al.,* 2013) and wind events (i.e. storms; Williams *et al.,* 2013), can produce significant additions to this background flux (3 to 17 times greater). Significant increases in diapycnal $\sum NO_x$ fluxes brought about by these episodic events could increase average seasonal estimates of new production, and thus rates of carbon fixation in temperate shelf seas. Also, spatial variation from synoptic observations (from satellite remote sensing platforms) have shown how productivity and chlorophyll-*a* (hereafter Chl-*a*) in surface waters are highly dynamic (Jonnson, Salisbury and Mahadevan, 2011). Variations in phytoplankton biomass and productivity, along with nutrient fluxes and availability, can range temporally from days to weeks and spatially on vertical scales of 1 to > 10 meters and horizontally on sub-mesoscale to mesoscale (Cullen, 2015).

Autonomous underwater gliders have proven themselves as key platforms for conducting complimentary biogeochemical and physical measurements allowing for new observations that highlight environmental variability (Johnson *et al.*, 2007; Testor *et al.*, 2010; Meyer, 2016; Rudnick, 2016). Short-term glider deployments allow for observations of rapid (hourly to days) transient events such as diel vertical migration and the effect of a storm on ocean surface layer dynamics and primary production (e.g. Baumgartner and Fratantoni, 2008; Rumyantseva *et al.*, 2015). Long-term glider deployments have been deployed to observe the seasonal cycle of primary production in the Atlantic and sub-Antarctic oceans (e.g. Thomalla *et al.*, 2011; Swart, Thomalla and Monteiro, 2015). Such deployments increase the spatial scales of observations in both the vertical and horizontal directions capturing ≤ 5 meter thick sub-surface Chl-*a* maximum (Hodges and Fratantoni, 2009) and ~15 kilometre wide eddies (Frajka-Williams *et al.,* 2009).

Here we combine high-resolution observations from gliders deployed with a microstructure profiler and a miniaturized Lab-on-Chip nutrient sensor to interrogate the physical processes driving the vertical fluxes of nitrate in much more detail than has previously been possible. Whilst previous studies that have relied on a limited dataset to estimate the vertical fluxes of nitrate (e.g.

Sharples *et al.,* 2007), we present *in situ*, sub-hourly profiles of turbulent dissipation and nitrate over 18 days during the summer SCM at central site in the Celtic sea.

4.2 Experimental

Physical and biogeochemical measurements were collected as part of the Shelf Sea Biogeochemistry project on a cruise from the 13th to 30th of July 2015 (DY033) at the Central Celtic Sea site (CCS; Figure 2.1). Two different glider setups were deployed, the first (hereafter defined as LoC glider), being a Seaglider (Kongsberg; Ogive fairing) with a Lab-on-Chip nutrient sensor (Ocean and technology and Engineering Group, National Oceanography Centre, Southampton) measuring nitrate + nitrite (hereafter defined as $\sum NO_x$). The second glider (hereafter defined as OMG glider), was a Slocum glider (Teledyne Webb research) with a Microrider microstructure package (Rockland Scientific International). Further details regarding the setup and deployment have been previously described in Palmer *et al.* (2015) and Vincent *et al.* (2018) and in Chapters 2 and 3 of this thesis. The OMG Glider was deployed from the 14th to 31st July 2015 and produced 1226 profiles of vertical turbulent kinetic energy, temperature and conductivity. The LoC Glider was deployed from the 13th and 30th of July 2015, and produced 1128 profiles of temperature, conductivity, Chl-*a* and 78 profiles consisting of 841 $\sum NO_x$ measurements.

4.2.1 Wind and Tide

Meteorological and tidal data was collected at CCS from a Met Office Ocean Data Acquisition System (ODAS) Buoy and Acoustic Doppler Current Profiler (ADCP) mounted on a frame on the seabed. The ODAS buoy provided hourly averages of wind speed (m^{-2}; including maximum gust speeds) and direction (degrees from north) 3 meters above sea level (Hopkins, *pers. comm*.). Neutral wind stress was calculated following Large and Pond (1981):

$$\tau = \mathrm{P}_a(C_d u10^2) \quad (4.1)$$

where P_a is the density of air (kg m^{-3}), C_d is the neutral drag coefficient at 10 meters, and $u10$ is the wind speed at 10 meters (m s^{-1}).

The upward facing ADCP (RDI 600 kHz workhorse) measured current magnitude (m^{-s} s^{-1}) and direction (degrees from north) at a vertical resolution of 2 meters every 2.5 minutes (Wihsgott, *pers. comm*.).

4.2.2 $\sum NO_x$, water column structure & Chlorophyll-*a*

A rosette package, consisting of a CTD (Seabird 911+) and Niskin bottle system, was used to collect discrete seawater samples following the GO-SHIP sampling and handling procedures (Hydes *et al.*, 2010). Samples for Chl-*a* were measured daily on a pre-calibrated (spinach extract, Sigma Aldrich) fluorometer (Turner Design Trilogy; Holm-Hansen *et al.,* 1965). $\sum NO_x$ was analysed on-board using a segmented-flow autoanalyzer (Bran & Luebbe) following the colorimetric procedures of Woodward and Rees (2001) and Brewer & Riley (1965).

The Lab-on-Chip nutrient sensor (hereafter defined as LoC $\sum NO_x$ sensor) was deployed in the science bay of the LoC glider and uses colorimetric detection, using the Griess assay (Grasshoff, Kremling and Ehrhardt, 1999), where NO_3^- is reduced to NO_2^- using an off-chip copper-activated cadmium column to enable $\sum NO_x$ to be determined. Reagents (Griess, Imidazole buffer), NO_3^- standard and artificial seawater blank solutions were stored in Flexboy bags (Sartorius, UK) and waste was collected into a 500 ml Flexboy bag within the science bay of the glider. A 6 µM NO_3^- standard was deployed for the cruise. A detection limit of 20 nM and linear range of up to 350 µM have been demonstrated in laboratory settings for the LoC $\sum NO_x$ sensor (Beaton *et al.,* 2012). Previous deployments of the LoC $\sum NO_x$ sensor have produced estimates of uncertainty between 0.14 – 1 µM (Yücel *et al.*, 2015; Beaton *et al.*, 2017b; Vincent *et al.*, 2018). During each glider dive, a minimum of one standard and one blank measurement was made. Cross validations were made against traditional ship-based autoanalyzer nutrient analyses undertaken at CCS within a spatial and temporal period of < 2 km and within 24 hrs (Vincent *et al.,* 2018). Detailed descriptions of the LoC $\sum NO_x$ sensor and the first deployment within a glider can be found in Beaton *et al.* (2011; 2012) and Vincent *et al.* (2018) respectively, and in Chapters 2 and 3 of this thesis.

The LoC glider sensor payload consisted of conductivity & temperature (un-pumped Sea-Bird SBE13 CT Sail, Seabird Electronics), pressure (Pain Electronics) and fluorescence and particulate optical backscatter (Triplet ECOPuck, WetLabs). Conductivity, temperature and pressure were collected at a frequency of 1 Hz and were initially checked for bounds, spikes and anomalies. Manufacturer-supplied coefficients were used for calibration, with further corrections to account for thermal lag caused by the thermal inertia of the conductivity cell (Lueck and Picklo, 1990; Garau *et al.,* 2011). Temperature and salinity, thus density, derived from the glider was calibrated against the ship-based CTD values taken from calibrated CTD casts (calibrated against discrete samples) < 2 km away from the gliders location. Comparison of values between 80 to 105 meters resulted in the adjustment of gliders values by -0.1126^{o}C and -0.0249 PSU for the July deployment. From these corrections density measurements were recalculated. Manufacturer calibrations were initially applied to data from the WetLabs Triplet for fluorescence by subtracting

the instrument blank and applying a scaling factor. Calibration to convert fluorescence to Chl-*a* is based on the sensor's response to a cultured diatom, *Thalassiosira weissflogii,* at a known Chl-*a* concentration (WetLabs, 2017).

4.2.3 Turbulence

The mixed layer depths within the water column were identified by applying a threshold method (Kara *et al.,* 2000). This uses a change in density (kg m^{-3}) from a reference depth to locate the mixed layer boundaries. This allowed the location of the base of the surface mixed layer (SML) and the top of the bottom mixed layer (BML) to be identified. An increase or decrease of 0.01 kg m^{-3} and 0.02 kg m^{-3} from a surface (15 m) or deep-water (80 m) reference value was used to identify the SML and BML (Hopkins, *pers. comm*.).

Profiles of vertical eddy diffusivity, temperature and conductivity collected by the OMG Glider enabled the investigation in the influence turbulent mixing had on diapycnal nutrient fluxes within and into the base of the pycnocline. Measurements were made from the surface to within 10 m of the seabed, with the upper 10 m being disregarded due to the presence of the ship's wake (Palmer, *pers. comm*.). For full details of the deployment of the microstructure package on a glider, and detailed post-processing, see Palmer *et al.* (2015).

Profiles of vertical eddy diffusivity, K_z (m^2 s^{-1}), were calculated using the diffusivity method (Osborn, 1980) from profiles of the rate of dissipation of turbulent kinetic energy, ε (m^2 s^{-3}), and the buoyancy frequency, N^2 (s^{-1}), via:

$$K_z = \Gamma \frac{\varepsilon}{N^2} \quad (4.2)$$

where Γ represents the constant mixing efficiency, which is regarded to be 0.2 (Osborn, 1980)debate.

The vertical variability of microstructure shear was used to estimate the dissipation of turbulent kinetic energy, ε, which can be estimated directly from the Microrider microstructure package (Yamazaki and Osborn, 1990), via:

$$\varepsilon = \frac{15}{2} \nu \overline{\left(\frac{\partial u'}{\partial z}\right)^2} \quad (4.3)$$

where ν is the kinematic viscosity of seawater (m^2 s^{-3}), *u'* is the fluctuation in turbulent velocity (m s^{-1}), and the overbar denotes a spatial average.

The buoyancy frequency, N^2, was calculated from temperature and conductivity measurements collected by the Microrider microstructure package, and is dependent on vertical structure of density (Gill, 1982):

$$N^2 = -\frac{g}{\rho}\left(\frac{\partial \rho}{\partial z}\right) \quad (4.4)$$

where g is gravity (9.81 m s^{-2}) and ρ is density (kg m^{-3}).

4.2.4 Calculating the ∑NOx flux

The instantaneous flux of $\sum NO_x$ (hereafter defined as $f\sum NO_x$; mM m^{-2} s^{-1}) into the base of the pycnocline was calculated based on the method of Sharples *et al.* (2007):

$$fNO_x = -K_z\left(\frac{\delta NO_x}{\delta z}\right) \quad (4.5)$$

where $\delta NO_x/\delta z$ is the vertical $\sum NO_x$ gradient (mM m^{-4}) from the LoC $\sum NO_x$ sensor and K_z is calculated from equation 4.2.

Both gliders were able to accurately collect high resolution profiles of density, along with the OMG glider measuring turbulent diffusivity and the LoC glider measuring $\sum NO_x$. The high-resolution profiles of $\sum NO_x$ and density collected by the LoC glider, combined with the complimentary CTD-derived data, allowed for sufficient data to generate a linear $\sum NO_x$:density regression for the whole deployment at CCS within the SCM. This allowed for 1) an increase in the vertical resolution of $\sum NO_x$ measurements compared to CTD based methods, and 2) the $\sum NO_x$ gradient can be applied to the turbulent diffusivity and density measurements taken from the same instrument in the same space and time. Both the LoC and OMG gliders were on average ~ 5 km apart and the $\sum NO_x$:density relationship measured by the LoC glider was applied to the OMG density profiles to calculate the $\sum NO_x$ gradient needed in equation 4.5.

Combining a strong linear $\sum NO_x$:density relationship, to profiles of density and dissipation of turbulent kinetic energy conducted on the same instrument allows the estimation of $f\sum NO_x$ into the base of the pycnocline to be simplified by combining equations 4.2, 4.3 and 4.4 to:

$$f\sum NO_x = m\frac{\Gamma \varepsilon p}{g} \quad (4.6)$$

where m (mmol m^{-3} (kg m^{-3})$^{-1}$) is the slope of the linear ∑NOx:density relationship (Figure 4.1).

$f\sum NO_x$ was calculated at a band 1m above and below the base of the pycnocline which coincided with the base of the SCM (Figure 4.2). A small band of 1m above and below the

pycnocline was used to estimate $f\sum NO_x$, as averaging ε over a broader band entrains a considerable amount of BML turbulence and selecting a band that include bins beyond the BML is contentious for describing the flux of nutrients (or other variable) from the BML into the base of the pycnocline, since that mixing acts at the first point of stratification (Palmer, *pers. comm*.) and in addition the nitrate can be taken up by phytoplankton very quickly (Raymont, 1980).

Turbulence throughout the water column was highly variable, both temporally and spatially, over the course of the deployment (see section 4.2.7), and therefore hourly average profiles of ε were used to calculate $f\sum NO_x$. To calculate the average hourly and daily instantaneous $f\sum NO_x$ values into the base of the pycnocline a Gaussian 'bootstrap' resampling method (Efron and Gong,

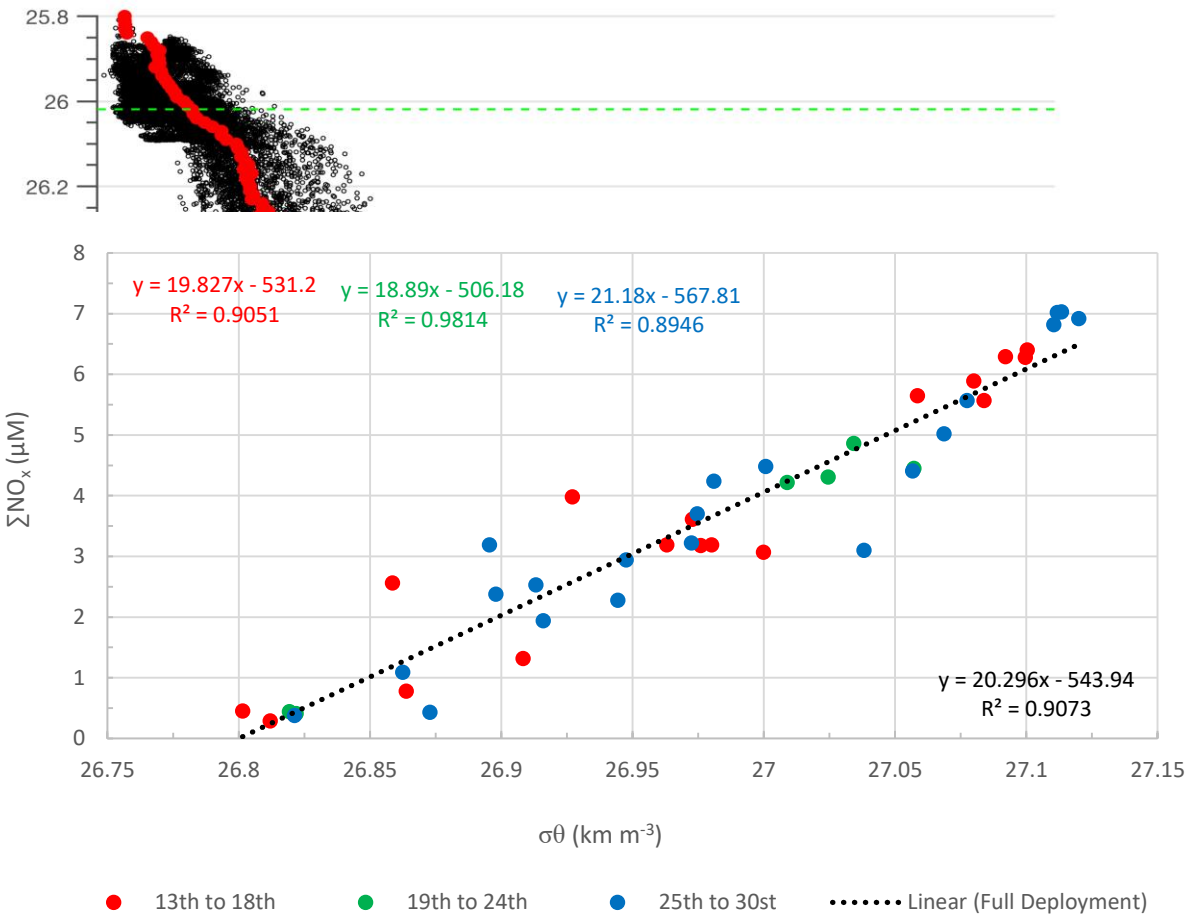

F

marking the range *f*∑NO_x was calculated from. ∑NO_x measurements used to form the ∑NO_x:density relationship were taken between the BML (lower dashed blue line) and all the top of the SCM (blue dotted line). of

the pycnocline via equation 4..

1983) with 95% confidence intervals was used from profiles of f∑NO_x and ε every ~40 minutes (Sharples *et al.*, 2007).

4.3 Results

4.3.1 Water column structure/characteristics

Water column structure was controlled by the variability in temperature rather than salinity, with a gradient between the SML and BML of ~0.1 PSU observed (data not shown). At the CCS sampling station, during July the water column consisted of two mixed layers separated by a well-defined pycnocline with variable temporal characteristics brought about due to the deepening and shoaling of the SML, as seen in the temperature data (Figure 4.3a). Average BML and SML temperatures were 10.2 ± 0.06°C and 16.3 ± 0.23°C, respectively. The temperature in the SML peaked at 17.1°C (2nd of July) during a period of increased surface temperature (19th to 23rd) temporarily causing the SML to become stratified before becoming homogeneous (24th). The thickness of the pycnocline remained broad (maximum of 46.6 m, minimum 20 m) during the first 10 days (14th-23rd July) of the deployment, with an average thickness of 31.4 ± 15.9 m, before narrowing in the final days (20.0 ± 5.0 m; Figure 4.3a). The top of the BML was at an average depth of 53.2 ± 2.9 m in a water column of ≈140 meters, and did not show variability during spring and neap tidal cycles but a clear semi-diurnal tidal signal observed with a regular amplitude of ~13 meters (Figure 4.5a). The strength of the stratification at the base of the pycnocline, characterised by N^2, was stable and had increased from the onset of stratification in Spring by 3.9 x 10^{-5} to 2.5 x 10^{-4} (data not shown). This highlights the potential of the strong seasonal stratification separating the SML and BML to limit the replenishment of nutrients to the SML.

The vertical profiles for Chl-*a* for July 2015 showed the defined structure of a sub-surface Chl-*a* maximum located near the base of the pycnocline at 52 ± 4 m (average density value of ~1027.9 kg m^{-3}; Figure 4.3b). Chl-*a* concentrations within the SML and BML were < 0.5 Chl-a mg m^{-3}. Depth integrated Chl-*a* concentrations within the pycnocline ranged from 20 to 50 mg m^{-2}, with an average concentration of 2.4 ± 0.9 mg m^{-3} and a maximum peak of 4.1 mg m^{-3}. At the base of the pycnocline, pulses (> 1 mg m^{-3}) of increased Chl-*a* were observed between the 20th to 23rd and from the 27th to the 30th which was the end of the deployment, indicating and increase in phytoplankton biomass (Figure 4.3b). Flow Cytometry data (data not shown) show an increase in heterotrophic bacteria and nanoplankton abundance (Mayers *et al.*, 2018). Photoinhibition was observed within the euphotic zone and assumed to have negligible effect on the SCM as shown by the decrease in surface Chl-*a* concentrations at midday, the average difference in Chl-*a* concentrations was 0.23 mg m^{-3} between midnight and midday.

$\sum NO_x$ concentrations were observed to be below the limit of detection (< 0.02 µM) within the SML (Figure 4.3c) while in the BML concentrations were 8.0 ± 0.2 µM and showed little

variation over the time of deployment similar to values reported from other studies (Hydes *et al.*, 2004). The distribution of $\sum NO_x$ suggests no significant external inputs from horizontal advection over the duration of the deployment or any sedimentary inputs. Mean $\sum NO_x$ concentrations within the pycnocline were 3.46 ± 1.79 µM indicating that $\sum NO_x$ was supplied to the pycnocline from the BML.

4.3.2 Physical forcing and water column turbulence

A number of wind events were observed that were higher than the deployment average, causing defined changes in wind stress within the surface boundary (Fig. 4.4). The average wind stress was 0.11 ± 0.09 N m^{-s}, with wind direction predominantly from the south west. For the first 10 days (13th-23rd July) wind stress remained within one standard deviation of the deployment mean with a variability of one order of magnitude occurring over <24 hr periods (e.g. 16th of July). Between the 24th to the 27th, two periods of rapid increases in wind stress, where 3 times the average wind stress was observed and peaked at 0.58 N m^{-s}. The tidal data showed a clear spring-neap signal, with peak spring tide occurring between the 17th and 18th July 2015 and neap between the 25th to 26th July 2015. The horizontal current magnitude peaked at 0.47 m s^{-1} during the peak spring tide period (17-18th July) and 0.53 m s^{-1} on 30th July at the end of the deployment approaching the next peak spring tide period. The tidal range during the spring tide period was double that observed during neap (0.1 m s^{-1}) with neap tides peaking at 0.2 m s^{-1}.

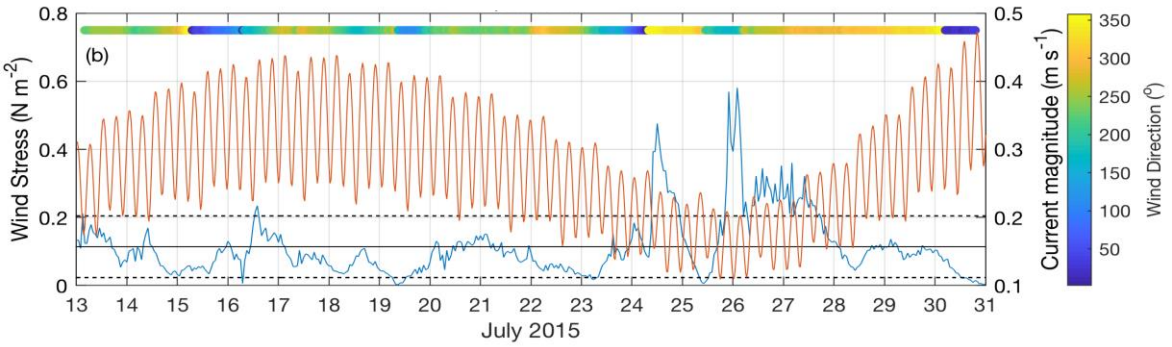

Figure 4.4: Hourly averages of wind stress (N m^{-2}; blue line) and current magnitude (m s^{-1}; orange line) corresponding to the gilder deployment period in July 2015. The mean wind stress is indicated by a black line and the 1x standard deviation a dotted line. Hourly wind direction (degrees from North) is plotted along the top.

Measurements of turbulence are important for determining fluxes of biogeochemical parameters in stratified waters by determining what physical parameters are driving turbulence.

Within the SML profiles of ε were primarily driven by the wind stress, with the highest observed rates of ε during the whole deployment observed at the surface (>$1x10^{-2.5}$) which coincided with the extended period of increased wind stress (24th to 28th July; Figure 4.4b). Following these periods of increased wind stress (Figures 4.4 and 4.5) shoaling of the SML was observed, indicating that wind stress controlled the depth and structure of near-surface dissipation. Throughout the water column ε varied by as much as 5 orders of magnitude with the least active area being observed within the pycnocline ($1x10^{-7}$; Figure 4.5c), with the higher rates only being observed during short-lived turbulence events at the boundaries or sporadic mid-water increases (e.g. 20th to 22nd and 26th to 28th). Within the BML, ε was dominated by the variability in tidal stress, with higher rates seen during the spring tide ($1x10^{-5}$ to $1x10^{-3}$ m^2 s^{-3}), with the turbulent bottom boundary layer extending to the base of the pycnocline, and lower rates observed during the neap tide ($1x10^{-7}$ to $1x10^{-5}$ m^2 s^{-3}). At the base of the pycnocline, where turbulence controls the flux of nitrate into the SCM, observed hourly averages of ε showed a tidal periodicity (Figure 4.5c), where again ε was higher during the spring tide ($5.4x10^{-7}$ to $5.4x10^{-5}$ m^2 s^{-3}) and lower during the neap tides ($3.9x10^{-7}$ to $4.1x10^{-6}$ m^2 s^{-3}) though the rates are highly variable as seen in the range of ε during both periods. Due to technical issues with the Microstructure profiler during the spring tide turbulence was not able to be collected, and therefore a 3-hour window either side will be used when referring to the spring tide period. This may result in under-estimates of ε during the spring tide.

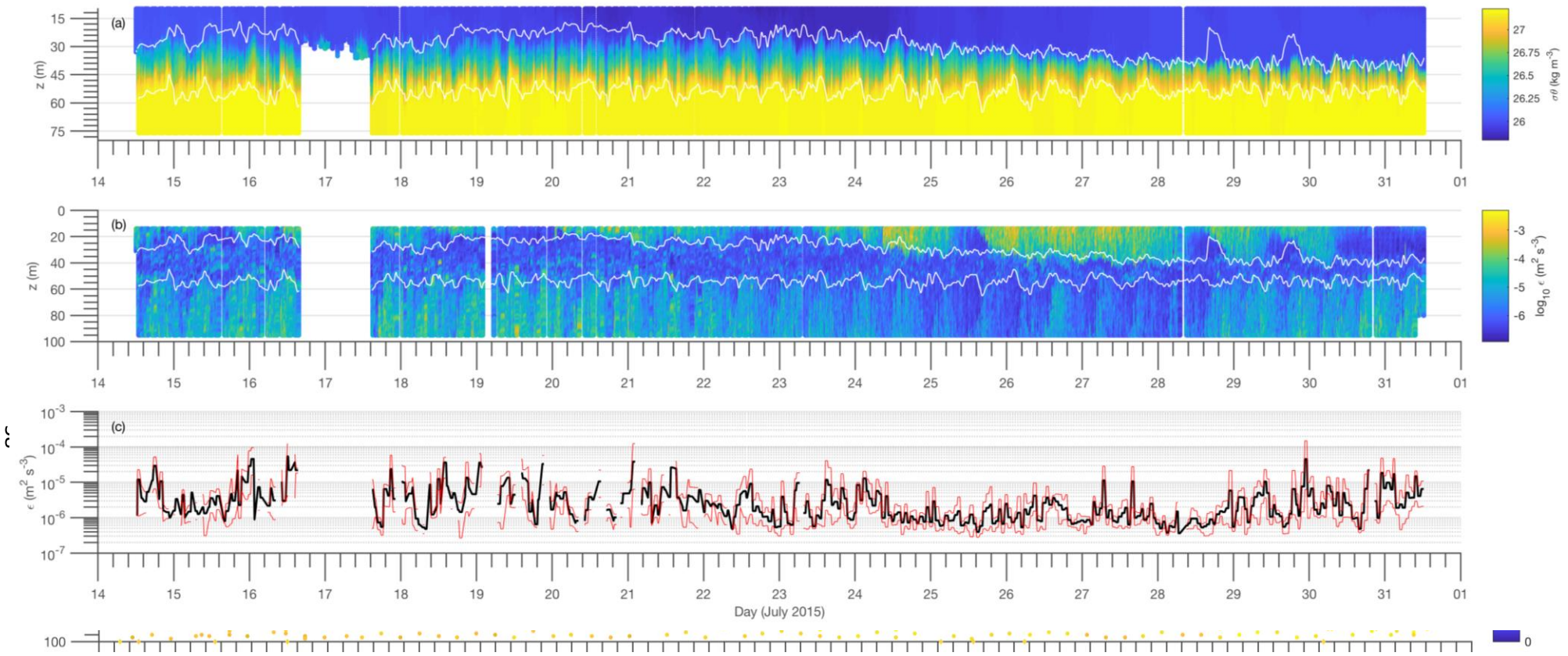

Figure 4.5: (a) Potential density (kg m^{-3}) and (b) dissipation of turbulent kinetic energy (m^2 s^{-3}) measurements obtained from a microstructure profiler mounted on a Slocom glider deployed from the 13th to 30th July 2015. The solid lines (white) denote the base of the SML and top of the BML. (c) Hourly averages of dissipation of turbulent kinetic energy taken from the base of the pycnocline (black line) with 95 % confidence intervals (red lines).

below the limit of detection (< 0.1 µM) are denoted by un-filled circles.

4.3.3 ∑NOx fluxes

Hourly time averages of $f\sum NO_x$ estimated at the base of the pycnocline also exhibited a strong spring-neap signal (Figur 4.6). However, superimposed on this spring-neap signal was short term variability in the $f\sum NO_x$, where the $f\sum NO_x$ varied by over an order of magnitude (0.3 to 48 mmol m^{-2} d^{-1}) over hourly timescales. The deployment average $f\sum NO_x$ was 4.2 ± 6.7 mmol m^{-2} d^{-1} and with such a high variability it is clear that short term fluxes have large impact on the average. The daily mean (with 95% confidence intervals) within the base of the pycnocline was 1.5 (1.3–1.7) mmol m^{-2} d^{-1} during the neap tide and 5.9 (3.6–10.1) mmol m^{-2} d^{-1} during the spring tide.

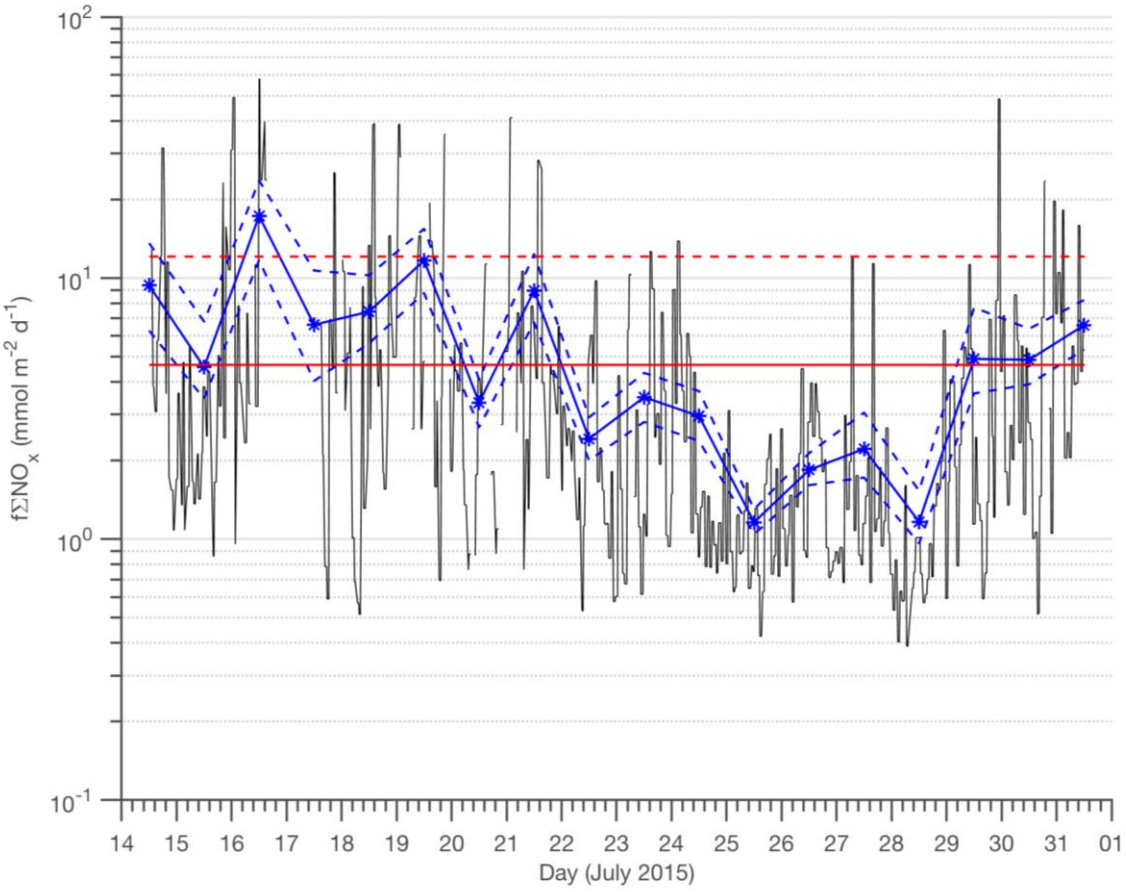

Figure 4.6: Hourly time series of $f\sum NO_x$ calculated at the base of the pycnocline (solid black line). Daily average $f\sum NO_x$ (solid blue line) with 95 % confidence intervals (dashed blue lines). The deployment average (4.03 ± 6.44 mmol m^{-2} d^{-1}) is denoted by the solid red line with the upper limit (+ standard deviation; dashed red line).

4.4 Discussion

4.4.1 Nutrient fluxes across the pycnocline

Here we report 1226 estimates of $f\sum NO_x$ calculated from observations of $\sum NO_x$ and dissipation of turbulent kinetic energy made every ~ 40 minutes over an 18-day period in July 2015. The estimated average $f\sum NO_x$ through the base of the pycnocline into the SCM was 4.2 ± 6.7 mmol m^{-2} d^{-1}, with the range reflecting the contribution of several higher $f\sum NO_x$ pulses to the mean (Figure 4.6). Our observations are from a flat seabed therefore the influence of increased mixing from turbulence processes affected by topography is limited (e.g. Sharples *et al.,* 2001; Tweddle *et al.,* 2012). All previous observations of $f\sum NO_x$ into the seasonal pycnocline over flat sea bed of the North West European shelf were lower (~2 mmol m^{-2} d^{-1}) and were driven by the barotropic tide and near inertial oscillations, and were calculated over time periods < 48 hours with < 200 estimates of $f\sum NO_x$ (e.g. Sharples *et al.,* 2001; Rippeth *et al.,* 2009, Tweddle *et al.,* 2012, Williams *et al.,* 2013). Such sampling strategies would likely alias short-term events (e.g. hourly) that this study was able to observe. A contrast between spring and neap tides $f\sum NO_x$ was reported by Sharples *et al.* (2007), at the shelf edge, and by Tweddle *et al.* (2012), over a bank in the Celtic sea, that was driven by an increase in ε at the base of pycnocline of ≈2 orders of magnitude observed between the two tidal periods. This study also observed such a contrast in ε, which resulted in a higher spring tide estimate of $f\sum NO_x$ (5.9 (3.6–10.1) mmol m^{-2} d^{-1}) compared to the estimated neap daily $f\sum NO_x$ of 1.5 (1.3–1.7) mmol m^{-2} d^{-1}, which was within the range of previously reported average estimates (~2 mmol m^{-2} d^{-1}). a*et al.,* .effectonpycnocline. As with previous studies within the Celtic shelf sea (e.g. Sharples *et al.,* 2001, 2007; Tweddle *et al.,* 2012; Williams *et al.,* 2013) ε had a first order control on the magnitude of the $f\sum NO_x$, with the deployment average of ε (10^{-6} m^2 s^{-3}) being within the range of previous studies on a flat shelf bed (10^{-9} to 10^{-6} m^2 s^{-3}; Sharples *et al.,* 2001; Tweddle *et al.,* 2012; Williams *et al.,* 2013), and below that observed on the shelf edge and Georges bank (10^{-5} to 10^{-4} m^2 s^{-3}; Sharples *et al.,* 2007; Tweddle *et al.,* 2012). While the average ε observed at the pycnocline was comparable to previous studies the deployment average $f\sum NO_x$ (4.2 mmol m^{-2} d^{-1}) was over double that of previously reported background $f\sum NO_x$ on a flat shelf bed (~2 mmol m^{-2} d^{-1}) and comparable to more turbulent locations such as the shelf edge during a spring tide (3.5 mmol m^{-2} d^{-1}). Our values are however, lower than the $f\sum NO_x$ estimated during the spring tide on Georges Bank (52 mmol m^{-2} d^{-1}). The higher deployment average reported here could be due to a number of factors. Firstly, by increasing the resolution of $\sum NO_x$ and the overall time period of observations we account for the influence of ε variability and higher $f\sum NO_x$ caused by episodic events to contribute to and increase

the estimated mean f$\sum NO_x$. The effect of under sampling turbulent events was shown by Sharples *et al.* (2007) where over 25-hour occupation observations of turbulence only took place 38% of the time, and as episodic events dominated their daily f$\sum NO_x$ estimate, and they estimate that continuous sampling would have raise the daily averaged spring tide f$\sum NO_x$ from 3 to approximately 9 mmol m^{-2} d^{-1}. Secondly, for the first time this deployment was able to capture more than just a single tidal cycle, our estimates also account for the transition between neap and spring tides. During the 17-day deployment over 72% of the daily estimates of f$\sum NO_x$ was > 2 mmol m^{-2} d^{-1} with sharp increases in f$\sum NO_x$ during the days either side of the neap tide period (e.g. 21st to 22nd, 23rd to 25th and 29th to 31st). By including these observed f$\sum NO_x$ (Figure 4.6) the average was more indicative of the full variability of the turbulent field affecting the production of fluxes at the pycnocline and therefore a better representation of the average f$\sum NO_x$ into the base of the SCM.

Higher f$\sum NO_x$ estimates have previously been reported that are orders of magnitude higher than the background flux (1–2 mmol m^{-2} d^{-1}) in physically dynamic regions (e.g. Shelf edge and banks), where ε at the base of the pycnocline was between 10^{-5} to 10^{-4} m^2 s^{-3} (e.g. Sharples *et al.,* 2007). Comparable higher f$\sum NO_x$ were observed in this study and ranged between 15-50 mmol m^{-2} d^{-1} and occurred during periods of high current magnitude (> 0.3 m s^{-1}), and where ε at the base of the pycnocline was >10^{-5} m^2 s^{-3}. For instance, f$\sum NO_x$ up to 52 mmol m^{-2} d^{-1} were reported by Tweddle *et al.* (2013) during the spring tide over Jones bank within the Celtic Sea and were forced by locally generated lee waves and internal mixing over the topographical features. Tweddle *et al.* (2013) suggested that without episodic mixing events, where ε was >10^{-5} m^2 s^{-3}, the daily supply of NO_3^- over the bank at spring tide would not be significantly different to the reported f$\sum NO_x$ over flat regions in the Celtic Shelf sea. Sharples *et al.* (2007) and Horne *et al.* (1996) report f$\sum NO_x$ of 1 to 11 mmol m^{-2} d^{-1} due to internal tides at the shelf edge and spring-neap adjustments at tidal mixing fronts on Georges Bank in the Celtic Sea. Interestingly our higher estimates are from a flat sea bed indicating the dynamic nature of f$\sum NO_x$ across the pycnocline. This is certainly also the case with this study, if f$\sum NO_x$ estimates greater than 1 standard deviation above the deployment mean (>10.9 mmol m^{-2} d^{-1}) are not included, then the estimated deployment average f$\sum NO_x$ decreases from 4.2 mmol m^{-2} d^{-1} to 2.7 mmol m^{-2} d^{-1} (median 1.7 mmol m^{-2} d^{-1}) indicating the importance of short-term mixing events in sustaining elevated f$\sum NO_x$ above background levels.

4.4.2 Influence of nitrate fluxes on primary production

Hickman *et al.* (2012) reported that irradiance within the SCM was ~5% of surface values, and therefore rates of new production could be limited due to both light and nitrate. If the amount of nitrate supplied to the SCM was surplus to that required by the light-limited rates of

primary production, the nitrate would be available to be utilised in the following days. This mechanism was observed by Sharples *et al.* (2007), where excess nitrate during spring was available for the following days, and the maximum Chl-*a* concentrations occurred ~3.5 days after maximum nitrate fluxes were observed. This mechanism could explain the significant increase in Chl-*a* (peaking at 4.1 mg m^{-3}) observed during this deployment from the 20th to 23rd of July (Figure 4.3b). The increase in PAR (% 62; data not shown from CEFAS SmartBouy) coincides with this increase in Chl-*a* and suggests that previously, primary production was light-limited and unable to utilise the available nutrients fluxed up through the pycnocline into the SCM 3-4 days earlier during the spring tide period.

Within the SML and top of the pycnocline (Figure 4.3c) $\sum NO_x$ was undetectable which suggests all $\sum NO_x$, and additional pulses of $\sum NO_x$ from the BML, is utilised by the phytoplankton community within the SCM for new production, and so estimating of the rate of carbon fixation supported based on these $f\sum NO_x$ estimates can be achieved. To estimate the rate of carbon fixation supported by the flux of $\sum NO_x$ to the base of the pycnocline requires a knowledge of the elemental stoichiometry of primary producers. The Redfield ratio suggests that the typical carbon (C) to nitrogen (N) ratio in phytoplankton is ≈6.6 mol:mol (Redfield, 1958). This has been reported to vary due to the different cellular quotas of different species and responses to changes in concentration within the water column but average values remain between 6.6 to 7.3 mol:mol (Redfield, Ketchum and Richards, 1963; Geider and La Roche, 2002; Ho *et al.*, 2003). However, Humphreys *et al.* (in press) reported that production of organic matter at CCS was C-rich, with the C:N ranging from 9 to 10 mol:mol. Using the average $f\sum NO_x$ into the base of the pycnocline reported in this study (4.2 mmol m^{-2} d^{-1}) and a C:N ratio of 9.5 mol:mol (mean observed by Humphreys et al. (in press)), 479 mg C m^{-2} d^{-1} (332 mg C m^{-2} d^{-1} where Redfield C:N = 6.6 is used) of new production would be able to be supported, Higher estimates during spring tides result in ~675 mg C m^{-2} d^{-1} (450 mg C m^{-2} d^{-1} where C:N = 6.6), and lower estimates during neaps ~171 mg C m^{-2} d^{-1} (125 mg C m^{-2} d^{-1} where C:N = 6.6) were observed using the average $f\sum NO_x$ during neap (1.5 mmol m^{-2} d^{-1}) and spring (5.9 mmol m^{-2} d^{-1}) tides. These new production estimates are comparable to previously reported estimates of new primary production (Carbon-14 methodology) in the seasonally stratified region of the Celtic Sea, where daily rates of 100 to 600 mg C m^{-2} d^{-1} in the summer months have been reported (Holligan *et al.*, 1984; Joint, Owens and Pomeroy, 1986; Hickman *et al.*, 2012). As part of the SSB program, Poulton *et al.* (2018) reported net primary production (NPP) rates (integrated within the euphotic zone using ^{14}C measurements) at CCS during this study (July 2015) ranged between 228.6 to 702.6 mg C m^{-2} d^{-1} with an average rate of 425.2 mg C m^{-2} d^{-1}. The average is very similar to that reported here calculate from $f\sum NO_x$

(479 mg C m^{-2} d^{-1}) indicating that flux of nitrate across the pycnocline is fully utilised by phytoplankton and needed to support their carbon fixation.

Assuming a summer stratified period of 120 days, the new production estimates presented here for July (2015) have been extrapolated to estimate the potential total summer new production in the SCM. The estimates of new production (479 mg C m^{-2} d^{-1}) supported by the estimated deployment average f$\sum NO_x$, with the neap and spring estimates of f$\sum NO_x$ being the lower and upper limits of the envelope, would result in 58 (21-80) g C m^{-2} of potential new production in the SCM over a summer period. The spring bloom has been estimated to contribute ~19 g C m^{-2} of new production annually (Joint *et al.,* 2001; Hickman *et al.,* 2012), therefore the SCM could contribute up to ~75 (52-80) % of spring-summer potential new production. While the lower estimate (52%) is comparable to the estimate reported in Hickman *et al.* (2012), more than likely due to the fact it is based on a neap f$\sum NO_x$ similar to those previously reported (1-2 mmol m^{-2} d^{-1}), the higher upper estimate (80%) is significantly higher. This higher estimate could be due to the higher f$\sum NO_x$ reported in this study compared to the lower f$\sum NO_x$ estimates used in Hickman *et al.* (2012) and also due to the higher C:N ratio used 9.5 is this study which would decrease SCM contribute of spring-summer potential new production to ~66 (44-74) %. This contribution is higher than estimates for the SCM in the North Sea ranging between 37% and 66% ((Richardson *et al.*, 2000; Weston *et al.*, 2005). Assuming that this estimate of contribution to new production over the summer growth period is representative of flat sea bed region, this produces an estimate of possible total new production of 6.42×10^{12} ($2.54\text{-}9.07 \times 10^{12}$) g C over the summer period over the entire Celtic Sea (total area estimated to be ~167,300 km^2; Tweddle *et al.* (2007)). Moreover, this estimate does not consider the contribution of enhanced f$\sum NO_x$ due to topographic features, such as 1.6×10^{11} g C of new production over banks and 1.9×10^{12} g C of new production from the shelf edge (e.g. Sharples *et al.,* 2001; Tweddle *et al.,* 2007).

4.5 Conclusions

Temperate shelf systems makes up 30% of the total continental shelf area of 24.7×10^6 km^2, with the mid to outer shelf waters being specifically shown to be key sinks of increasing atmospheric CO_2 (Cai, Dai and Wang, 2006; Laruelle *et al.*, 2010), and also play a significant part in the ability of the global continental shelves to contribute 10–30% of global marine primary production and estimated supply of up to 50% of the organic carbon to the deep open ocean to be locked away from the euphotic zone (Jahnke, 2010; Liu *et al.*, 2010). Determining the amount of new production, and thus carbon fixation, supported by the f$\sum NO_x$ from the BML is crucial for understanding the role shelf sea biogeochemistry plays in the global carbon sequestration via

mechanisms such as the '*continental shelf pump*' (Tsunogai *et al.,* 1999). The contribution of new production estimated in this study supported by the f$\sum NO_x$ into the SCM reported in this study (58 (21-80) g C m^{-2}) could support all of the estimate annual new production of 81.8 g C m^{-2} in the Celtic sea reported by Joint *et al.* (2001) just in the SCM during the summer period (120 days). If this under-estimation of the contribution of the summer SCM to the annual new production shown here in the Celtic shelf sea is indicative in all other continental shelf seas of the Northern Hemisphere, then their estimated ability to be net sinks of CO_2 (−0.24 Pg C yr^{-1}; Laruelle *et al.*, 2010) could be underestimated.

Chapter 5: Estimating particulate organic carbon and phytoplankton carbon biomass using bio-optical sensors from glider observations in a seasonal shelf sea

5.1 Introduction

The optical characteristics of open ocean waters are dominated by phytoplankton components and their covariant by-products (e.g. degradation products), resulting in a relatively simple optical signature when compared to coastal waters (Loisel *et al.*, 2013). Coastal waters, however, also include groups of substances defined as coloured dissolved organic matter (CDOM) and mineral particles, with the latter shown to dominate the optical signature in many cases (Loisel *et al.*, 2007; Souza, Holt and Proctor, 2007). Shelf sea regions are shallow and tidally active, and the penetration of light can be strongly attenuated by particulate and dissolved organic matter that originates from rivers, or is re-suspended from the seabed (Babin *et al.*, 2003), complicating the observation of bio-optical parameters (e.g. fluorescence, scatter and absorbance) by either remote or *in situ* observations. These bio-optical parameters have been observed to have a relationship with variables such as chlorophyll-*a* (Chl-*a*), Particulate Organic Carbon (POC) and phytoplankton carbon biomass estimates (C_{phyto}), and are therefore used as proxies for these (McClain, 2009; Sathyendranath *et al.*, 2009). These relationships have been applied to surface data collected by satellites and shown to hold, to an extent, in a variety of water/environmental characteristics (Loisel *et al.*, 2002; Behrenfeld *et al.*, 2005; Evers-King *et al.*, 2017).

Shelf seas are dynamic and highly productive regions that are reported to generate 15 – 30 % of total oceanic primary production (Wollast, 1998; Simpson and Sharples, 2012). This therefore makes these regions globally significant for the fixing and sequestering of atmospheric carbon. Shelf seas are seasonally stratified from spring throughout summer, with a sub-surface chlorophyll maximum (SCM) forming at the base of the pycnocline (Simpson and Sharples, 2012). Phenomena such as the SCM are under-sampled, not only by satellites, but by traditional ship-based platforms as well. Through the use of increased sampling, studies reported $\sum NO_x$ fluxes

twice that of previous observations, estimating the potential of the summer SCM to supply a significant proportion of the annual new production (Chapter 4: Vincent *et al.,* 2018).

The ability to observe the dynamics and spatial heterogeneity of phytoplankton biomass and associated carbon parameters (e.g. POC and C_{phyto}) at relevant temporal and spatial scales is vital to improving our understanding of the biogeochemical role of phytoplankton in the carbon cycle in open ocean waters, but also in complex productive regions such as the shelf seas, where processes known as the '*biological pump*' and '*continental shelf pump'* are globally important (Tsunogai *et al.*, 1999; Thomas *et al.*, 2004; Legendre et al., 2015). To increase the spatial and temporal coverage of observations and combat the general under-sampling of phytoplankton biomass and associated carbon parameters, bio-optical sensors have been increasingly used on *in situ* platforms and AUVs (Johnson *et al.*, 2009; Claustre *et al.*, 2010). Similar to how *in situ* measurements (from fixed observatories or cruises) are used for the calibration and '*quality control*' of remotely sensed data, autonomous underwater vehicle platforms (e.g. Bio-optical ARGO floats and autonomous underwater gliders) can be used for such a purpose, providing high resolution datasets within spatial and temporal domains that traditional observational methodology is unable to attain (Testor *et al.*, 2010; Wojtasiewicz *et al.*, 2018). There is a need to better understand the capabilities of bio-optical observations from gliders within optically complex shelf seas (case 2 waters) to not only increase our bio-optical observations and validate and calibrate methodology honed within case 1 waters, but also to be able to reliably observe and predict the role of shelf seas in the global carbon cycle (Bauer *et al.*, 2013; Loisel *et al.*, 2013; Laliberté *et al.*, 2018).

This study applied the established bio-optical satellite remote sensing methodology used to estimate POC and C_{phyto}, which are usually used in studies in the open ocean (case 1 waters), to a dynamic shelf environment (case 2 waters) using optical sensors deployed on a Seaglider. Over two month-long deployments during the two key periods in a seasonal shelf sea, the spring bloom and summer SCM, a comparison was made between periodic discrete seawater samples measuring POC and of C_{phyto} and estimates of POC and C_{phyto} derived using empirical relationships between bio-optical parameters observed from optical instruments deployed on a Seaglider.

5.2 Methods

The data presented in this chapter is obtained from the fluorescence and backscatter observations from an Environmental Characterisation Optics (ECO) puck (BBFL2VMT; WetLabs, USA; hereafter referred to as ECOp) deployed on an autonomous Seaglider (Kongsberg). The Seaglider was deployed at the Central Celtic Sea site (CCS; Figure 2.1) between the 4th to 25th of April 2015 and 13th to 30th of July 2015, collecting 1547 and 1128 profiles, respectively, to a depth of ~ 120 meters along a saw-tooth trajectory at typical vertical speeds of 0.1 m s^{-1} (Rudnick *et al.*, 2004). In addition to the ECOp, a Conductivity and Temperature sail (Seabird Electronics, USA) measuring conductivity (salinity), temperature, pressure, and a Lab-on-Chip sensor measuring nitrite + nitrate (defined as $\sum NO_x$; National Oceanographic Centre, UK) were also deployed on the Seaglider, making co-located observations. Further details on the processing, quality control and calibration of the physical (e.g. conductivity and temperature) and $\sum NO_x$ have been described in detail in chapters two and three of this thesis.

5.2.1 Data from RSS Discovery at CCS

In addition to the measurements from the Seaglider, water column profiles and discrete samples were collected using both a stainless-steel and titanium frame rosette system. On each rosette a Conductivity, Temperature and Depth package was mounted, consisting of a CTD (Seabird 911+), backscattering meter (ECO BB, WetLabs, USA), and fluorimeter (Chelsea Technologies Group, Aquatracka MKIII), which were deployed from the *R.S.S. Discovery* during April and July (2015) at CCS. Discrete seawater samples were collected for Chl-*a*, POC and phytoplankton biomass. The GO-SHIP sampling and handling procedures were used for all discrete seawater sampling (Hydes *et al.*, 2010). Salinity (calculated from conductivity and temperature) and Chl-*a* (fluorescence, emissions wavelength at 682 nm) measurements obtained from CTD casts were calibrated daily on-board using discrete seawater samples. Salinity samples were analysed on an Autosal 8400B salinometer (Guildline). Chl-*a* samples were filtered through 0.7 µm glass microfiber filters (Whatman GF/F) and extracted in 90 % acetone overnight, before being measured on a pre-calibrated (spinach chlorophyll-*a* standard, Sigma) fluorimeter (Turner Design Trilogy; Holm-Hansen et al. 1965). All CTD profile data was supplied by the British Oceanographic Data Centre (www.bodc.ac.uk).

Discrete seawater samples for phytoplankton biomass (C_{phyto}) estimates were taken during casts undertaken during pre-dawn (02:00-06:00) at six light depths (60, 40, 20, 10, 5 and 1 %) at CCS. It was assumed that the base of the SML was at or close to the depth of the euphotic zone

(i.e. 1 % of surface irradiance) for April (2015). In July (2015) the SCM occurred at or close to a depth of 5 % surface irradiance. These measurements from the six light depths were then integrated to calculate the inventories for the euphotic zone (Humphreys *et al.*, 2018). C_{phyto} was estimated using the method reported in Poulton *et al.* (2018), whereby cell abundances for the major phytoplankton groups were analysed using flow cytometry and light microscopy according to Tarran, Heywood and Zubkov (2006) and (Widdicombe, Eloire and Harbour, 2010), respectively. Cell abundances from flow cytometer counts were converted to biomass using literature values (Tarran, Heywood and Zubkov, 2006) and cellular biomass for light microscope counted taxa were estimated from cell dimensions following (Kovala, 1966) on an individual species basis.

For POC analysis, discrete seawater samples were collected from 6 to 8 depths (5 casts in April and 4 casts in July 2015). The volume of water filtered onto a 0.7 µm filter (Whatman GF/F, pre-combusted for 4 hours at 450 °C) was measured. Filters were then frozen at -20 ^{o}C before laboratory analysis at the University of Liverpool undertaken by Dr Clare Davis (Davis *et al.*, 2018). Samples were analysed in duplicate after vapour phase decarbonation using a Carlo Erba Instruments NC2500 elemental analyser (Yamamuro and Kayanne, 1995). A two-point calibration was performed using High Organic Sediment Standard OAS (Elemental Microanalysis Ltd, NIST certified values), which were then analysed twice as an unknown during the run. The results were always within the uncertainty limits of the certified value which are 7.17 ± 0.09 % carbon with detection limits of 100 ppm (Davis *et al.*, 2018).

5.2.2 Fluorescence processing

Chl-*a* fluorescence (a proxy for phytoplankton concentration) was observed at excited/emissions wavelengths at 470/685 nm. The raw counts (*rawCounts*) from the ECOp from the Seaglider were converted to a concentration of Chl-*a* (mg m^{-3}) following:

$$Chla = (rawCounts - darkcounts) * scalingFactor \quad (5.1)$$

Where the darkCount value used was 48 and the scalingFactor values were 0.0122 for Chl-*a*. Initial calibration of the tested fluorescence sensors were performed by the manufacturer, using a *Thalassiosira weissflogii* standard for chlorophyll-*a* fluorescence (WetLabs, 2017). The measurement range and sensitivity for Chl-*a* were 0-30 (mg m^{-3}) and 0.015 (mg m^{-3}) respectively. Further details on the processing of Chl-*a* data and quality control can be found in Chapter 2 of this thesis. A visual comparison between calibrated Chl-*a* profiles from the Seaglider and calibrated CTD bottle-samples was done to facilitate quality control. Profiles of Chl-*a* were compared and showed no large systematic variation between the datasets; the small-scale variability between Seaglider and calibrated CTD collected data was likely due to the variation

between the datasets as a product of a greater number of Seaglider profiles (CTD profiles = <25, Seaglider profiles = >1100), lateral distance and the period of time between compared profiles.

5.2.3 Particle backscattering processing

The backscattering coefficient, $b_b(\lambda)$, is related to light scattered from a beam in the backward direction and is directly related to the concentration and size of particles, but also to their composition (i.e. organic vs inorganic). The particulate backscattering coefficient, $b_{bp}(\lambda)$, assumes DOM has a negligible effect on scattering and is derived by subtracting the scattering by pure water, $b_w(\lambda)$, from $b_{bp}(\lambda)$ (Zhang, Hu and He, 2009).

The ECOp (Seaglider) and ECO BB (CTD) sensor provides counts of VSF, $\beta(\theta,\lambda)$, with units of m^{-1}, where θ was 124° and 117°, respectively, and λ was 650 nm. Initially values were checked to be in the threshold of the range of the ECOp sensor (range of 0-5 (m^{-1})) and spikes from raw counts were separated using a 5 and 7 point running median filter according to protocols detailed in Briggs *et al.* (2011). From the CTD bottles files, values of backscatter coefficient (b_b; m^{-1}) were used. Following the procedure established by Schmechtig *et al.* (2018) and Thomalla *et al.* (2017), the particulate backscattering coefficient, $b_{bp}(\lambda)$ with the units of m^{-1}, was calculated following Boss and Pegau (2001):

$$\mathrm{bbp}(\lambda) = 2\pi\chi[(rawCounts - darkCounts) * scalingFactor - \beta_{sw}(650)] \quad (5.1)$$

Where χ is a conversion factor 1.076 (Schmechtic *et al.,* 2015; Sullivan *et al.,* 2013), *rawCounts* are the raw output counts, *darkCounts* were 47 and 0.061 for the ECOp and ECO BB, respectively, which are the factory measured signal output of the backscattering meter in clean water with black tape over the detector. ScaleFactor were $3.941e^{-6}$ and $2.365e^{-3}$ in $(m^{-1})/counts^{-1}$ for the ECOp and ECO BB, respectively. $\beta_{sw}(650)$ is the contribution to the VSF by pure seawater at a wavelength of 650 nm, which depends on temperature and salinity, and was estimated from MATLAB code written by Zhang, Hu and He (2009).

5.3 Results and Discussion

5.3.1 General Hydrography and Chl-*a*

The water column structure at CCS during both the Spring (April) and Summer (July) 2015 deployments has been extensively discussed in chapters 3 and 4 of this thesis, respectively. To summarize, during April the water column went from being fully mixed to stratified over ~21 days

as an increase in solar heating overcame the destabilising mixing energy from tidal and wind inputs leading to the water column becoming stratified (Simpson and Sharples, 2012; Figure 5.1a). At the beginning of the April deployment surface Chl-*a* concentrations were 1.68 mg m^{-3} and, as the water column became stratified, a strong thermocline formed defining a SML. Phytoplankton were now confined within the SML, where both PAR and nutrient availability were high, leading to the onset of the spring bloom (Pingree *et al.*, 1976; Hopkins *et al.,* in prep; Figure 5.1c). The bloom had a distinct peak in Chl-*a* of (> 8 mg m^{-3}) on the 17th of April 2015 and resulted in the drawdown of $\sum NO_x$ (Vincent *et al.,* 2018) concentration within the SML to below the limit of detection (Birchill *et al.,* 2017). Euphotic zone inventories of Chl-*a* ranged between 49.6–152.6 mg m^{-2}, peaking during the middle of the deployment. The drawdown of $\sum NO_x$ limited phytoplankton growth, forming a warm buoyant nutrient-deplete SML separated from the cooler nutrient-replete BML by a thermocline (Figure 3.4b). By the summer, the contrast between these layers had increased, with a strongly defined thermocline with nutrients below the limit of detection with the SML (Figure 4.4). A sub-surface chlorophyll maximum (SCM) had formed at the base of the pycnocline (figure 5.2c), located within the water column between 30-60 m with an average Chl-*a* concentration of 2.4 ± 0.9 mg m^{-3} and a maximum peak of 4.1 mg m^{-3}. Concentrations within the surface and bottom mixed layers were < 0.5 Chl-*a* mg m^{-3} due to being light or nutrient limited (Simpson and Sharples, 2012). Euphotic zone inventories of Chl-*a* were lower during summer when the SCM was present and ranged from 22.1 to 38.9 mg m^{-2}.5.1of chlorophyll *a*

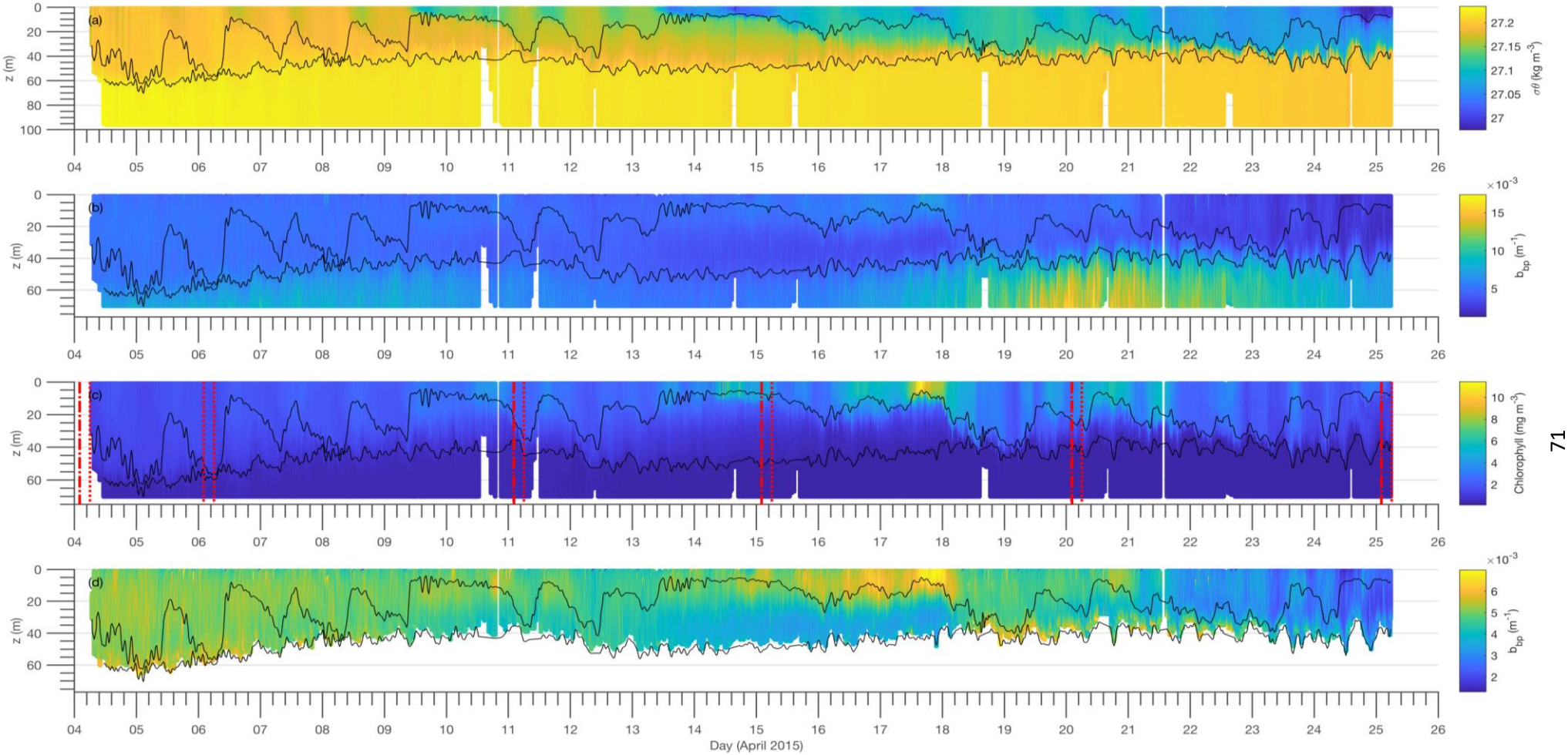

Figure 5.1: (a) Sigma-theta (kg m^{-3}), (b) particulate backscattering coefficient (650 nm; m^{-1}), (c) Chlorophyll-a (mg m^{-3}) and particulate backscattering coefficient with the BML values removed (650 nm; m^{-1}). Measurements obtained from one Seaglider deployment from the 4th to 25th April 2015. Black lines denote the SML and BML. Dashed red lines mark the time a cast for POC measurements were made. Dotted red lines mark the period CTD cast were undertaken for C_{phyto} observations.

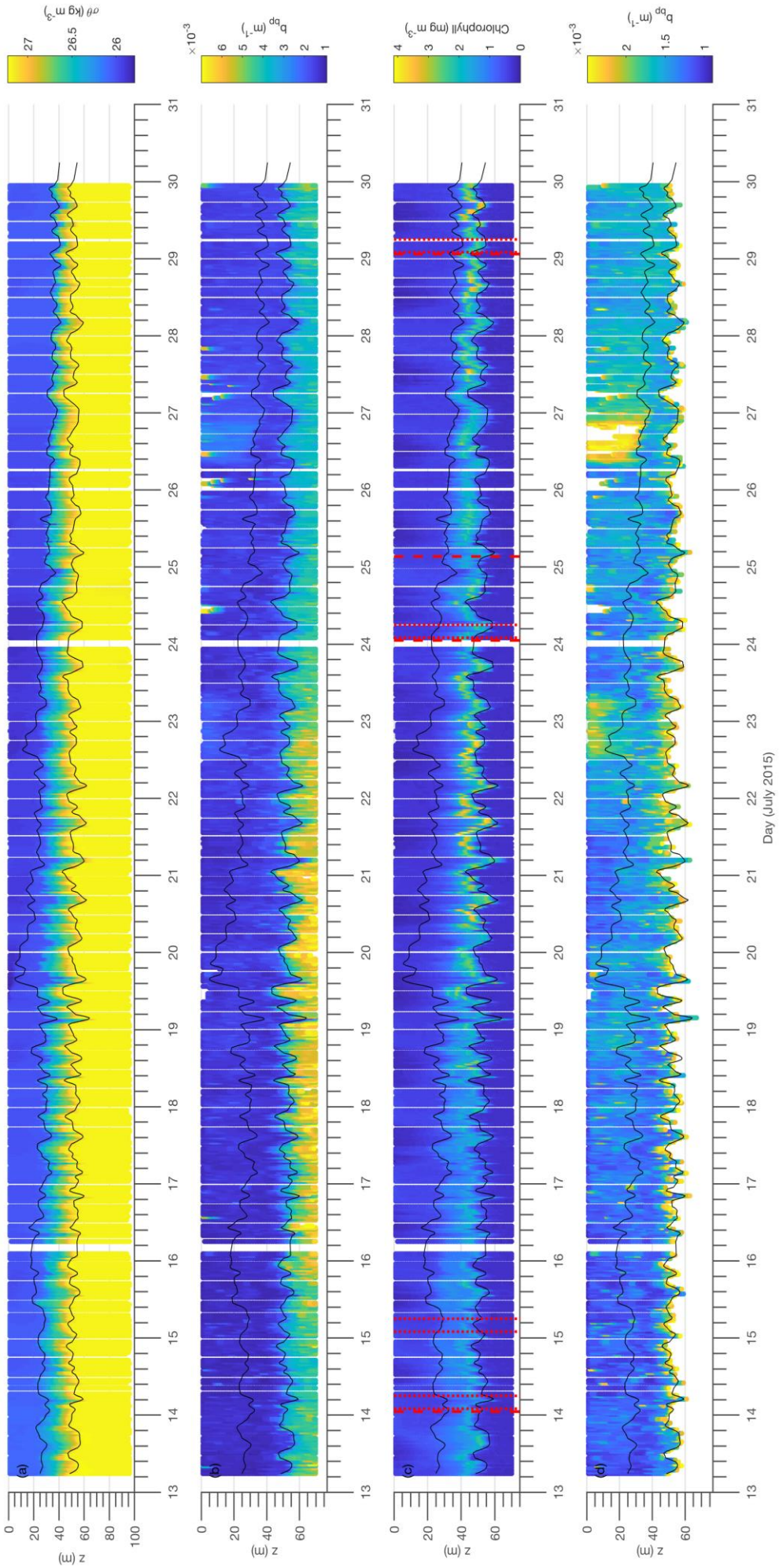

Figure 5.2: (a) Sigma-theta (kg m^{-3}), (b) particulate backscattering coefficient (650 nm; m^{-1}), (c) Chlorophyll-a (mg m^{-3}) and particulate backscattering coefficient with the BML values removed (650 nm; m^{-1}). Measurements obtained from one Seaglider deployment from the 13th to 30th July 2015. Black lines denote the SML and BML. Dashed red lines mark the time a cast for POC measurements were made. Dotted red lines mark the period CTD cast were undertaken for C_{phyto} observations.

5.3.2 Particulate backscatter and POC

During both the spring and summer deployments, a vertical b_{bp} gradient was observed with a stark contrast between the mixed layers, where b_{bp} values within the BML were either 2-fold or 3-fold higher (e.g. 20th of April, 20th of July) than the values seen in the SML. b_{bp} values in spring were higher for both the SML (0.001 - 0.007 m^{-1}) and BML (0.005-0.016) than during the summer (0.001-0.003 and 0.004-0.007 m^{-1} for SML and BML, respectively; Figures 5.1b and 5.2b). Within the BML during deployments a semi-diurnal and spring-neap signal was also observed (Figure 5.1b & 5.2b) with higher b_{bp} values (~ double), corresponding to times of higher turbulence observed during the spring tide periods (Figure 4.5b for July; April data not shown).

There was a strong positive relationship between Chl-*a*:b_{bp} in April within the SML (r^2 = 0.62, n = 15866; Figure 5.3a; Observed from the Seaglider). As the on-set of the spring bloom progressed, an increase was observed in both Chl-*a* and b_{bp} values, with a maxima observed during the peak of the bloom (Figure 5.1c; ~17th April). A tighter fit to the regression line was observed during the peak spring bloom period, with subsequent periods each side of the bloom showing a decrease in both Chl-*a* and b_{bp} and more variation away from the regression line. In July however, there was only a weak positive correlation between b_{bp} values and Chl-*a* (r^2 = 0.27, n = 9138; Figure 5.4b) suggesting a decoupling between Chl-*a* and b_{bp}.

POC concentrations within the euphotic zone were shown to be 7 times higher in April (maxima of 28 µM) than during winter (4.1 µM; Davis *et al.* 2018), and 3.5 times higher than in July (8 µM). During April, POC increased by a factor of 4 from the beginning of the cruise (4th April), to midway through (15th April), where it reached its maxima value observed from discrete samples. Euphotic zone inventories of POC showed higher concentrations in April (5059 (3126-6511) mg m^{-2}), compared to the lower concentrations observed in July (3739 (3243-4576) mg m^{-2}; Davis *et al.* 2018). Fluorescence data from the glider, however, clearly shows that the peak of the bloom was on the 17th April (Figure 5.1c), when no discrete POC samples were taken. Using derived POC concentrations from this period, a maxima of 6645.6 (6346-6852) mg m^{-2} was determined with a maxima Chl-*a* euphotic zone inventory of 136.8 (128.8-142.5) mg m^{-2}. In the summer (July 2015), when the SCM was established, little variation in the discrete seawater POC concentrations was observed, where concentrations ranged from 6.11 to 8.19 µM (Figure 5.4). BML (> 60 m) POC concentrations during both April and July 2015 remained relatively stable, ranging from 3.14 to 5.19 (µM) and 2.83 to 4.81 (µM), respectively. During both time periods the water column POC concentrations were observed to be related to the regions of higher Chl-*a,* and thus primary production, with higher POC concentrations observed in April (Figure 5.4a) within

the SML (0 to 25 m), as the on-set of the spring bloom progressed (Figure 5.1c), and in July (Figure 5.4b), within the thermocline (30 to 50 m) where the SCM was located (Figure 5.2c). For both time periods there was no relationship between discrete seawater POC concentrations and their respective b_{bp} values from the glider (Figures 5.5). However, there was a strong correlation between POC concentrations and Chl-*a* (r^2= 0.79; $p < 0.001$) during April (Figure 5.6), which was also seen during the Autumn bloom (Davies *et al*., 2019). This correlation was, however, weaker in July, with lower Chl-*a* and b_{bp} values (Figure 5.7) due to decoupling between POC and Chl-*a* in the SCM (p=0.008).

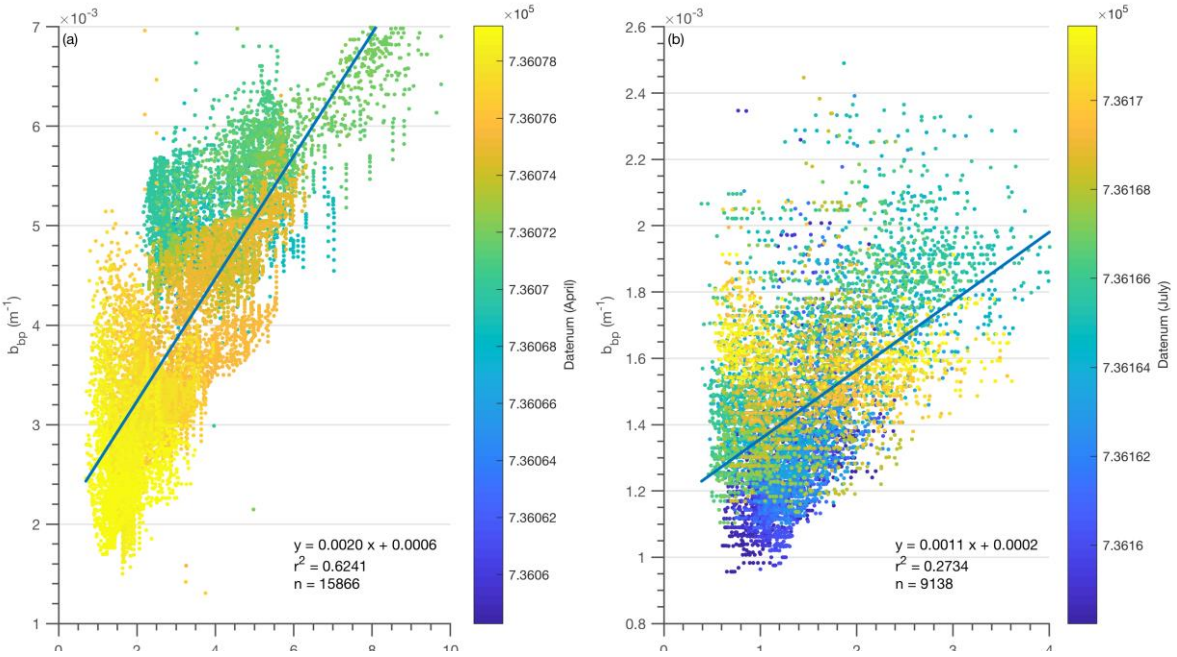

Figure 5.3: Particulate backscattering coefficient (650 nm; m^{-1}) as a function of chlorophyll-a (mg m^{-3}) with the colour bar denoting time (datenumber). (a) Observations from the SML during the spring bloom (April 2015). (b) Observations from the thermocline during the summer bloom (July 2015).

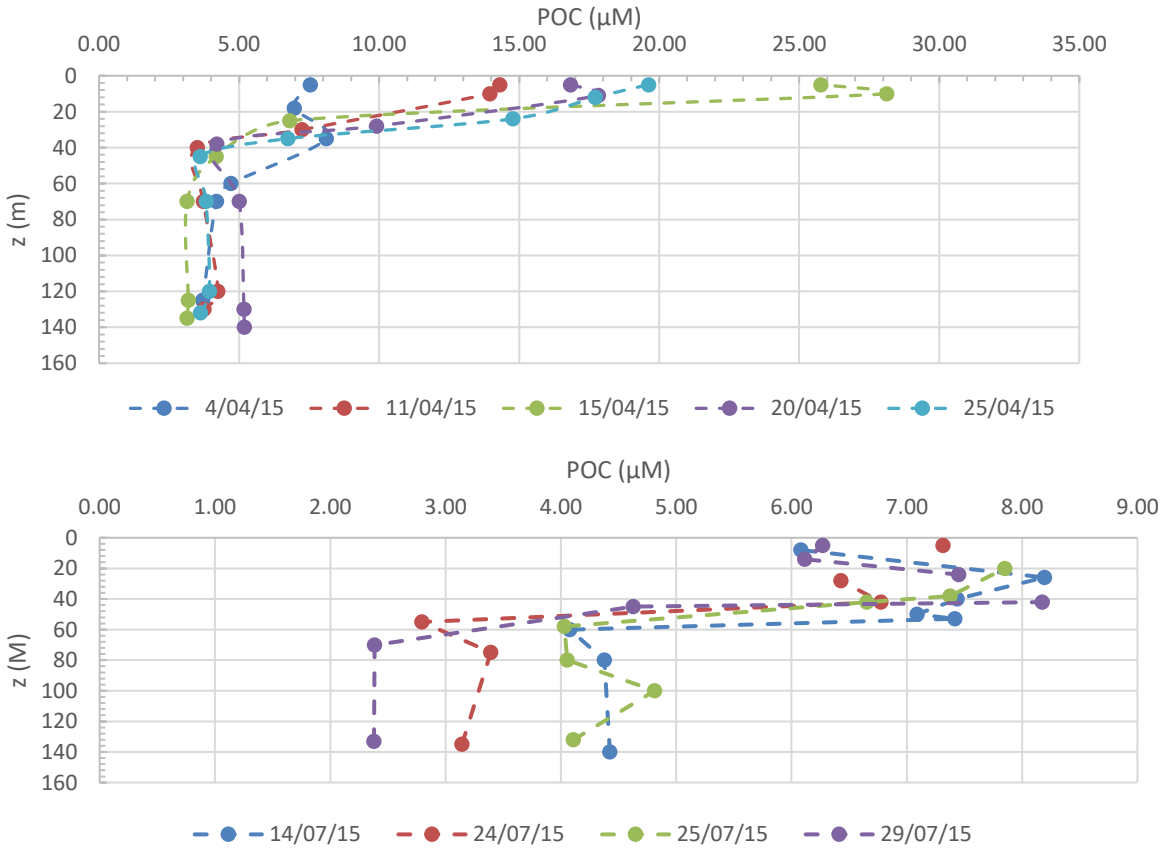

Figure 5.4: POC (µM) profiles measured from discrete CTD sampling at CCS during, (a) the spring (April 2015), and (b), the summer (July 2015) deployments.

5.3.3 Deriving POC from b_{bp} and Chl-*a*

In the open ocean, b_{bp} generally covaries with POC, and is therefore used as a proxy (Stramski *et al.*, 1999; Loisel *et al.*, 2002; Bishop and Wood, 2009). While this relationship holds true across different oceanic regions, changes in the nature (composition and size) of the particle assemblage may cause large variability in the b_{bp} signal and, therefore, in the POC:b_{bp} relationship (Gardner, Mishonov and Richardson, 2006; Stramski *et al.*, 2008; Bishop and Wood, 2009). Previous (Behrenfeld *et al.*, 2005; Evers-King *et al.*, 2017) have used this POC:b_{bp} relationship calculated from discrete samples to enable POC estimates from a glider, whereby the backscatter observations made by both the glider and CTD used the same wavelength of 650 nm. As there was no relationship between discrete samples of POC and their respective b_{bp} measurements in this study, such a methodology could not be used (Figures 5.6). This study did, however, observe a strong correlation between POC and Chl-*a* concentrations (Figure 5.6). While the July data showed a poor r^2 (r^2 = 0.26) compared to the April data set (r^2 = 0.84), the full data set was combined to calculate the POC:Chl-*a* relationship During the April sprint bloom r^2= 0.79; $p < 0.001$), and, by using the POC:Chl-*a* relationship, estimates of POC concentrations were derived from glider bio-optical data (e.g. fluorescence).

Shelf seas are dynamic regions with regards to phytoplankton biomass, nutrient availability, irradiance and temperature (Simpson and Sharples, 2012), which can all affect the Chl-*a*:POC relationship. However, when using large datasets from multiple oceanographic regimes the large range in Chl-*a* and POC concentrations observed indicate a robust relationship between these parameters, regardless of the environmental difference that (e.g. contrasting locations, nutrients and irradiance; Eppley *et al.*, 1977). Legendre and Michaud (1999) notes that although the linear relationship was robust, it may not hold in extreme environments (e.g. areas with large continental organic inputs or polar seas during the winter night months). Although in this study no relationship between POC:b_{bp} was observed, a very clear relationship between Chl-*a*:POC was seen, enabling the estimation of POC from the fluorescence sensor on the glider.

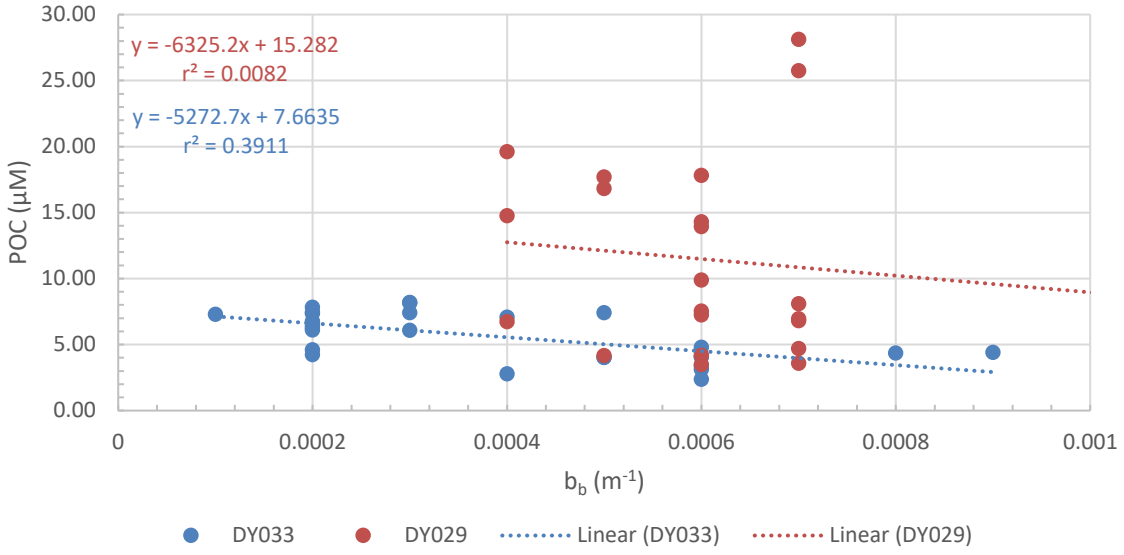

Figure 5.5: POC (µM) as a function of b_b (m^{-1}) measured from discrete CTD sampling and CTD casts within the SML at CCS during the spring (April 2015; orange dots) and summer (July 2015; blue dots) deployments.

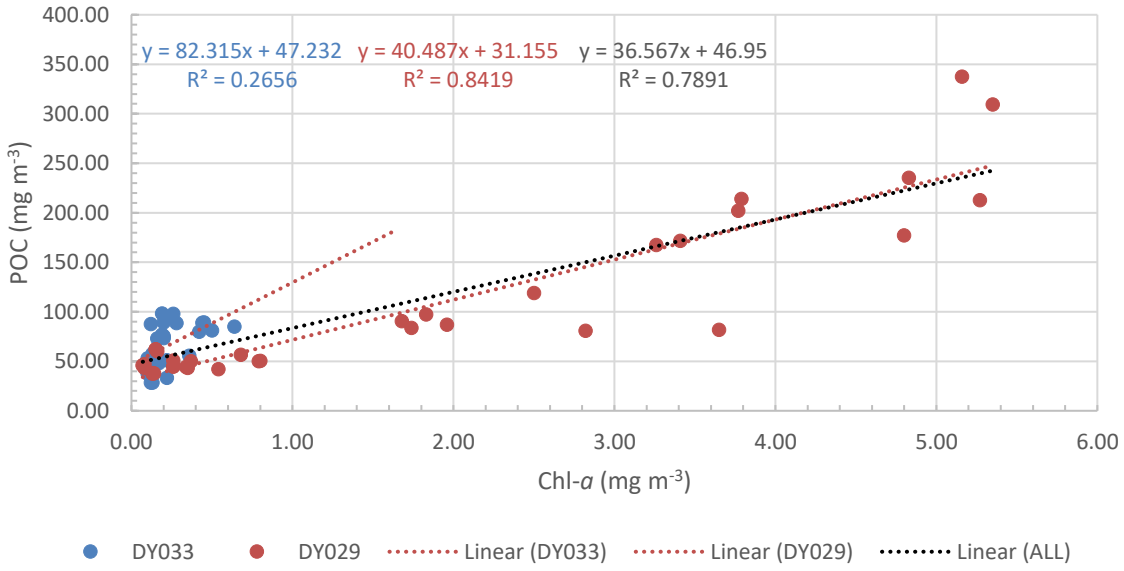

Figure 5.6: POC (mg m^{-3}) as a function of Chl-a (mg m^{-3}) measured from discrete CTD sampling at CCS during the spring (red; 4th to 25th April 2015) and summer (blue; 13th to 30th July 2015) deployments. The equation of the linear fit, r^2 black line is from the combination of both cruise data.

5.3.4 Phytoplankton carbon biomass

As with inventories of euphotic zone-integrated Chl-*a* and POC from discrete samples, CTD derived euphotic zone inventories of C_{phyto} (Table 5.3)showed a clear seasonal progression, with higher C_{phyto} values in April (180 (153-247) mmol C m^{-2}) than July (110 (79-200) mmol C m^{-2}; Table 5.1, Poulton et al., 2018). As this study used Chl-*a* to derive POC, from which C_{phyto} is then estimated, it is vital to compare observations collected from different platforms (e.g. discrete seawater samples and bio-optical sensors on the glider) and those estimated using different techniques (e.g. cell counts with pmol C averages and fluorescence data established using empirical relationships). When euphotic zone inventories of Chl-*a*, estimated from both discrete samples and glider measurements, were compared (Table 5.1), these were comparable during both deployments, with the exception of two outliers in April 15th and 25th April (2015). The variation observed between the two methods used to calculate C_{phyto} could likely be due to the natural variation between the two local water masses sampled by each platform method (note: glider was within 3.2 ± 5.4 km of CTD deployment) and/or the contribution of each individual measurement within a profile used in the calculation of the integration. Higher estimates of the euphotic zone Chl-*a* inventories were reported during the 15th and 25th April 2015 deployment from discrete water samples (Table 5.1; Poulton *et al.,* 2018), which were close to double those obtained from the glider during this time period. However, these higher inventories are similar to the Chl-*a* inventory from the glider during the peak of the bloom (17th April: 136.8 (128.8-142.5) mg m^{-2}; Figure 5.1c). While variation can be seen between the two methods, in general all glider observations and euphotic inventories during these periods were comparable. Taking the three Chl-*a* profiles from the glider closest in time to both the CTD profiles in question (15th & 25th April 2015), no variations in average Chl-*a* inventories from within the euphotic zone (3.1 ± 1.4 mg m^{-3} and 1.4 ± 0.7 mg m^{-3}) were observed. Moreover, using all the available glider profiles on the 2 days in question during the 'pre-dawn' time period (n=14 on 15th April and n=12 on the 25th April) the Chl-*a* inventories were similar to the three profiles closest in time to the CTD deployment within the 95 % confidence level (Table 5.1).

It is possible a single discrete sample (6 discrete samples were taken per cast) could have increased the euphotic zone inventory of Chl-*a*. In addition, the mean estimated Chl-*a* inventory from the glider incorporates more observations per cast (n = ~38) and more profiles within the 'pre-dawn' sampling window than discrete samples from one CTD cast used by Poulton *et al.* (2018; 02:00 – 06:00). Moreover, during this time period, the glider is observing not a single point but a wider spatial area (see Figure 2.1 for full glider deployment locations). Therefore, it can be argued the gilder data could be more representative of the water column and the spatial patchiness often seen with phytoplankton communities (1 to 10 km; Sharples *et al.,* 2001).

ThereforeCare must be taken when comparing (or to an extent calibrating) a derived value (e.g. POC) calculated from a relationship (e.g. POC:Chl-*a*) from high resolution glider data (increase in vertical and temporal resolution) to a single cast of limited discrete samples.

To derive C_{phyto} from the calculated POC concentrations, this study used two methods reported in the literature (Behrenfeld *et al.* 2005; Sathendranath *et al.,* 2009). reported yThe consideredb$_{bp}$) canused in this study using platform to greatly increase our observational capacity and provide first order

It must be noted that the processes used in the estimation of C_{phyto} was done using a two-step process (e.g. b_{bp}/Chl-*a* -> POC -> C_{phyto}), similar to other reported methods (e.g. Thomalla *et al*., 2017), and therefore any uncertainty at each stage will propagate through the calculations. The firstly methodology used is based on a study by Behrenfeld *et al.* (2005), who summarized ranges of field-based C_{phyto}:POC ratios from different studies (e.g. Eppley, Chavez and Barber, 1992; Durand, Olson and Chisholm, 2001; Gundersen *et al.*, 2001; Oubelkheir, 2001) in a range of oceanic regions (e.g. oligotrophic to eutrophic) to obtain an average phytoplankton contribution to total POC of ∼30 % (reported percentages ranged from 19 % to 49 %). Studies suggest that over seasonal cycles (Durand, Olson and Chisholm, 2001) and across oligotrophic to eutrophic conditions (Oubelkheir, 2001) phytoplankton contribute a relatively consistent fraction to POC. When applied to this study (30 % POC represents average phytoplankton contribution), estimates of euphotic zone inventories of C_{phyto} from glider observations were half that of estimates obtained from discrete samples (Table 5.1). While the derived POC estimates are within the same order of magnitude, using an literature based average (30 %) from different regions shows it is vital to consider the local characteristics. During both deployments the average phytoplankton contribution to total POC was 48 ± 12 % and 37 ± 13 % for April and July, respectively (calculated using the C_{phyto} from discrete water samples and POC). While these estimates are within the range reported by Behrenfeld *et al.* (2005), using the April and July average (48 ± 12 % and 37 ± 13 % respectively) an improvement in the comparability to discrete samples was observed (Table 5.1).

The second methodology used in this study was reported by Sathendranath *et al.* (2009), who suggested that any observation of POC could be partitioned into living organic carbon (e.g. phytoplankton) and a residual (heterotrophs and various detritus), and that an increase in the residual components would increase the total POC without increasing Chl-*a*. Therefore, at any observed Chl-*a* concentration, the lowest POC concentration observed represents the C_{phyto} associated with that Chl-*a* concentration. This relationship can be found using quantile regression (Koenker and Bassett, 1978). To find the regression for the lowest quantile consistent with the criterion of robustness, Rogers (1992) advises that the minimum quantile, q, should satisfy the

condition q > 5/n, where n is the total number of observations, therefore a 10th percentile was used (q = 0.1) whereby the line lies below 90 % of the observations. When (POC = 15.5108Chl-*a* + 108.8269), based on the Sathendranath *et al.* (2009) methodology, applied to this study, estimates of euphotic zone inventories of C_{phyto} from glider observations were shown to be bot comparable to discrete samples (r^2 = 0.47). This could be due to the fact that this methodology considers the local variability that a single average estimate could not, and that the lowest POC concentration observed represents the C_{phyto} associated, and therefore dampens the effect of higher POC concentrations caused by an increase in the residual components (e.g. heterotrophs and various detritus). 5.2of Particulate Organic Carbon

5.3of

5.4 Conclusions

Primary production within seasonal shelf seas, is controlled by water column structure and the availability of nutrients and light, and these characteristics vary seasonally. Phytoplankton biomass and therefore, the amount of carbon contributed to the POC pool by phytoplankton can vary on temporal and spatial times scales (Raymont, 1980; Simpson and Sharples, 2012). During the spring bloom (April 2015) Chl-*a* (and co-varying products) showed a good correlation with b_{bp} signal (r^2 = 0.62) and POC (r^2 = 0.79), but these parameters were decoupled during the summer, when the SCM was present (July 2015; Figure 5.3b). This results in poor estimates for POC and therefore C_{phyto} using established empirical relationships during the summer. During the spring bloom, conditions are suited to support faster growing phytoplankton with a larger cell size, which are carbon-rich (Poulton *et al.,* 2018) and therefore, contribute not only to the POC pool but also contribute to the b_{bp} signal within the surface layer, far away from the resuspension of finer sediment at the seabed. Coccolithophores, were also observed during the spring bloom period (data not shown; Mayers *et al.*, 2018), which contribute significantly to the b_{bp} signal (Balch *et al.,* 2001). The seasonal water column characteristics change during summer, whereby primary production and the hence, the main contribution to POC is confined to the SCM, which has lower light, and supply of nutrients from below the pycnocline (Chapter 4). During this time period, the b_{bp} signal is now not dominated by larger cells but mainly by bacterial influence (Poulton *et al.,* 2018) which contribute ~60% of the total primary production (Platt, Subba Rao and Irwin, 1983). In addition, the b_{bp} signal is dominated by resuspended sedimentary material due to the proximity with the BML (Figure 5.2b).

While care must be taken when comparing (or to an extent calibrating) a derived value (e.g. POC) calculated from a relationship (e.g. POC:Chl-*a*) from high resolution glider data collected over a large special area (~ 5 km^2) to a single cast of limited discrete samples, this study showed using bio-optical sensors on gliders can produce comparable values of POC (Table 5.2; $p > 0.05$) and Cphyto (Table 5.3; $p > 0.05$) to discrete samples from CTD casts. Therefore, using methodology that use established empirical relationships can be used to predict a first order estimation of POC, and thus C_{phyto}, in a dynamic shelf system indicating the potential for bio-optical sensors on gliders to be used in shelf seas. The use of bio-optically equipped ARGO floats has produced new data (BGC-Argo database; Barbieux, Organelli, *et al.*, 2017), that have shown to be a useful tool for the validation of remotely sensed bio-optical data within the case 1 waters of the open ocean (Blondeau-Patissier *et al.*, 2014). There are still many challenges to overcome with regards to bio-optical remote sensing in coastal areas (Loisel *et al.*, 2013) and it is therefore, important to develop methods capable of detecting biogeochemical properties from bio-optical instruments on autonomous platforms for the development and validating robust parameterisation of both remote sensing algorithms and numerical models. To be able to determine phytoplankton biomass, POC and C_{phyto} directly and to understand its seasonal variability, will improve not only the phytoplankton growth models within a dynamic shelf sea system (Souza, Holt and Proctor, 2007; Holt *et al.*, 2016, 2017) but will allow us to better evaluate the role of seasonal shelf seas, as CO_2 sinks through the continental shelf pump mechanism (Tsunogai, Watanabe and Sato, 1999; Thomas *et al.*, 2004; Takahashi *et al.*, 2009), in the global carbon cycle shelf seas play and how it might vary in the context of a changing climate (Behrenfeld *et al.*, 2006; Gruber *et al.*, 2010; Gruber, 2011; Honjo *et al.*, 2014).

Chapter 6: Summary and Future work

6.1 Introduction

The main objective of this thesis was to use novel wet chemical sensors to determine the temporal variability of nitrate + nitrite (hereafter defined as $\sum NO_x$), alongside established methods for estimating turbulence and the use of bio-optical sensors to determine the role of nitrate availability on primary production within an area of flat sea bed in a tidally active temperate shelf sea. To achieve this, a pair of autonomous underwater vehicles (Kongsberg Seaglider and Teledyne Slocum glider) were deployed to continuously profile at the central Celtic Sea sampling site (CCS; 49°24'N, 8°36'W; Figure 2.1) from the 4th to 29th April (2015), and from the 13th to 30th of July (2015), as part of the Shelf Seas Biogeochemistry program (SSB; http://www.uk-ssb.org/). On both gliders a suite of sensors for temperature, conductivity and pressure were installed. The Seaglider (Kongsberg) also had a fluorescence sensor, optical backscatter and LoC $\sum NO_x$ sensor, while the Slocum (Teledyne) also measured turbulent velocity using a microstructure profiler. Auxiliary data was used to compliment and calibrate data collected by the gliders, and consisted of tidal and meteorological data, nutrients, Particulate Organic Carbon (POC) and chlorophyll-*a* concentrations (Chl-*a*), collected from a mooring and seabed frame, and periodic CTD and discrete bottle sampling from the *R.S.S Discovery* at CCS. During the two continuous deployments the gliders were able to observe physical and biogeochemical parameters at high resolution producing ~1500 profiles ever ~40 minutes to a depth of ~140 meters. These glider deployments took place during the spring bloom (April 2015) and when a sub-surface chlorophyll maximum was present (SCM; July 2015). High resolution data from these deployments provided new insights into the physico-chemical and biological cycling during these vital periods for shelf sea primary production and are outlined below.

The thesis produced 4 main findings:

1. A wet chemical microfluidic Lab-on-Chip (LoC) nutrient sensor was shown to be able to accurately determine $\sum NO_x$ with excellent agreement with traditional discreet water sample methods (r^2 = > 0.98; n = 151; p = < 0.001) (Vincent *et al.,* 2018)

2. High resolution estimations of the diapycnal flux of $\sum NO_x$ ($f\sum NO_x$) into the base of the SCM reported in this study (4.2 mmol m^{-2} d^{-1}) were shown to be double that of previously reported values (~2 mmol m^{-2} d^{-1}) in the Celtic Shelf Sea
3. The contribution of new production estimated in this study supported by the $f\sum NO_x$ into the SCM (58 (21-80) g C m^{-2}) could support all the estimated annual new production of 81.8 g C m^{-2} in the Celtic Sea solely in the SCM during the summer period (120 days)
4. Within a dynamic shelf region, established empirical bio-optical relationships can be used to estimate POC from Chl-*a* and therefore predict phytoplankton carbon (C_{phyto}), during the spring bloom and summer SCM from bio-optical sensors deployed on a glider

6.2 Integrating a wet chemical LoC in an autonomous underwater glider

For the first time a novel wet chemical LoC $\sum NO_x$ sensor (Ocean Technology and Engineering group, National Oceanographic Centre, UK) was integrated and successfully deployed in an autonomous underwater Seaglider for two cruises in a shelf sea system, lasting 18 and 21 days during April and July (2015), respectively. During these deployments the LoC $\sum NO_x$ sensor produced 619 & 457 blank (artificial seawater; n = 155 & 78) and standard (NO_3^-; n = 199 & 97) corrected $\sum NO_x$ measurements. An excellent agreement between LoC $\sum NO_x$ sensor measurements and autoanalyzer analysis of discrete water samples was shown (Figure 3.2), with a correlation of r^2 = > 0.99 (n = 9; p = < 0.001) when deployed on a CTD rosette and an estimated analytical uncertainty of 0.14 µM (n = 10). When profiles from each platform were compared (1 – 10 hr window; ±3 metersdepth ; < 2km between profiles), again a good correlation was observed, r^2 = > 0.98 (n = 51; p = < 0.001), with an average estimated analytical uncertainty for the LoC $\sum NO_x$ sensor during this period of 0.19 µM (n = 142).

Over the 21-day April (2015) deployment the LoC $\sum NO_x$ sensor was able to accurately capture the large drawdown of $\sum NO_x$ within the surface mixed layer due to the onset of the spring bloom (Figure 3.4). Concentrations decreased from 5.74 µM (4^{th}) to 1.42 µM (25^{th}), whilst bottom layer NO_3^- concentrations remained constant (6.86 ±0.16 µM) (continuous sampling for 18days)

The temporal and spatial variability of biogeochemical processes has previously been successfully measured using remote sensing, time series moorings and ship-based methods, but these, to an extent, fall short in resolving the dynamic temporal and spatial elements with long-term endurance in a low-cost package. Therefore, there has been a strong call for the development of biogeochemical sensors to be deployed on stationary and mobile platforms, to provide *in situ* measurements as part of sensor networks aimed at providing long term monitoring within a low-resource package (Johnson *et al.*, 2009; Adornato *et al.*, 2010). The LoC $\sum NO_x$ sensor deployed within the Seaglider in this study clearly demonstrates that nitrate & nitrite can be accurately determined over monthly timescales due to the sensor's low resource use, small size and *in situ* calibration abilities. Moreover, deployed within a glider with other physical and biochemical data (e.g. CTD and the WetLabs Triplet sensor measurements), it provided a powerful tool for resolving dynamic biogeochemical processes within a dynamic shelf system.The research presented in this Chapter 3 has been published in *Marine Chemistry*:

Vincent, A.G., Pascal, R.W., Beaton, A., Walk, J., Hopkins, J.E., Woodward, E.M.S., Mowlem, M. and Lohan, M.C. (2018), Nitrate drawdown during a shelf sea spring bloom revealed using a novel microfluidic in-situ chemical sensor deployed within an autonomous underwater glider, *Mar. Chem.* https://doi.org/10.1016/j.marchem.2018.07.005.

6.3 Quantifying new production supported by the flux of $\sum NO_x$ into the SCM during summer

- In Chapter 4 high resolution $\sum NO_x$ and dissipation of turbulent kinetic energy observations were made during summer (21 days; July 2015) using a Microrider microstructure package (Rockland Scientific) and LoC $\sum NO_x$ sensor deployed on a Slocum glider and Seaglider, allowing the investigation of how the flux of $\sum NO_x$ across the pycnocline drives new production within the sub-surface chlorophyll maximum (SCM). This methodology allowed for the continuous observation over a 21-day time period over a flat seabed in a shelf sea system (one profile every ~ 40 minutes; 1226 total profiles), therefore increasing the observational ability to capture highly dynamic fluxes of $\sum NO_x$ into the base of the SCM, which had not been achieved in previous studies within the Celtic Shelf Sea. (e.g. Sharples *et al.* 2007) 1-61-2 and reported an average background range of 1-2 mmol m^{-2} d^{-1} in the Celtic Sea. By subsampling the f$\sum NO_x$ dataset of this study for periods of 12 and 24 hrs on spring and neap tides (similar periods reported in previous studies; e.g. Sharples *et al.,* 2007 and Williams *et al.,* 2013)…

- Compare to different subsamples… Is there a different magnitude? What's the variability like? Are the subsamples similar to those of previous studies?

as estimates are not based on smaller datasets biased to short sampling windows to reduce uncertainty and Table 6.1: Average Flux of ∑NOx across the pycnocline

Using this methodology we were able to estimate a more representative average f$\sum NO_x$ at the pycnocline, which included the contributions of semi-diurnal and spring-neap variability and the augmentation of higher fluxes of $\sum NO_x$ (Figure 4.6), caused by the episodic increase of turbulence at the pycnocline. By having a more representative average f$\sum NO_x$ estimate we were able to reliably estimate the potential of the f$\sum NO_x$ to support new production in the SCM during the summer growth period in a shelf sea environment. The temporal average (4.2 ± 6.4 mmol m^{-2} d^{-1}) was dominated by short mixing events that could potentially supply larger (> 15 mmol m^{-2} d^{-1}) intermittent fluxes of $\sum NO_x$ into the SCM. The deployment average was double (~4 mmol m^{-2} d^{-1}) that of previously reported averages (~2 mmol m^{-2} d^{-1}) in the Celtic Sea, likely due to the contribution of a number of higher f$\sum NO_x$ pulses around the transition into, and including, the spring tide period (Figure 4.6; 15th to 21st July 2015). Using the spring and neap tide f$\sum NO_x$ estimates to represent the envelope limits, the contribution of new production supported by the f$\sum NO_x$ into the SCM during the summer period (120 days) reported in this study is 58 (21-80) g C m^{-2} could support all of the estimated annual new production of 81.8 g C m^{-2} in the Celtic Sea (reported by Joint *et al.* (2001)). If this under-estimation of the contribution of the summer SCM to the annual new production shown here in the Celtic Shelf Sea is indicative of all other continental shelf seas of the Northern Hemisphere, then their estimated ability to be net sinks of CO_2 (−0.24 Pg C yr^{-1}; Laruelle *et al.*, 2010) could be underestimated.

This research will be submitted to *Geophysical Research Letters.*

6.4 Assessing the estimation of particulate organic carbon and phytoplankton carbon biomass from glider chlorophyll-a observations

In Chapter 5, high resolution Chl-*a* and particulate backscatter (b_{bp}) observations were made during both the spring bloom (18 days; April 2015) and summer sub-surface chlorophyll maximum (SCM; 21 days; July 2015), using a WetLabs Triplet ECOPuck (BBFL2VMT; WetLabs,

USA;) deployed on a Seaglider. By applying established empirical bio-optical relationships to the bio-optical sensors deployed on a Seaglider enabled an investigation of seasonal phytoplankton biomass, particulate organic carbon (POC) and phytoplankton carbon (C_{phyto}) dynamics. The validation of applying these established empirical bio-optical relationships to the bio-optical sensors deployed on a Seaglider, was undertaken by comparing estimated euphotic zone inventories of Chl-*a*, POC and C_{phyto}, measured from discrete seawater bottle samples taken periodically at CCS during the two time periods. Both discrete samples and glider measurements were comparable (Table 5.1), apart from two larger outliers in April 15th and 25th April (2015). The variation observed between the two methods used to calculate C_{phyto} could likely be due to the natural variation between the two local water masses sampled by each platform method (note: glider was within 3.2 ± 5.4 km of CTD deployment) and/or the contribution of each individual measurement within a profile used in the calculation of the integration.

While in the open ocean, b_{bp} generally covaries with POC, and is therefore used as a proxy (Loisel *et al.*, 2002), POC discrete bottles samples showed no relationship to their respective b_{bp} measurements from either the glider or the CTD in this study, therefore this methodology was not valid. This study did, however, observe a strong correlation between POC and Chl-*a* concentrations (r^2= 0.79; $p < 0.001$), and, by using the POC:Chl-*a* relationship, estimates of POC concentrations were derived from glider bio-optical data (e.g. fluorescence). During the spring bloom (April 2015) Chl-*a* concentrations (and co-varying products) also showed a good correlation with b_{bp} signal (r^2 = 0.62), but both these parameters were decoupled during the summer, when the SCM was present (July 2015; Figure 5.3b). This resulted in poor estimates for POC and hence C_{phyto} using established empirical relationships during the summer. We hypotheses this was because the b_{bp} signal was no longer dominated by larger cells but mainly by bacterial influence (Poulton *et al.,* 2018) which can contribute ~60% of the total primary production (Platt, Subba Rao and Irwin, 1983). In addition, the b_{bp} signal is dominated by resuspended sedimentary material due to the proximity with the BML (Figure 5.2b). This work highlighted the potential for the application, established empirical bio-optical relationships can be used to estimate POC from Chl-a and therefore predict C_{phyto}, during the spring bloom and potentially the summer SCM from bio-optical sensors deployed on a glider within a dynamic shelf region.

6.5

novel LoC nutrient sensor.W in blank corrected samples (limited to 24 measurements per cast, non-continuous over longer timescales), it's vertical resolution has two limitations. Firstly,

un-like the CTD cast methodology which the users have the ability to control where a sample is taken (setting the pressure at which a Niskin bottle will fire) the LoC and Glider setup is currently unable to do so. Therefore the user is unable to focus in on a boundary of interest in any great detail (i.e. the base of the thermocline with a thickness) or to be able to

er (< 6 day deployments)Equation 4.6; density unlocked densityWhile this studyfollowed the method of these previous studies,there was the upon themby of biogeochemical and mixing measurements using the density to calculate at the base of the SCMUnfortunately, the set differencebetween the slopes into 6 day periods (Figure 4.1). I 4.2using this by and should be prioritised in future workBoth deployments but er (> 4 weeks) fully due to low power levels in the battery. A longer deployment period could provide in-sight into reagent longevity, the power draw of the LoC on the Gliders , the decrease in efficiency of the cadmium column in a real-world use testpotential of the 0.45µ sample filter (who deployed gliders)inputacurrent project. The project is undertaking sustained multi-glider deployments, to provide a detailed methodology of the deployment strategy, piloting, and calibration process. The analysis will deliver methods for the synoptic interpretation of all ocean variables over multiple timescales and has already deployed 22 gliders over 17 months (Palmer *et al.,* 2018)Once the work has been published it will hopefully shed some light on the true long-term capabilities of a LoC and to set a baseline of which to improve.

6.6 Future Work

Since the practical components of this study, $\sum NO_x$ sensors and other analyte versions (e.g. pH, PO_4 and silicate) have been successfully deployed within glacial runoff (~14 days), a freshwater ecosystem (River Avon, UK; 63 days), an estuarine system (Southampton waters, UK; > 56 days) and in the subtropical oligotrophic waters of Kaneohe Bay (Hawaii, USA; 30 days; Beaton *et al.*, 2017b; Clinton-Bailey *et al.*, 2017; Grand *et al.*, 2017). All of these were on stationary platforms unlike this study which used an AUV for the first time. However, with further developments currently being undertaken to improve the analytical capabilities of the LoC sensor platform (e.g. chip architecture, filters, runtime methodology), this opens up the possibility for a swarm of gliders to be deployed equipped with a full contingent of macronutrient LoC sensors. Having a sensor suite such as this on an autonomous platform provides an opportunity for high resolution data sets producing blank and standard corrected macronutrients observations with a low operational resource footprint and the analytical strengths of wet chemical analysis (e.g. lower analytical uncertainty and limit of detection). It must also be mentioned that within the

field of microfluidics there have been new research ideas that, although currently in their infancy, could result in an increase in the resolution of wet chemical microfluidics. Nightingale *et al.* (2017) reported the use of a methodology using a micropump to form droplets, whereby droplet generation was achieved using the pulsatile nature of peristaltic pumps to deliver temporally separated oil and aqueous phases like that seen in traditional segmented flow analysis. This could have the potential for a wet chemical LoC sensor to undertake continuous sample analysis with a droplet generation frequency of ~ 0.2Hz, allowing for a blank and standard corrected $\sum NO_x$ measurement every ~2 meters, assuming the average vertical velocity of a glider is ~0.1m s^{-1} (Rudnick *et al.*, 2004; Nightingale, *per. comm.*). This would allow for new insight into the vertical structure of biogeochemical variables akin to the resolution of physical sensors (e.g. temperature, salinity etc.).

This research has proved that, by integrating a LoC nutrient sensor in an autonomous glider it is possible to undertake continuous high-resolution observations for just under one month. From this, the next progressive steps are to firstly undertake longer deployments, and secondly to integrate the LoC nutrients sensors into the growing selection of autonomous marine vehicles worldwide. Integration with an array of autonomous vehicles that are non-ship-dependent, such as submersible platforms like the Autosub LR (Furlong *et al.*, 2012) and Slocum (Jones, 2012), and surface vehicles such as the AutoNaut (Johnston and Poole, 2017), ASV C-Enduro (*ASV Global*, 2018) and Waveglider (Hine *et al.*, 2009), would increase our observational capabilities in a temporal and spatial scale between moorings, ship-based observations and remote sensing platforms in an array of different operational capacities. Back-to-back seasonal deployments for multiple years in the setting of a shelf sea ecosystem would allow for investigation into events and processes such as the autumn bloom (Pingree *et al.*, 1976a), on-shelf advection (Stabeno and Meurs, 1999; Hydes *et al.*, 2004), remineralisation, and even shelf systems with a higher pycnocline flux potential (e.g. New Zealand; Sharples *et al.,*2001), and the year-on-year variation of macronutrient inventories (Proctor, Chen and Tett, 2003; Humphreys *et al.*, 2018). With the addition of oxygen and bio-optical sensors, measuring beam attenuation, and backscatter and irradiance alongside nutrient sensors a rich dataset observing the spatial and temporal variability of parameters such as plankton community composition, primary and net community production, and export efficiency would provide a fuller picture of the biological carbon cycle within the shelf sea (Alkire *et al.*, 2012; Cetinić *et al.*, 2015; Hemsley *et al.*, 2015; Briggs *et al.*, 2018). Similarly, within other regions these deployments would provide new insights into biogeochemical areas of interest such as within gyres and eddies (Sherwin *et al.*, 2012; Thomsen *et al.*, 2015), oxygen minimum zones (Breitburg *et al.*, 2018) or in low nutrient and chlorophyll regions (Karl and Letelier, 2008). These types of investigations would provide insights into the processes controlling

primary production in globally significant shelf sea systems and beyond, and aid in models predicting the ecosystem and biogeochemical responses to climate-driven variations and anthropogenic pressures.

The data availability in continental shelf seas is strongly biased towards the temperate regions of the Northern Hemisphere, countries with larger research budgets, and during operationally favourable seasons. Therefore, key shelf sea systems in the higher latitudes are currently severely under-sampled. The ability of the LoC nutrient platform to function remotely for extended periods of time within a polar setting has been proved by Beaton *et al.* (*per. comm.*; 2017), whereby a LoC nutrient sensor was deployed within glacial runoff and on a mooring during a yearlong deployment off the coast of Svalbard. By combing autonomous gliders, moorings, and landers, an array of biogeochemical sensors could be deployed to observe the inputs of glacial meltwaters, pelagic and benthic components within the coastal regions, and transects out across the continental shelf. This would allow us to greatly improve our understanding of the variability within the complex biogeochemical system of the polar coastal and continental shelf regions that are already strongly influenced by the changing climate (Schofield *et al.*, 2010; Kaufman *et al.*, 2014; Randelhoff, Sundfjord and Reigstad, 2015).

List of Reference

Adornato, L., Cardenas-Valencia, A., Kaltenbacher, E., Byrne, R., Daly, K., Larkin, K., Hartman, S., Mowlem, M., Prien, R. and Garcon, V. (2010). 'In Situ Nutrient Sensors for Ocean Observing Systems', In: Hall, J., Harrison, D. E., and Stammer, D. (eds) *Proceedings of OceanObs'09: Sustained Ocean Observations and Information for Society*. European Space Agencey, pp. 9–18. doi: 10.5270/OceanObs09.cwp.01.

Aiken, J., Bruce, R. H. and Lindley, J. A. (1977). 'Ecological Investigations with the Undulating Oceanographic Recorder : The Hydrography and Plankton of the Waters Adjacent to the Orkney and Shetland Islands', *Marine Biology,* 39(1), pp. 77–91.

Alkire, M. B., D'Asaro, E., Lee, C., Jane Perry, M., Gray, A., Cetinić, I., Briggs, N., Rehm, E., Kallin, E., Kaiser, J. and González-Posada, A. (2012). 'Estimates of net community production and export using high-resolution, Lagrangian measurements of O 2, NO 3-, and POC through the evolution of a spring diatom bloom in the North Atlantic', *Deep-Sea Research Part I: Oceanographic Research Papers*, 64, pp. 157–174. doi: 10.1016/j.dsr.2012.01.012.

Arrigo, K. R. (2005). 'Marine microorganisms and global nutrient cycles', *Nature,* 437, pp. 349–355. doi: 10.1038/nature04158.

ASV Global (2018). Available at: http://www.asvglobal.com (Accessed: 16 December 2018).

Babin, Marcel, Morel, André, Fournier-Sicre, Vincent, Fell, Frank, Stramski, Dariusz, (2003). 'Light scattering properties of marine particles in coastal and open ocean waters as related to the particle mass concentration', *Limnology and Oceanography*, 2, doi: 10.4319/lo.2003.48.2.0843.

Balch, W. M., Bowler, B. C., Drapeau, D. T., Lubelczyk, L. C. and Lyczkowski, E. (2018) .'Vertical Distributions of Coccolithophores, PIC, POC, Biogenic Silica, and Chlorophyll a Throughout the Global Ocean', *Global Biogeochemical Cycles*, 32(1), pp. 2–17. doi: 10.1002/2016GB005614.

Balch, W. M., Drapeau, D., Bowler, B. and Booth, E. (2007). 'Prediction of pelagic calcification rates using satellite measurements', *Deep Sea Research Part II Tropical Studies in Oceanography,* 54(5-7), pp. 478–495. doi: 10.1016/j.dsr2.2006.12.006.

Barbieux, M., Uitz, J., Bricaud, A., Organelli, E., Poteau, A., Schmechtig, C., Claustre, H. (2018). 'Assessing the variability in the relationship between the particulate backscattering coefficient and the chlorophyll a concentration from a global Biogeochemical-Argo database'. *Journal of Geophysical Research: Oceans*, 123, 1229– 1250. https://doi.org/10.1002/2017JC013030

Bauer, J. E., Cai, W. J., Raymond, P. A., Bianchi, T. S., Hopkinson, C. S. and Regnier, P. A. G. (2013). 'The changing carbon cycle of the coastal ocean', *Nature*, 504(7478), pp. 61–70. doi: 10.1038/nature12857.

Baumgartner, M. F. and Fratantoni, D. M. (2008). 'Diel periodicity in both sei whale vocalization rates and the vertical migration of their copepod prey observed from ocean gliders', *Limnology and Oceanography*, 53(5part2), pp. 2197–2209. doi: 10.4319/lo.2008.53.5_part_2.2197.

Beaton, A. D., Cardwell, C. L., Thomas, R. S., Sieben, V. J., Legiret, F.-E., Waugh, E. M., Statham, P. J., Mowlem, M. C. and Morgan, H. (2012). 'Lab-on-chip measurement of nitrate and nitrite for in situ analysis of natural waters.', *Environmental science & technology*. doi: 10.1021/es300419u.

Beaton, A. D., Sieben, V. J., Floquet, C. F. a., Waugh, E. M., Abi Kaed Bey, S., Ogilvie, I. R. G., Mowlem, M. C. and Morgan, H. (2011). 'An automated microfluidic colourimetric sensor applied in situ to determine nitrite concentration', *Sensors and Actuators B: Chemical*. Elsevier B.V.,

156(2), pp. 1009–1014. doi: 10.1016/j.snb.2011.02.042.

Beaton, A. D., Wadham, J. L., Hawkings, J., Bagshaw, E. A., Lamarche-Gagnon, G., Mowlem, M. C. and Tranter, M. (2017). 'High-Resolution in Situ Measurement of Nitrate in Runoff from the Greenland Ice Sheet', *Environmental Science & Technology*. doi: 10.1021/acs.est.7b03121.

Behrenfeld, M. J. and Boss, E. (2003). 'The beam attenuation to chlorophyll ratio : an optical index of phytoplankton physiology in the surface ocean ?', 50, pp. 1537–1549. doi: 10.1016/j.dsr.2003.09.002.

Behrenfeld, M. J., Boss, E., Siegel, D. A. and Shea, D. M. (2005). 'Carbon-based ocean productivity and phytoplankton physiology from space', *Global Biogeochemical Cycles*, 19(1), pp. 1–14. doi: 10.1029/2004GB002299.

Behrenfeld, M. J., O'Malley, R. T., Siegel, D. a, McClain, C. R., Sarmiento, J. L., Feldman, G. C., Milligan, A. J., Falkowski, P. G., Letelier, R. M. and Boss, E. S. (2006). 'Climate-driven trends in contemporary ocean productivity', *Nature*, 444(7120), pp. 752–5. doi: 10.1038/nature05317.

Birchill, A. J., Milne, A., S. Woodward, E. M., Harris, C., Annett, A., Rusiecka, D., Achterberg, E. P., Gledhill, M., Ussher, S. J., Worsfold, P. J., Geibert, W. and Lohan, M. C. (2017) .'Seasonal iron depletion in temperate shelf seas', *Geophysical Research Letters*, (3), pp. 8987–8996. doi: 10.1002/2017GL073881.

Bishop, J. K. B. and Wood, T. J. (2009). 'Year-round observations of carbon biomass and flux variability in the Southern Ocean', *Global Biogeochemical Cycles,* 23(March), pp. 1–12. doi: 10.1029/2008GB003206.

Blondeau-Patissier, D., Gower, J. F. R., Dekker, A. G., Phinn, S. R. and Brando, V. E. (2014). 'A review of ocean color remote sensing methods and statistical techniques for the detection, mapping and analysis of phytoplankton blooms in coastal and open oceans', *Progress in Oceanography*, 123, pp. 123–144. doi: 10.1016/j.pocean.2013.12.008.

Borges, A. V., Delille, B. and Frankignoulle, M. (2005). 'Budgeting sinks and sources of CO 2 in the coastal ocean: Diversity of ecosystems counts', *Geophysical Research Letters*, 32(14), p. n/a-n/a. doi: 10.1029/2005GL023053.

Boss, E. and Behrenfeld, M. (2010). 'In situ evaluation of the initiation of the North Atlantic phytoplankton bloom', 37(June), pp. 1–5. doi: 10.1029/2010GL044174.

Boss, E. and Pegau, W. S. (2001). 'Relationship of light scattering at an angle in the backward direction to the backscattering coefficient', *Applied Optics*, 40(30), p. 5503. doi: 10.1364/AO.40.005503.

Breitburg, D., Levin, L. A., Oschlies, A., Grégoire, M., Chavez, F. P., Conley, D. J., Garçon, V., Gilbert, D., Gutiérrez, D., Isensee, K., Jacinto, G. S., Limburg, K. E., Montes, I., Naqvi, S. W. A., Pitcher, G. C., Rabalais, N. N., Roman, M. R., Rose, K. A., Seibel, B. A., Telszewski, M., Yasuhara, M. and Zhang, J. (2018). 'Declining oxygen in the global ocean and coastal waters', *Science*, 359(6371), p. eaam7240. doi: 10.1126/science.aam7240.

Brewer, P. G. and Riley, J. P. (1965). 'The automatic determination of nitrate in sea water', *Deep Sea Research and Oceanographic Abstracts*, 12(6), pp. 765–772. doi: 10.1016/0011-7471(65)90797-7.

Briggs, N., Guemundsson, K., Cetinić, I., D'Asaro, E., Rehm, E., Lee, C. and Perry, M. J. (2018). 'A multi-method autonomous assessment of primary productivity and export efficiency in the springtime North Atlantic', *Biogeosciences*, 15(14), pp. 4515–4532. doi: 10.5194/bg-15-4515-2018.

Le Bris, N., Sarradin, P. M., Birot, D. and Alayse-Danet, a. M. (2000). 'A new chemical analyzer for in situ measurement of nitrate and total sulfide over hydrothermal vent biological communities', *Marine Chemistry*, 72(1), pp. 1–15. doi: 10.1016/S0304-4203(00)00057-8.

Butenschon, M., Clark, J., Aldridge, J. N., Icarus Allen, J., Artioli, Y., Blackford, J., Bruggeman, J., Cazenave, P., Ciavatta, S., Kay, S., Lessin, G., Van Leeuwen, S., Van Der Molen, J., De Mora, L., Polimene, L., Sailley, S., Stephens, N. and Torres, R. (2016). 'ERSEM 15.06: A generic model for marine biogeochemistry and the ecosystem dynamics of the lower trophic levels', *Geoscientific Model Development*, 9(4), pp. 1293–1339. doi: 10.5194/gmd-9-1293-2016.

Cai, W. J., Dai, M. and Wang, Y. (2006). 'Air-sea exchange of carbon dioxide in ocean margins: A province-based synthesis', *Geophysical Research Letters*, 33(12). doi: 10.1029/2006GL026219.

Carrillo, L., Souza, A. J., Hill, A. E., Brown, J., Fernand, L. and Candela, J. (2005). 'Detiding ADCP data in a highly variable shelf area: The Celtic Sea', *Journal of Atmospheric and Oceanic Technology*, 22(1), pp. 84–97. doi: 10.1175/JTECH-1687.1.

Castelao, R., Glenn, S., Schofield, O., Chant, R., Wilkin, J. and Kohut, J. (2008). 'Seasonal evolution of hydrographic fields in the central Middle Atlantic Bight from glider observations', *Geophysical Research Letters*, 35(3), pp. 6–11. doi: 10.1029/2007GL032335.

Cetinić, I., Perry, M. J., D'Asaro, E., Briggs, N., Poulton, N., Sieracki, M. E. and Lee, C. M. (2015). 'A simple optical index shows spatial and temporal heterogeneity in phytoplankton community composition during the 2008 North Atlantic Bloom Experiment', *Biogeosciences*, 12(7), pp. 2179–2194. doi: 10.5194/bg-12-2179-2015.

Cetinić, I., Toro-Farmer, G., Ragan, M., Oberg, C. and Jones, B. H. (2009). 'Calibration procedure for Slocum glider deployed optical instruments.', *Optics express*, 17(18), pp. 15420–15430. doi: 10.1364/OE.17.015420.

Chen, C. A. and Borges, A. V (2009). 'Deep-Sea Research II Reconciling opposing views on carbon cycling in the coastal ocean : Continental shelves as sinks and near-shore ecosystems as sources of atmospheric CO2', 56, pp. 578–590. doi: 10.1016/j.dsr2.2008.12.009.

Chester, R. and Jickells, T. (2012). Nutrients, Oxygen, Organic Carbon and the Carbon Cycle in Seawater. In: Marine Geochemistry (eds R. Chester and T. Jickells). doi:10.1002/9781118349083.ch9

Church, M. J., Lomas, M. W. and Muller-karger, F. (2013) .'Deep-Sea Research II Sea change : Charting the course for biogeochemical ocean time-series research in a new millennium', *Deep-Sea Research Part II*, 93, pp. 2–15. doi: 10.1016/j.dsr2.2013.01.035.

Claustre, H., Claustre, H., Claustre, H., Claustre, H., Claustre, H., Claustre, H., Claustre, H., Claustre, H., Claustre, H., Claustre, H., Claustre, H., Claustre, H. and Claustre, H. (2010) .'Bio-Optical Profiling Floats as New Observational Tools for Biogeochemical and Ecosystem Studies: Potential Synergies with Ocean Color Remote Sensing.', *Proceedings of OceanObs'09: Sustained Ocean Observations and Information for Society*, (1), pp. 177–183. doi: 10.5270/OceanObs09.cwp.17.

Clinton-Bailey, G. S., Grand, M. M., Beaton, A. D., Nightingale, A. M., Owsianka, D. R., Slavik, G. J., Connelly, D. P., Cardwell, C. L. and Mowlem, M. C. (2017). 'A Lab-on-Chip Analyzer for *in Situ* Measurement of Soluble Reactive Phosphate: Improved Phosphate Blue Assay and Application to Fluvial Monitoring', *Environmental Science & Technology*, 51(17), pp. 9989–9995. doi: 10.1021/acs.est.7b01581.

Council, N. R. (2011). *Assessing the Requirements for Sustained Ocean Color Research and Operations*. Washington, DC: The National Academies Press. doi: 10.17226/13127.

Cullen, J. J. (2015). 'Subsurface chlorophyll maximum layers: enduring enigma or mystery solved?', *Annual review of marine science*, 7, pp. 207–39. doi: 10.1146/annurev-marine-010213-135111.

Dafner, E. V. (2015). 'Segmented continuous-flow analyses of nutrient in seawater: Intralaboratory comparison of Technicon AutoAnalyzer II and Bran+Luebbe Continuous Flow AutoAnalyzer III', *Limnology and Oceanography: Methods*, 13(10), pp. 511–520. doi: 10.1002/lom3.10035.

Daly, K. L., Byrne, R. H., Dickson, A. G., Gallager, S. M. and Tivey, M. K. (2004). 'Chemical and Biological Sensors for Time-Series Research : Current Status and New Directions', *Marine Technology Society Journal,* 38(2), pp. 121–143.

Daly, K. L., Byrne, R. H., Dickson, A. G., Gallager, S., Perry, M. J. and Tivey, M. K. (2004).'Chemical and Biological Sensors for time series research: current status and new directions', *Marine Technology Society Journal*, 38(2), pp. 121–143.

Davidson, K., Gilpin, L. C., Pete, R., Brennan, D., McNeill, S., Moschonas, G. and Sharples, J. (2013). 'Phytoplankton and bacterial distribution and productivity on and around Jones Bank in the Celtic Sea', *Progress in Oceanography*, 117, pp. 48–63. doi: 10.1016/j.pocean.2013.04.001.

Davis, C. E., Blackbird, S., Wolff, G., Woodward, M. and Mahaffey, C. (2018). 'Seasonal organic matter dynamics in a temperate shelf sea', *Progress in Oceanography*. doi: 10.1016/j.pocean.2018.02.021.

Davis, R. E., Ohman, M. D., Rudnick, D. L., Sherman, J. T. and Hodges, B. a (2008). 'Glider surveillence of physics and biology in the southern California Current System', *Limnol. Oceanogr.*, 53(5, part 2), pp. 2151–2168. doi: 10.4319/lo.2008.53.5_part_2.2151.

Delory, E. and Haugan, P. M. (2016). 'Cost and value of multidisciplinary fixed-point ocean observatories', *Marine Policy*, 71(September), pp. 138–146. doi: 10.1016/j.marpol.2016.05.029.

Dickey, T. D., Itsweire, E. C., Moline, M. and Perry, M. J. (2008). 'Introduction to the Limnology and Oceanography Special Issue on Autonomous and Lagrangian Platforms and Sensors (ALPS)', *Limnology and Oceanography*, 53, pp. 2057–2061. doi: 10.4319/lo.2008.53.5_part_2.2057.

Dugdale, R. C. and Goering, J. J. (1967). 'Uptake of New and Regenerated Forms of Nitrogen in Primary Productivity', *Limnology and Oceanography*, 12(2), pp. 196–206. doi: 10.4319/lo.1967.12.2.0196.

Durand, M. D., Olson, R. J. and Chisholm, S. W. (2001). 'Phytoplankton population dynamics at the Bermuda Atlantic Time-series station in the Sargasso Sea', *Deep-Sea Research Part II: Topical Studies in Oceanography*, 48(8–9), pp. 1983–2003. doi: 10.1016/S0967-0645(00)00166-1.

Dutt, J. and Davis, J. (2002).'Current strategies in nitrite detection and their application to field analysis', *Journal of Environmental Monitoring,* 4(3), pp. 465–471. doi: 10.1039/B202670H.

Eppley, R. W., Chavez, F. P. and Barber, R. T. (1992). 'Standing stocks of particulate carbon and nitrogen in the equatorial Pacific at 150°W', *Journal of Geophysical Research*, 97(C1), pp. 655–661. doi: 10.1029/91JC01386.

Eppley, R. W., Harrison, W. G., Chisholm, S. W. and Stewart, E. (1977). 'Particulate organic matter in surface waters off Southern California and its relationship to phytoplankton', *Journal of Marine. Research*, (35), pp. 671–696.

Eppley, R. W., Rogers, J. N. and Mccarthy, J. J. (1969). 'Half-Saturation Constants for Uptake of Nitrate and Ammonium by Marine Phytoplankton', *Limnology and Oceanography*, 14(6), pp. 912–920. doi: 10.4319/lo.1969.14.6.0912.

Eriksen, C. C., Osse, T. J., Light, R. D., Wen, T., Lehman, T. W., Sabin, P. L., Ballard, J. W. and Chiodi, A. M. (2001). 'Seaglider: A long-range autonomous underwater vehicle for oceanographic research', *IEEE Journal of Oceanic Engineering*, 26(4), pp. 424–436. doi: 10.1109/48.972073.

Esaias, W. E., Abbott, M. R., Barton, I., Brown, O. B., Campbell, J. W., Carder, K. L., Clark, D. K., Evans, R. H., Hoge, F. E., Gordon, H. R., Balch, W. M., Letelier, R. and Minnett, P. J. (1998). 'An Overview of MODIS Capabilities for Ocean Science Observations', *IEEE Transactions on Geoscience and Remote Sensing*, vol. 36, issue 4, pp. 1250-1265

Evers-King, H., Martinez-Vicente, V., Brewin, R. J. W., Dall'Olmo, G., Hickman, A. E., Jackson, T., Kostadinov, T. S., Krasemann, H., Loisel, H., Röttgers, R., Roy, S., Stramski, D., Thomalla, S., Platt, T. and Sathyendranath, S. (2017). 'Validation and Intercomparison of Ocean Color Algorithms for Estimating Particulate Organic Carbon in the Oceans', *Frontiers in Marine Science*, 4(August), pp. 1–20. doi: 10.3389/fmars.2017.00251.

Falkowski, P. G. and Kolber, Z. (1995). 'Variations in Chlorophyll Fluorescence Yields in Phytoplankton in the World Oceans', *Functional Plant Biology*, 22(2), pp. 341–355. Available at: https://doi.org/10.1071/PP9950341.

Falkowski, P. G. and Raven, J. A. (1997). *Aquatic Photosynthesis*. Blackwell Science, UK.

Fasham, M. J. R., Holligan, P. M. and Pugh, P. R. (1983). 'The Spatial and Temporal Development of the Spring Phytoplankton Bloom in the Celtic Sea , April 1979', *Progress in Oceanography*, 12, pp. 87–145. doi: 10.1016/0079-6611(83)90007-1.

Fasham, M. J. R., Holligan, P. M., Pugh, P. R. (1983). 'The Spatial and Temporal Development of the Spring Phytoplankton Bloom in the Celtic Sea , April 1979', *Progress in Oceanography*, 12, pp. 87–145. doi: 10.1016/0079-6611(83)90007-1.

Fennel, K. (2010).'The role of continental shelves in nitrogen and carbon cycling : Northwestern North Atlantic case study', *Ocean Science,* 6, pp. 539–548. doi: 10.5194/os-6-539-2010.

Fick, A. (1855). 'Ueber Diffusion', *Annalen der Physik*. John Wiley & Sons, Ltd, 170(1), pp. 59–86. doi: 10.1002/andp.18551700105.

Frajka-Williams, E., Eriksen, C. C., Rhines, P. B. and Harcourt, R. R. (2011). 'Determining vertical water velocities from Seaglider', *Journal of Atmospheric and Oceanic Technology*, 28(12), pp. 1641–1656. doi: 10.1175/2011JTECHO830.1.

Frajka-Williams, E., Rhines, P. B. and Eriksen, C. C. (2009). 'Physical controls and mesoscale variability in the Labrador Sea spring phytoplankton bloom observed by Seaglider', *Deep Sea Research Part I: Oceanographic Research Papers*, 56(12), pp. 2144–2161. doi: 10.1016/j.dsr.2009.07.008.

Frankignoulle, M. and Borges, A. (2001) 'European continental shelf as a significant sink for atmospheric carbon dioxide', *Global Biogeochemical Cycles*, 15(3), pp. 569–576. Available at: http://onlinelibrary.wiley.com/doi/10.1029/2000GB001307/full (Accessed: 7 November 2014).

Friedrichs, M. A. M., Dusenberry, J. A., Anderson, L. A., Armstrong, R. A., Chai, F., Christian, J. R., Doney, S. C., Dunne, J., Fujii, M., Hood, R., McGillicuddy, D. J., Moore, J. K., Schartau, M., Spitz, Y. H. and Wiggert, J. D. (2007). 'Assessment of skill and portability in regional marine biogeochemical models: Role of multiple planktonic groups', *Journal of Geophysical Research: Oceans*, 112(8), pp. 1–22. doi: 10.1029/2006JC003852.

Furlong, M. E., Paxton, D., Stevenson, P., Pebody, M., McPhail, S. D. and Perrett, J. (2012). 'Autosub Long Range: A long range deep diving AUV for ocean monitoring', *2012 IEEE/OES Autonomous Underwater Vehicles, AUV 2012*, (January 2016). doi: 10.1109/AUV.2012.6380737.

Gallager, S. and Whelan, J. (2003). *Report of the workshop on the next generation of in situ biological and chemical sensors in the ocean.* Woods Hole Oceanographic Institution.

Garau, B., Ruiz, S., Zhang, W. G., Pascual, A., Heslop, E., Kerfoot, J. and Tintoré, J. (2011). 'Thermal lag correction on slocum CTD glider data', *Journal of Atmospheric and Oceanic Technology*, 28(9), pp. 1065–1071. doi: 10.1175/JTECH-D-10-05030.1.

Gardner, W. D., Mishonov, A. V and Richardson, M. J. (2006). 'Global POC concentrations from in-situ and satellite data', *Deep Sea Research Part II: Topical Studies in Oceanography*, 53(5), pp. 718–740. doi: https://doi.org/10.1016/j.dsr2.2006.01.029.

Gattuso, J.-P., Frankignoulle, M. and Wollast, R. (1998). 'Carbon and Carbonate Metabolism in Coastal Aquatic Ecosystems', *Annual Review of Ecology and Systematics*, 29, pp. 405–434.

Gattuso, J. P., Magnan, A., Billie, R., Cheung, W. W. L., Howes, E. L. and Joos, F. (2015). 'Contrasting futures for ocean and society from different anthropogenic CO2 emissions scenarios.', *Science*, 349(6243).

Geider, R. J. and La Roche, J. (2002) .'Redfield revisited: Variability of C:N:P in marine microalgae and its biochemical basis', *European Journal of Phycology*, 37(1), pp. 1–17. doi: 10.1017/S0967026201003456.

Gill, A. (1982). *Atmosphere-Ocean Dynamics*. London, England: Acedemic Press.

Gordon, H. R., Clark, D. K., Brown, J. W., Brown, O. B., Evans, R. H. and Broenkow, W. W. (1983). 'Phytoplankton pigment concentrations in the Middle Atlantic Bight : comparison of ship determinations and CZCS estimates', *Applied* Optics, 22(1), pp. 20-36.

Gould, J., Roemmich, D., Wijffels, S., Freeland, H., Ignaszewsky, M., Jianping, X., Pouliquen, S., Desaubies, Y., Send, U., Radhakrishnan, K., Takeuchi, K., Kim, K., Danchenkov, M., Sutton, P., King, B., Owens, B. and Riser, S. (2004). 'Argo profiling floats bring new era of in situ ocean observations', *Transactions American Geophysical Union*, 85(19), p. 185. doi: 10.1029/2004EO190002.

Grand, M. M., Clinton-Bailey, G. S., Beaton, A. D., Schaap, A. M., Johengen, T. H., Tamburri, M. N., Connelly, D. P., Mowlem, M. C. and Achterberg, E. P. (2017). 'A Lab-On-Chip Phosphate Analyzer for Long-term In Situ Monitoring at Fixed Observatories: Optimization and Performance Evaluation in Estuarine and Oligotrophic Coastal Waters', *Frontiers in Marine Science*, 4(August), pp. 1–16. doi: 10.3389/fmars.2017.00255.

Grasshoff, K., Kremling, K. and Ehrhardt, M. (1999). *Method of Seawater Analysis*. Edited by K. Grasshoff, K. Kremling, and M. Ehrhardt. John Wiley & Sons.

Gregg, W. W. and Casey, N. W. (2004). 'Global and regional evaluation of the SeaWiFS chlorophyll data set', 93, pp. 463–479. doi: 10.1016/j.rse.2003.12.012.

Gregg, M.C., D'Asaro, E.A., Riley, J.J. and Kunze, E. (2018) Annual Review of Marine Science (2018) 'Mixing Efficiency in the Ocean', 10(1), pp. 443-473.

Griess, P. (1879). 'Griess reagent: a solution of sulphanilic acid and $α$-naphthylamine in acetic acid which gives a pink colour on reaction with the solution obtained after decomposition of nitrosyl complexes', *Chem. Ber*, 12, p. 427.

Gruber, N. (2008). 'The Marine Nitrogen Cycle: Overview and Challenges', *Nitrogen in the Marine Environment*. Elsevier Inc., pp. 1–50.

Gruber, N. (2011). 'Warming up, turning sour, losing breath: ocean biogeochemistry under global

change.', *Philos. Trans. A Math. Phys. Eng. Sci.*, 369, pp. 1980–1996.

Gruber, N. and Galloway, J. N. (2008). 'An Earth-system perspective of the global nitrogen cycle.', *Nature*, 451(7176), pp. 293–6. doi: 10.1038/nature06592.

Gundersen, K., Orcutt, K. M., Purdie, D. A., Michaels, A. F. and Knap, A. H. (2001), 'Particulate organic carbon mass distribution at the Bermuda Atlantic Time-series Study (BATS) site', *Deep-Sea Research Part II: Topical Studies in Oceanography*, 48(8–9), pp. 1697–1718. doi: 10.1016/S0967-0645(00)00156-9.

Hales, B., Geen, A. Van and Takahashi, T. (2004). 'High-frequency measurement of seawater chemistry : Flow-injection analysis of macronutrients', *Limnology and Oceacnography: Methods 2,* pp. 91–101.

Harris, R. (2010). 'The L4 time-series: The first 20 years', *Journal of Plankton Research*, 32(5), pp. 577–583. doi: 10.1093/plankt/fbq021.

Hemsley, V. S., Smyth, T. J., Martin, A. P., Frajka-Williams, E., Thompson, A. F., Damerell, G. and Painter, S. C. (2015). 'Estimating Oceanic Primary Production Using Vertical Irradiance and Chlorophyll Profiles from Ocean Gliders in the North Atlantic', *Environmental Science and Technology*, 49(19), pp. 11612–11621. doi: 10.1021/acs.est.5b00608.

Heslop, E. E., Tintoré, J., Testor, P. and Mortier, L. (2015). *A report on the operation and data analysis of glider experiments in the SES. PERSEUS Project.*

Hickman, A. E., Holligan, P. M., Moore, C. M., Sharples, J., Krivtsov, V. and Palmer, M. R. (2009). 'Distribution and chromatic adaptation of phytoplankton within a shelf sea thermocline', *Limnology and Oceanography*, 54(2), pp. 525–536.

Hickman, A., Moore, C., Sharples, J., Lucas, M., Tilstone, G., Krivtsov, V. and Holligan, P. (2012). 'Primary production and nitrate uptake within the seasonal thermocline of a stratified shelf sea', *Marine Ecology Progress Series*, 463, pp. 39–57. doi: 10.3354/meps09836.

Hine, R., Willcox, S., Hine, G. and Richardson, T. (2009) .'The Wave Glider: A Wave-Powered autonomous marine vehicle', *OCEANS 2009, MTS/IEEE Biloxi - Marine Technology for Our Future: Global and Local Challenges*, (December 2014), pp. 1–6. doi: 10.1080/00365540701649554.

Ho, T.-Y., Quigg, A., Finkel, Z. V, Milligan, A. J., Wyman, K., Falkowski, P. G. and Morel, F. M. M. (2003). 'The Elemental Composition of Some Marine Phytoplankton', *Journal of Phycology*, 39(6), pp. 1145–1159. doi: 10.1111/j.0022-3646.2003.03-090.x.

Hodges, B. A. and Fratantoni, D. M. (2009). 'A thin layer of phytoplankton observed in the Philippine Sea with a synthetic moored array of autonomous gliders', 114(October), pp. 1–15. doi: 10.1029/2009JC005317.

Holligan, P. M. (1978). 'Patchiness is subsurface populations on the Northwest European Continental Shelf', In: Steele, J. H. (ed.) *Spatial patterns in plankton communities*. New York: Plenum Press, pp. 222–238.

Holligan, P., Williams, Pj., Purdie, D. and Harris, R. (1984). 'Photosynthesis, respiration and nitrogen supply of plankton populations in stratified, frontal and tidally mixed shelf waters', *Marine Ecology Progress Series*, 17, pp. 201–213. doi: 10.3354/meps017201.

Holm-Hansen, O., Lorenzo, C. J., Holmes, R. W. and Strickland, J. D. H. (1965). 'Fluorometric Determination of Chlorophyll', *Journal du conseil International pour l'Exploration de Mer*, 30(1), pp. 3–15.

Holt, J., Hyder, P., Ashworth, M., Harle, J., Hewitt, H. T., Liu, H., New, A. L., Pickles, S., Porter, A., Popova, E., Icarus Allen, J., Siddorn, J. and Wood, R. (2017). 'Prospects for improving the representation of coastal and shelf seas in global ocean models', *Geoscientific Model Development*, 10(1), pp. 499–523. doi: 10.5194/gmd-10-499-2017.

Horne, E. P. W., Loder, J. W., Naimief, C. E. and Oakey, N. S. (1996). 'Turbulence dissipation rates and nitrate supply in the upper water column on Georges Bank', *Deep-Sea Research Part II: Topical Studies in Oceanography*, 43(7–8), pp. 1683–1712. doi: 10.1016/S0967-0645(96)00037-9.

Humphreys, M. P., Achterberg, E. P., Hopkins, J. E., Chowdhury, M. Z. H., Griffiths, A. M., Hartman, S. E., Hull, T., Smilenova, A., Wihsgott, J. U., Woodward, E. M. S. and Moore, C. M. (2018). 'Mechanisms for a nutrient-conserving carbon pump in a seasonally stratified, temperate continental shelf sea', *Progress in Oceanography*. doi: 10.1016/j.pocean.2018.05.001.

Hydes, D. ., Le Gall, A. ., Miller, A. E. ., Brockmann, U., Raabe, T., Holley, S., Alvarez-Salgado, X., Antia, A., Balzer, W., Chou, L., Elskens, M., Helder, W., Joint, I. and Orren, M. (2001) .'Supply and demand of nutrients and dissolved organic matter at and across the NW European shelf break in relation to hydrography and biogeochemical activity', *Deep Sea Research Part II: Topical Studies in Oceanography*, 48(14–15), pp. 3023–3047. doi: 10.1016/S0967-0645(01)00031-5.

Hydes, D. ., Gowen, R. ., Holliday, N. ., Shammon, T. and Mills, D. (2004) .'External and internal control of winter concentrations of nutrients (N, P and Si) in north-west European shelf seas', *Estuarine, Coastal and Shelf Science*, 59(1), pp. 151–161. doi: 10.1016/j.ecss.2003.08.004.

Hydes, D., Aoyama, M., Aminot, A., Bakker, K., Becker, S., Coverly, S., Daniel, A., Dickson, A. G., Grosso, O., Kerouel, R., van Ooijen, J., Sato, K., Tanhua, T., Woodward, E. M. S. and Zhang, J. Z. (2010). 'Determination of dissolved nutrients (N, P, Si) in seawater with high precision and inter-comparability using gas-segmented continuous flow analysers', *The GO-SHIP Repeat Hydrography Manual IOCCP Report*, 134(14), pp. 1–87. Available at: http://archimer.ifremer.fr/doc/00020/13141/.

IPCC (2014). '*Climate Change 2014: Impacts, Adaptation, and Vulnerability. Part A: Global and Sectoral Aspects. Contribution of Working Group II to the Fifth Assessment Report of the Intergovernmental Panel on Climate Change',* Cambridge, United Kingdom and New York, NY, USA: Cambridge University Press.

Jahnke, R. A. (2010). 'Global Synthesis', In: Lui, K. K., Atkinson, L., Quiñones, R., and Talaue-McManus, L. (eds) *Carbon and Nutrient Fluxes in Continental Margins: A Global Synthesis*. Berlin: Springer-Verlag.

Johnson, K., Berelson, W., Boss, E., Chase, Z., Claustre, H., Emerson, S., Gruber, N., Körtzinger, A., Perry, M. J. and Riser, S. (2009). 'Observing Biogeochemical Cycles at Global Scales with Profiling Floats and Gliders: Prospects for a Global Array', *Oceanography*, 22(3), pp. 216–225. doi: 10.5670/oceanog.2009.81.

Johnson, K. S. (2003). 'Chemical Sensors for Autonomous and Lagrangian Platforms Prepared for the Autonomous and Lagrangian Platforms Workshop, March 31 to April 2, 2003, MBARI'.

Johnson, K. S. and Coletti, L. J. (2002). 'In situ ultraviolet spectrophotometry for high resolution and long-term monitoring of nitrate, bromide and bisulfide in the ocean', *Deep Sea Research Part I: Oceanographic Research Papers*, 49(7), pp. 1291–1305. doi: 10.1016/S0967-0637(02)00020-1.

Johnson, K. S., Coletti, L. J., Jannasch, H. W., Sakamoto, C. M., Swift, D. D. and Riser, S. C. (2013). 'Long-Term Nitrate Measurements in the Ocean Using the in situ Ultraviolet Spectrophotometer: Sensor Integration into the APEX Profiling Float', *Journal of Atmospheric and Oceanic Technology*, 30(8), pp. 1854–1866. doi: 10.1175/JTECH-D-12-00221.1.

Johnson, K. S., Needoba, J. A., Riser, S. C. and Showers, W. J. (2007). 'Chemical sensor networks for the aquatic environment', *Chemical Reviews*, 107(2), pp. 623–640. doi: 10.1021/cr050354e.

Johnston, P. and Poole, M. (2017). 'Marine surveillance capabilities of the AutoNaut wave-propelled unmanned surface vessel (USV)', *OCEANS 2017 - Aberdeen*, 2017–October, pp. 1–4. doi: 10.1109/OCEANSE.2017.8084782.

Joint, I., Owens, N. and Pomeroy, A. (1986). 'Seasonal production of photosynthetic picoplankton and nanoplankton in the Celtic Sea ', *Marine Ecology Progress Series*, 28, pp. 251–258. doi: 10.3354/meps028251.

Joint, I., Wollast, R., Chou, L., Batten, S., Elskens, M., Edwards, E., Hirst, a., Burkill, P., Groom, S., Gibb, S., Miller, a., Hydes, D., Dehairs, F., Antia, a., Barlow, R., Rees, a., Pomroy, a., Brockmann, U., Cummings, D., Lampitt, R., Loijens, M., Mantoura, F., Miller, P., Raabe, T., Alvarez-Salgado, X., Stelfox, C. and Woolfenden, J. (2001). 'Pelagic production at the Celtic Sea shelf break', *Deep-Sea Research Part II: Topical Studies in Oceanography*, 48(14–15), pp. 3049–3081.

Jokerst, J. C., Emory, J. M. and Henry, C. S. (2012). 'Advances in microfluidics for environmental analysis', *Analyst*, 137(1), pp. 24–34. doi: 10.1039/C1AN15368D.

Jones, C. P. (2012). 'Slocum glider persistent oceanography', *2012 IEEE/OES Autonomous Underwater Vehicles, AUV 2012*. doi: 10.1109/AUV.2012.6380738.

Jonnson, B. F., Salisbury, J. E. and Mahadevan, A. (2011) .'Large variability in continental shelf production of phytoplankton carbon revealed by satellite', *Biogeosciences*, (8), pp. 1213–1223. doi: 10.5194/bg-8-1213-2011.

Kamenkovich, I., Cheng, W., Sarachik, E. S. and Harrison, D. E. (2009). 'Simulation of the Argo observing system in an ocean general circulation model', *Journal of Geophysical Research: Oceans*, 114(9), pp. 1–16. doi: 10.1029/2008JC005184.

Kara, A. B., Rochford, P. A. and Hurlburt, H. E. (2000). 'An optimal definition for ocean mixed layer depth', *Journal of Geophysical Research: Oceans*, 105(C7), pp. 16803–16821. doi: 10.1029/2000JC900072.

Karl, D. M. and Church, M. J. (2014). 'Microbial oceanography and the Hawaii Ocean Time-series programme', *Nature Reviews Microbiology*, 12(10), pp. 699–713. doi: 10.1038/nrmicro3333.

Karl, D. M. and Letelier, R. M. (2008). 'Nitrogen fixation-enhanced carbon sequestration in low nitrate, low chlorophyll seascapes', *Marine Ecology Progress Series*, 364, pp. 257–268. doi: 10.3354/meps07547.

Kaufman, D. E., Friedrichs, M. A. M., Smith, W. O., Queste, B. Y. and Heywood, K. J. (2014). 'Biogeochemical variability in the southern Ross Sea as observed by a glider deployment', *Deep-Sea Research Part I: Oceanographic Research Papers*, 92, pp. 93–106. doi: 10.1016/j.dsr.2014.06.011.

Kawai, Y. and Wada, A. (2007). 'Diurnal sea surface temperature variation and its impact on the atmosphere and ocean: A review', *Journal of Oceanography*, 63(5), pp. 721–744. doi: 10.1007/s10872-007-0063-0.

Kirk, J. T. O. (1994). '*Light and photosynthesis in aquatic ecosystems*'. Cambridge University Press.

Koenker, R. and Bassett, G. (1978) .'Regression quantiles', *Econometrica*, (46), pp. 33–50.

Kolber, Z. and Falkowski, P. G. (1993). 'Use of active fluorescence to estimate phytoplankton photosynthesis in situ', *Limnology and Oceanography* 38(8), pp. 1646–1665.

Kovala, P. E. (1966). 'Computation of phytoplankton cell numbers, cell volume, cell surface and plasma volume per liter, from microscopical counts', *Spec.Rep.* Dep.Oceanogr.Univ.Washington, 38, pp. 1–91.

Laliberté, J., Larouche, P., Devred, E. and Craig, S. (2018). 'Chlorophyll-a concentration retrieval in the optically complex waters of the St. Lawrence Estuary and Gulf using principal component analysis', *Remote Sensing*, 10(2). doi: 10.3390/rs10020265.

Large, W. G. and Pond, S. (1981). 'Open Ocean Momentum Flux in Moderate to Strong Winds', *Journal of Physical Oceanography*, 11, pp. 324–336.

Laruelle, G. G., Dürr, H. H., Slomp, C. P. and Borges, A. V. (2010). 'Evaluation of sinks and sources of CO<inf>2</inf> in the global coastal ocean using a spatially-explicit typology of estuaries and continental shelves', *Geophysical Research Letters*, 37(15), pp. 1–6. doi: 10.1029/2010GL043691.

Legendre, L. and Michaud, J. (1999). 'Chlorophyll a to estimate the particulate organic carbon available as food to large zooplankton in the euphotic zone of oceans', *Journal of Plankton Research*, 21(11), pp. 2067–2083. doi: 10.1093/plankt/21.11.2067.

Lehman, P. W. (2000). 'Phytoplankton Biomass, Cell Diameter, and Species Composition in the Low Salinity Zone of Northern San Francisco Bay Estuary', *Estuaries*, 23(2), pp. 216–230. doi: 10.2307/1352829.

Liu KK., Atkinson L., Quiñones R.A., Talaue-McManus L. (2010) Biogeochemistry of Continental Margins in a Global Context. In: Liu KK., Atkinson L., Quiñones R., Talaue-McManus L. (eds) Carbon and Nutrient Fluxes in Continental Margins. Global Change – The IGBP Series. Springer, Berlin, HeidelbergLiu, K. K., Yung Tang, T., Gong, G. C., Chen, L. Y. and Shiah, F. K. (2000). 'Cross-shelf and along-shelf nutrient fluxes derived from flow fields and chemical hydrography observed in the southern East China Sea off northern Taiwan', *Continental Shelf Research*, 20(4–5), pp. 493–523. doi: 10.1016/S0278-4343(99)00083-7.

Loisel, H., Mériaux, X., Berthon, J. F. and Poteau, A. (2007). 'Investigation of the optical backscattering to scattering ratio of marine particles in relation to their biogeochemical composition in the eastern English Channel and southern North Sea', *Limnology and Oceanography*, 52(2), pp. 739–752. doi: 10.4319/lo.2007.52.2.0739.

Loisel, H., Nicolas, J.-M., Deschamps, P.-Y. and Frouin, R. (2002) .'Seasonal and inter-annual variability of particulate organic matter in the global ocean', *Geophysical Research Letters*, 29(24), pp. 49-1-49–4. doi: 10.1029/2002GL015948.

Loisel, H., Vantrepotte, V., Jamet, C. and Dat, D. N. (2013) .'Challenges and New Advances in Ocean Color Remote Sensing of Coastal Waters', In: Zambianchi, E. (ed.) *Topics in Oceanography*. Intechopen. doi: 10.5772/50266.

Lomas, M. W., Bates, N. R., Johnson, R. J., Knap, A. H., Steinberg, D. K. and Carlson, C. A. (2013). 'Two decades and counting: 24-years of sustained open ocean biogeochemical measurements in the Sargasso Sea', *Deep-Sea Research Part II: Topical Studies in Oceanography*, 93, pp. 16–32. doi: 10.1016/j.dsr2.2013.01.008.

Long, G. L. and Winefordner, J. D. (1983). 'Limit of Detection: A Closer Look at the IUPAC Definition', *Analytical Chemistry*, 55(7), p. 712A–724A. doi: 10.1021/ac00258a001.

Lueck, R. G. and Picklo, J. J. (1990). 'Thermal Inertia of Conductivity Cells: Observations with a Sea-Bird Cell', *Journal of Atmospheric and Oceanic Technology*, pp. 756–768. doi: 10.1175/1520-0426(1990)007<0756:TIOCCO>2.0.CO;2.

Many, G., Bourrin, F., Durrieu, X., Madron, D., Ody, A., Doxaran, D. and Cauchy, P. (2018).

'Progress in Oceanography Glider and satellite monitoring of the variability of the suspended particle distribution and size in the Rhône ROFI', 163, pp. 123–135. doi: 10.1016/j.pocean.2017.05.006.

Mawji, E., Schlitzer, R., Dodas, E. M., Abadie, C., Abouchami, W., Anderson, R. F., Baars, O., Bakker, K., Baskaran, M., Bates, N. R., Bluhm, K., Bowie, A., Bown, J., Boye, M., Boyle, E. A., Branellec, P., Bruland, K. W., Brzezinski, M. A., Bucciarelli, E., Buesseler, K., Butler, E., Cai, P., Cardinal, D., Casciotti, K., Chaves, J., Cheng, H., Chever, F., Church, T. M., Colman, A. S., Conway, T. M., Croot, P. L., Cutter, G. A., De Baar, H. J. W., De Souza, G. F., Dehairs, F., Deng, F., Dieu, H. T., Dulaquais, G., Echegoyen-Sanz, Y., Lawrence Edwards, R., Fahrbach, E., Fitzsimmons, J., Fleisher, M., Frank, M., Friedrich, J., Fripiat, F., Galer, S. J. G., Gamo, T., Solsona, E. G., Gerringa, L. J. A., Godoy, J. M., Gonzalez, S., Grossteffan, E., Hattaa, M., Hayes, C. T., Heller, M. I., Henderson, G., Huang, K. F., Jeandel, C., Jenkins, W. J., John, S., Kenna, T. C., Klunder, M., Kretschmer, S., Kumamoto, Y., Laan, P., Labatut, M., Lacan, F., Lam, P. J., Lannuzel, D., Le Moigne, F., Lechtenfeld, O. J., Lohan, M. C., Lua, Y., Masqué, P., McClain, C. R., Measures, C., Middag, R., Moffett, J., Navidad, A., Nishioka, J., Noble, A., Obata, H., Ohnemus, D. C., Owens, S., Planchon, F., Pradoux, C., Puigcorbé, V., Quaya, P., Radic, A., Rehkämper, M., Remenyi, T., Rijkenberg, M. J. A., Rintoul, S., Robinson, L. F., Roeske, T., Rosenberg, M., Van Der Loeff, M. R., Ryabenko, E., Saito, M. A., Roshan, S., Salt, L., Sarthou, G., Schauer, U., Scott, P., Sedwick, P. N., Sha, L., Shiller, A. M., Sigman, D. M., Smethie, W., Smith, G. J., Sohrin, Y., Speich, S., Stichel, T., Stutsman, J., Swift, J. H., Tagliabue, A., Thomas, A., Tsunogai, U., Twining, B. S., Van Aken, H. M., Van Heuven, S., Van Ooijen, J., Van Weerlee, E., Venchiarutti, C., Voelker, A. H. L., Wake, B., Warner, M. J., Woodward, E. M. S., Wu, J., Wyatt, N., Yoshikawa, H., Zheng, X. Y., Xue, Z., Zieringer, M. and Zimmer, L. A. (2014). 'The GEOTRACES Intermediate Data Product 2014', *Marine Chemistry*, 177, pp. 1–8. doi: 10.1016/j.marchem.2015.04.005.

Mayers, K. M. J., Poulton, A. J., Daniels, C. J., Wells, S. R., Woodward, E. M. S., Tarran, G. A., Widdicombe, C. E., Mayor, D. J., Atkinson, A. and Giering, S. L. C. (2018) 'Growth and mortality of coccolithophores during spring in a temperate Shelf Sea (Celtic Sea, April 2015)', *Progress in Oceanography*. doi: 10.1016/j.pocean.2018.02.024.

McClain, C. R. (2009) 'A Decade of Satellite Ocean Color Observations', *Annual Review of Marine Science*, 1(1), pp. 19–42. doi: 10.1146/annurev.marine.010908.163650.

Meyer, D. (2016).'Glider Technology for Ocean Observations: A Review', *Ocean Science Discussions*, (July), pp. 1–26. doi: 10.5194/os-2016-40.

Millero, F. J. (1996). *Chemical Oceanography, Second Edition*. Taylor & Francis (Marine Science Series).

Monismith, S., Koseff, J. & White, B. (2018). 'Mixing Efficiency in the Presence of Stratification: When Is It Constant?', *Geophysical Research Letters*. 45. doi:10.1029/2018GL077229.

Moorcroft, M. J., Davis, J. and Compton, R. G. (2001). 'Detection and determination of nitrate and nitrite : a review', 54, pp. 785–803.

Morison, J., Andersen, R., Larson, N., D'Asaro, E. and Boyd, T. (1994). 'The Correction for Thermal-Lag Effects in Sea-Bird CTD Data', *Journal of Atmospheric and Oceanic Technology*. American Meteorological Society, 11(4), pp. 1151–1164. doi: 10.1175/1520-0426(1994)011<1151:TCFTLE>2.0.CO;2.

Moum, J. N. and Nash, J. D. (2000) .'Topographically Induced Drag and Mixing at a Small Bank on the Continental Shelf', *Journal of Physical Oceanography*, 30(8), pp. 2049–2054. doi: 10.1175/1520-0485(2000)030<2049:TIDAMA>2.0.CO;2.

Moum, J. N., and J. D. Nash. (2009) 'Mixing measurements on an equatorial ocean mooring'. *J.*

Atmos. Oceanic Technol., **26**, pp.317–336.

Muller-Karger, F. E. (2005). 'The importance of continental margins in the global carbon cycle', *Geophysical Research Letters*, 32(1), L01602. doi: 10.1029/2004GL021346.

Nightingale, A. M., Beaton, A. D. and Mowlem, M. C. (2015). 'Trends in Microfluidic Systems for In Situ Chemical Analysis of Natural Waters', *Sensors and Actuators B: Chemical*, 221, pp. 1398–1405. doi: 10.1016/j.snb.2015.07.091.

Olmo, D., Analytical, M. J., Graff, J. R., Westberry, T. K., Milligan, A. J., Brown, M. B., Dall, G., Dongen-vogels, V. Van, Reifel, K. M. and Behrenfeld, M. J. (2015).'Analytical phytoplankton carbon measurements spanning diverse ecosystems', *Deep-Sea Research Part I*, 102, pp. 16–25. doi: 10.1016/j.dsr.2015.04.006.

Olsen, A., Key, R. M., Van Heuven, S., Lauvset, S. K., Velo, A., Lin, X., Schirnick, C., Kozyr, A., Tanhua, T., Hoppema, M., Jutterström, S., Steinfeldt, R., Jeansson, E., Ishii, M., Pérez, F. F. and Suzuki, T. (2016). 'The global ocean data analysis project version 2 (GLODAPv2) - An internally consistent data product for the world ocean', *Earth System Science Data*, 8(2), pp. 297–323. doi: 10.5194/essd-8-297-2016.

Osborn, T. R. (1980). 'Estimates of the Local Rate of Vertical Diffusion from Dissipation Measurements', *Journal of Physical Oceanography*, pp. 83–89. doi: 10.1175/1520-0485(1980)010<0083:EOTLRO>2.0.CO;2.

Oubelkheir, K. (2001). '*Biogeochemical characterization of various oceanic provinces through optical indicators over various space and time scales'*. Univ. de la Me´diter./CNRS, Marseille, France.

P.Christensen, P.J. and Melling, H. (2009). '*Correcting Nitrate Profiles Measured by the In Situ Ultraviolet Spectrophotometer in Arctic Ocean Waters*', *The Open Oceanography Journal*. doi: 10.2174/1874252100903010059.

Pai, S. C., Yang, C. C. and P. Riley, J. (1990) .'Formation kinetics of the pink azo dye in the determination of nitrite in natural waters', *Analytica Chimica Acta*, 232(C), pp. 345–349. doi: 10.1016/S0003-2670(00)81252-0.

Palmer, M. R., Rippeth, T. P. and Simpson, J. H. (2008). 'An investigation of internal mixing in a seasonally stratified shelf sea', *Journal of Geophysical Research*, 113(C12), C12005. doi: 10.1029/2007JC004531.

Palmer, M. R., Stephenson, G. R., Inall, M. E., Balfour, C., Düsterhus, a and Green, J. a M. (2015). 'Turbulence and mixing by internal waves in the Celtic Sea determined from ocean glider microstructure measurements', *Journal of Marine Systems*, 144, pp. 57–69. doi: 10.1016/j.jmarsys.2014.11.005.

Palmer, M.R., Williams, C. and Horsburgh, K. (2018). 'Synoptic multi-variable glider study', AtlantOS Deliverable, D4.3 *AtlantOS,* pp. 25. doi: 10.3289/atlantos d4.3

Pascual, A., Faugère, Y., Larnicol, G. and Le Traon, P. Y. (2006). 'Improved description of the ocean mesoscale variability by combining four satellite altimeters', *Geophysical Research Letters*, 33(2), pp. 2–5. doi: 10.1029/2005GL024633.

Pasqueron De Fommervault, O., D'Ortenzio, F., Mangin, A., Serra, R., Migon, C., Claustre, H., Lavigne, H., Ribera D'Alcalà, M., Prieur, L., Taillandier, V., Schmechtig, C., Poteau, A., Leymarie, E., Dufour, A., Besson, F. and Obolensky, G. (2015). 'Seasonal variability of nutrient concentrations in the Mediterranean Sea: Contribution of Bio-Argo floats', *Journal of Geophysical Research: Oceans*, 120(12), pp. 8528–8550. doi: 10.1002/2015JC011103.

Pingree, R. D., Holligan, P. M. and Mardell, G. T. (1978). 'The effects of vertical stability on phytoplankton distributions in the summer on the northwest European Shelf', *Deep-Sea Research*, 25(11). doi: 10.1016/0146-6291(78)90584-2.

Pingree, R. D., Holligan, P. M., Mardell, G. T. and Head, R. N. (1976). 'The influence of physical stability on spring, summer and autumn phytoplankton blooms in the Celtic Sea', *Journal of the Marine Biological Association of the United Kingdom*. Cambridge University Press, 56(04), pp. 845–873. doi: 10.1017/S0025315400020919.

Pingree, R. D., Mardell, G. T. and Cartwright, D. E. (1981). 'Slope Turbulence, Internal Waves and Phytoplankton Growth at the Celtic Sea Shelf-Break [and Discussion]', *Philosophical Transactions of the Royal Society A: Mathematical, Physical and Engineering Sciences*, 302(1472), pp. 663–682. doi: 10.1098/rsta.1981.0191.

Platt, T., Subba Rao, D. V. and Irwin, B. (1983). 'Photosynthesis of picoplankton in the loigotrophic ocean', *Nature*, 301, pp. 517–520. doi: 10.1038/301517a0.

Poulton, A. J., Davis, C. E., Daniels, C. J., Mayers, K. M. J., Harris, C., Tarran, G. A., Widdicombe, C. E. and Woodward, E. M. S. (2018). 'Seasonal phosphorus and carbon dynamics in a temperate shelf sea (Celtic Sea)', *Progress in Oceanography*. doi: 10.1016/j.pocean.2017.11.001.

Prien, R. D. (2007). 'The future of chemical in situ sensors', *Marine Chemistry*, 107(3), pp. 422–432. doi: 10.1016/j.marchem.2007.01.014.

Proctor, R., Chen, F. and Tett, P. (2003). 'Carbon and nitrogen fluxes across the Hebridean shelf break, estimated by a 2D coupled physical–microbiological model', *The Science of The Total Environment*, 314–316(03), pp. 787–800. doi: 10.1016/S0048-9697(03)00084-6.

Provin, C., Fukuba, T., Okamura, K. and Fujii, T. (2013). 'An Integrated Microfluidic System for Manganese Anomaly Detection Based on Chemiluminescence: Description and Practical Use to Discover Hydrothermal Plumes Near the Okinawa Trough', *IEEE Journal of Oceanic Engineering*, 38(1), pp. 178–185. doi: 10.1109/JOE.2012.2208849.

Le Quere, C. (2015). 'Global carbon budget 2014', *Earth System Science Data*, 7(1), pp. 47–85. doi: 10.5194/essd-7-47-2015.

Queste, B. Y. (2013). '*Hydrographic Observations of Oxygen and Related Physical Variables in the North Sea and Western Ross Sea Polynya*'. Doctoral Thesis, University of East Anglia.

Queste, B. Y., Fernand, L., Jickells, T. D., Heywood, K. J. and Hind, A. J. (2016). 'Drivers of summer oxygen depletion in the central North Sea', *Biogeosciences*, 13(4), pp. 1209–1222. doi: 10.5194/bg-13-1209-2016.

Queste, B. Y., Heywood, K. J., Kaiser, J., Lee, G. a., Matthews, A., Schmidtko, S., Walker-Brown, C. and Woodward, S. W. (2012). 'Deployments in extreme conditions: Pushing the boundaries of Seaglider capabilities', *IEEE/OES Autonomous Underwater Vehicles*. doi: 10.1109/AUV.2012.6380740.

Randelhoff, A., Sundfjord, A. and Reigstad, M. (2015). 'Seasonal variability and fluxes of nitrate in the surface waters over the Arctic shelf slope', *Geophysical Research Letters*, 42(9), pp. 3442–3449. doi: 10.1002/2015GL063655.

Raymont, J. E. G. (1980). 'Plankton and Productivity in the Oceans'. doi: 10.1016/B978-0-08-021551-8.50009-7.

Redfield, A. C. (1958). 'The Biological contral of chemical factors in the environment', *American Scientist*, 46(3), p. 230A–221.

Redfield, A. C., Ketchum, B. H. and Richards, F. A. (1963). 'The influence of organisms on the composition of sea water', In: *The Sea, ideas and observations on progress in the study of the sea*. New York: J. Wiley and Sons, pp. 26–77.

Rees, A. P., Joint, I. and Donald, K. M. (1999). 'Early spring bloom phytoplankton-nutrient dynamics at the Celtic Sea shelf edge', *Deep-Sea Research Part I: Oceanographic Research Papers*, 46(3), pp. 483–510.

Rees, A.P., Robinson, C., Smyth, T., Aiken, J., Nightingale, P. and Zubkov, M. (2015). '20 years of the Atlantic Meridional Transect—AMT', *Limnology and Oceanography Bulletin*, 24(4), pp. 101–107. doi: 10.1002/lob.10069.

Rérolle, V. M. C., Floquet, C. F. A., Harris, A. J. K., Mowlem, M. C., Bellerby, R. R. G. J. and Achterberg, E. P. (2013). 'Development of a colorimetric microfluidic pH sensor for autonomous seawater measurements', *Analytica Chimica Acta*, 786, pp. 124–131. doi: 10.1016/j.aca.2013.05.008.

Richardson, K., Rasmussen, B., Bunk, T. and Mouritsen, L. T. (2000). 'Multiple subsurface phytoplankton blooms occurring simultaneously in the Skagerrak', *Journal of Plankton Research*, 25(7). pp. 799-813.

Richardson, K., Visser, A. and Pedersen, F. (2000). 'Subsurface phytoplankton blooms fuel pelagic production in the North Sea', *Journal of Plankton Research*, 22(9), pp. 1663–1671. doi: 10.1093/plankt/22.9.1663.

Rippeth, T.P. and Inall, M. (2002). 'Observations of the internal tide and associated mixing across the Malin Shelf', *Journal of Geophysical Research: Oceans,* 107(C4). pp. 3-1-3-14.

Rippeth, T. P. (2005). 'Mixing in seasonally stratified shelf seas: a shifting paradigm.', *Philosophical transactions. Series A, Mathematical, physical, and engineering sciences*, 363(1837), pp. 2837–54. doi: 10.1098/rsta.2005.1662.

Rippeth, T. P. (2005). 'Thermocline mixing in summer stratified continental shelf seas', *Geophysical Research Letters*, 32(5), L05602. doi: 10.1029/2004GL022104.

Rippeth, T. P., Wiles, P., Palmer, M. R., Sharples, J. and Tweddle, J. (2009). 'The diapcynal nutrient flux and shear-induced diapcynal mixing in the seasonally stratified western Irish Sea', *Continental Shelf Research*, 29(13), pp. 1580–1587. doi: 10.1016/j.csr.2009.04.009.

Riser, S. C., Freeland, H. J., Roemmich, D., Wijffels, S., Troisi, A., Belbéoch, M., Gilbert, D., Xu, J., Pouliquen, S., Thresher, A., Le Traon, P. Y., Maze, G., Klein, B., Ravichandran, M., Grant, F., Poulain, P. M., Suga, T., Lim, B., Sterl, A., Sutton, P., Mork, K. A., Vélez-Belchí, P. J., Ansorge, I., King, B., Turton, J., Baringer, M. and Jayne, S. R. (2016). 'Fifteen years of ocean observations with the global Argo array', *Nature Climate Change*, 6(2), pp. 145–153. doi: 10.1038/nclimate2872.

Roemmich, D., Boebel, O., Desaubies, Y., Freeland, H., Kim, K., King, B., Letraon, P., Molinari, R., Owens, W. B., Riser, S. C., Send, U., Takeuchi, K. and Wijffels, S. (2001). 'Argo: the global array of profiling floats.' In: Koblinsky CJ, Smith NR (eds) Observing the oceans in the 21st century. GODAE Project Office, Bureau of Meteorology, Melbourne, pp 248–258

Roemmich, D. and Steering Team, and the A. (2009). 'Argo The challenge of continuing 10 Years of Progress', *Oceanography*, 22(3), pp. 26–35. doi: 10.1148/114.3.741.

Rogers, W. (1992). 'Quantile regression standard errors', *Stata Technical Bulletinl*, 2(9), pp. 133–137.

Rudnick, D. L. (2016). 'Ocean Research Enabled by Underwater Gliders', *Annual Review of Marine*

Science, 8(1), pp. 519–541. doi: 10.1146/annurev-marine-122414-033913.

Rudnick, D. L., Davis, R. E., Eriksen, C. C., Fratantoni, D. M. and Perry, M. J. (2004). 'Underwater Gliders for Ocean Research', *Marine Technology Society Journal*, 38(2), pp. 73–84.

Rumyantseva, A., Lucas, N., Rippeth, T., Martin, A., Painter, S. C., Boyd, T. J. and Henson, S. (2015). 'Ocean nutrient pathways associated with the passage of a storm', *Global Biogeochemical Cycles*, 29, pp. 1179–1189. doi: 10.1002/2015GB005097.

Sackmann, B. S., Perry, M. J. and Eriksen, C. C. (2008). 'Seaglider observations of variability in daytime fluorescence quenching of chlorophyll- a in Northeastern Pacific coastal waters', *Biogeosciences Discussions*, 5, pp. 2839–2865. doi: 10.5194/bgd-5-2839-2008.

Sakamoto, C. M., Johnson, K. S. and Coletti, L. J. (2009). 'Improved algorithm for the computation of nitrate concentrations in seawater using an in situ ultraviolet spectrophotometer', *Limnology and Oceanography: Methods*, 7, pp. 132–143. doi: 10.4319/lom.2009.7.132.

Sathyendranath, S., Stuart, V., Nair, A., Oka, K., Nakane, T., Bouman, H., Forget, M. H., Maass, H. and Platt, T. (2009). 'Carbon-to-chlorophyll ratio and growth rate of phytoplankton in the sea', *Marine Ecology Progress Series*, 383, pp. 73–84. doi: 10.3354/meps07998.

Sauzède, R., Bittig, H. C., Claustre, H., Pasqueron de Fommervault, O., Gattuso, J.-P., Legendre, L. and Johnson, K. S. (2017). 'Estimates of Water-Column Nutrient Concentrations and Carbonate System Parameters in the Global Ocean: A Novel Approach Based on Neural Networks', *Frontiers in Marine Science*, 4(March), pp. 128. doi: 10.3389/fmars.2017.00128.

Schmechtig, C., Poteau, A., Claustre, H., D'Ortenzio, F., Dall'Olmo, G. and Boss, E. (2018). '*Processing Bio-Argo particle backscattering at the DAC level*'. UPMC Université Paris 06, UMR 7093, LOV, Observatoire océanologique, Villefranche-sur-Mer, France: Ifremer. doi: 10.13155/39459.

Schofield, O., Ducklow, H. W., Martinson, D. G. and Meredith, M. P. (2010). 'How Do Polar Marine Ecosystems', *Science*, 328(5985), pp. 1520–1523. doi: 10.1016/S0378-4347(97)00255-7.

Schofield, O., Kohut, J., Aragon, D., Creed, L., Graver, J., Haldeman, C., Kerfoot, J., Roarty, H., Jones, C., Webb, D. and Glen, S. (2007). 'Slocum Gliders: Robust and Ready', *Journal of Field Robotics*, 24(6), pp. 473–485. doi: 10.1002/rob.

Sea-Bird Scientific, (2017). '*User manual ECO Fluorometers and Scattering Sensors*'. Seabird Available at: http://www.seabird.com/eco-triplet-fluorometer-and-backscattering-sensor (Accessed: 25 October 2017).

Sharples, J. (2008). 'Potential impacts of the spring-neap tidal cycle on shelf sea primary production', *Journal of Plankton Research,* 30(2), pp. 183-197. doi: 10.1093/plankt/fbm088.

Sharples, J., Ellis, J. R., Nolan, G. and Scott, B. E. (2013) 'Fishing and the oceanography of a stratified shelf sea', *Progress in Oceanography*, 117, pp. 130–139. doi: 10.1016/j.pocean.2013.06.014.

Sharples, J. and Moore, C. (2009). 'Internal tidal mixing as a control on continental margin ecosystems', *Geophysical Research Letters*, 36, pp. L23603. doi: 10.1029/2009GL040683.

Sharples, J., Moore, M. C., Rippeth, T. P., Holligan, P. M., Hydes, D. J., Fisher, N. R., Simpson, J. H., Moore, C. M., Rippeth, T. P., Holligan, P. M., Hydes, D. J., Fisher, N. R. and Simpson, J. H. (2001). 'Phytoplankton distribution and survival in the thermocline', *Limnology and Oceanography*, 46(3), pp. 486–496. doi: 10.4319/lo.2001.46.3.0486.

Sharples, J., Tweddle, J. F., Green, J. A. M., Palmer, M. R., Kim, Y., Hickman, A. E., Holligan, P. M., Moore, C. M., Rippeth, T. P., Simpson, J. H. and Krivtsov, V. (2007). 'Spring – neap modulation of internal tide mixing and vertical nitrate fluxes at a shelf edge in summer', *Limnology and Oceanography*, 52(5), pp. 1735–1747.

Sherman, J., Davis, R. E., Owens, W. B. and Valdes, J. (2001). 'The autonomous underwater glider" Spray', *IEEE Journal of Oceanic Engineering*, 26(4), pp. 437–446.

Sherwin, T. J., Read, J. F., Holliday, N. P. and Johnson, C. (2012). 'The impact of changes in North Atlantic Gyre distribution on water mass characteristics in the Rockall Trough', *ICES Journal of Marine Science*, 69, pp. 751–757.

Sieben, V. J., Floquet, C. F., Ogilvie, I. R. G. G., Mowlem, M. C. and Morgan, H. (2010). 'Microfluidic colourimetric chemical analysis system: Application to nitrite detection', *Analytical Methods*, 2(5), pp. 484–491. doi: 10.1039/c002672g.

Simpson, J. H., Crawford, W. R., Rippeth, T. P., Campbell, A. R. and Cheok, J. V. S. (1996). 'The Vertical Structure of Turbulent Dissipation in Shelf Seas', *Journal of Physical Oceanography*, pp. 1579–1590. doi: 10.1175/1520-0485(1996)026<1579:TVSOTD>2.0.CO;2.

Simpson, J. H. and Hunter, J. R. (1974) 'Fronts in the Irish Sea', *Nature*, 250(5465), pp. 404–406. doi: 10.1038/250404a0.

Simpson, J. H. and Sharples, J. (2012). '*Introduction to the Physical and Biological Oceanography of Shelf Seas*'. Cambridge University Press. doi: 10.1017/CBO9781139034098.

Smyth, T. J. (2004), 'A methodology to determine primary production and phytoplankton photosynthetic parameters from Fast Repetition Rate Fluorometry', *Journal of Plankton Research*, 26(11), pp. 1337–1350.

Smyth, T. J., Fishwick, J. R., Al-Moosawi, L., Cummings, D. G., Harris, C., Kitidis, V., Rees, A., Martinez-Vicente, V. and Woodward, E. M. S. (2010), 'A broad spatio-temporal view of the Western English Channel observatory', *Journal of Plankton Research*, 32(5), pp. 585–601. doi: 10.1093/plankt/fbp128.

Souza, A. J., Holt, J. T. and Proctor, R. (2007), 'Modelling SPM on the NW European shelf seas', *Geological Society, London, Special Publications*, 274(1), pp. 147–158. doi: 10.1144/GSL.SP.2007.274.01.14.

Stabeno, P. J. and Meurs, P. V. (1999). 'Evidence of episodic on-shelf flow in the southeastern Bering Sea', *Journal of Geophysical Research: Oceans,* 104(C12), pp. 2971-29720.

Statham, P. J., Connelly, D. P., German, C. R., Brand, T., Overnell, J. O., Bulukin, E., Millard, N., McPhail, S., Pebody, M., Perrett, J., Stevenson, P. and Webb, A. (2005). 'Spatially Complex Distribution of Dissolved Manganese in a Fjord as Revealed by High-Resolution in Situ Sensing Using the Autonomous Underwater Vehicle Autosub', *Environmental Science & Technology*, 39(24), pp. 9440–9445. doi: 10.1021/es050980t.

Stramski, D., Reynolds, R. A., Babin, M., Kaczmarek, S., Lewis, M. R., Sciandra, A., Stramska, M., Twardowski, M. S., Franz, B. A., Stramski, D., Reynolds, R. A., Babin, M., Kaczmarek, S. and Lewis, M. R. (2008). 'Relationships between the surface concentration of particulate organic carbon and optical properties in the eastern South Pacific and eastern Atlantic Oceans', *Biogeosciences,* 5, pp. 171-201.

Stramski, D., Reynolds, R. A., Kahru, M. and Mitchell, B. G. (1999). 'Estimation of Particulate Organic Carbon in the Ocean from Satellite Remote Sensing', *Science*, 285(July), pp. 239–243.

Strutton, G., Boss, E., Taylor, L., Brickley, P., Zaneveld, R. and Darling, I. C. (2013). 'Observations of pigment and particle distributions in the western from North Atlantic an autonomous float and ocean color satellite', *Limonlogy and* Oceanography, 53(1), pp. 2112–2122. doi.org/10.4319/lo.2008.53.5_part_2.2112.

Sverdrup, H. U. (1952). 'On Conditions for the Vernal Blooming of Phytoplankton'. J. Cons. Explor. Mer., 18(287), pp. 18–287.

Swart, S., Thomalla, S. J. and Monteiro, P. M. S. (2015), 'The seasonal cycle of mixed layer dynamics and phytoplankton biomass in the Sub-Antarctic Zone: A high-resolution glider experiment', *Journal of Marine Systems*, 147, pp. 103–115. doi: 10.1016/j.jmarsys.2014.06.002.

Takahashi, T., Sutherland, S. C., Wanninkhof, R., Sweeney, C., Feely, R. A., Chipman, D. W., Hales, B., Friederich, G., Chavez, F., Sabine, C., Watson, A., Bakker, D. C. E., Schuster, U., Metzl, N., Yoshikawa-Inoue, H., Ishii, M., Midorikawa, T., Nojiri, Y., Körtzinger, A., Steinhoff, T., Hoppema, M., Olafsson, J., Arnarson, T. S., Tilbrook, B., Johannessen, T., Olsen, A., Bellerby, R., Wong, C. S., Delille, B., Bates, N. R. and de Baar, H. J. W. (2009), 'Climatological mean and decadal change in surface ocean pCO2, and net sea-air CO2 flux over the global oceans', *Deep-Sea Research Part II: Topical Studies in Oceanography*, 56(8–10), pp. 554–577. doi: 10.1016/j.dsr2.2008.12.009.

Talley, L. D., Feely, R. A., Sloyan, B. M., Wanninkhof, R., Baringer, M. O., Bullister, J. L., Carlson, C. A., Doney, S. C., Fine, R. A., Firing, E., Gruber, N., Hansell, D. A., Ishii, M., Johnson, G. C., Katsumata, K., Key, R. M., Kramp, M. and Langdon, C. (2016). 'Changes in Ocean Heat , Carbon Content , and Ventilation : A Review of the First Decade of GO-SHIP Global Repeat Hydrography ', *Annual Review of Marine Science,* 8(1) pp. 185–218. doi: 10.1146/annurev-marine-052915-100829.

Tarran, G. A., Heywood, J. L. and Zubkov, M. V (2006). 'Latitudinal changes in the standing stocks of nano- and picoeukaryotic phytoplankton in the Atlantic Ocean', *Deep Sea Research Part II: Topical Studies in Oceanography*, 53(14), pp. 1516–1529. doi: https://doi.org/10.1016/j.dsr2.2006.05.004.

Tennekes, H. and Lumley, J. (1972).'*A First Course in Turbulence*', Cambridge, Massachusetts, and London: The MIT Press. doi: 10.1017/S002211207321251X.

Testor, P., Meyers, G., Pattiaratchi, C., Bachmeyer, R., Hayes, D., Pouliquen, S., Petit de la Villeon, L., Carval, T., Ganachaud, A., Gourdeau, L., Mortier, L., Claustre, H., Taillandier, V., Lherminier, P., Terre, T., Visbeck, M., Karstensen, J., Krahmann, G., Alvarez, A., Rixen, M., Poulain, P.-M., Osterhus, S., Tintore, J., Ruiz, S., Garau, B., Smeed, D., Griffiths, G., Merckelbach, L., Sherwin, T., Schmid, C., Barth, J. A., Schofield, O., Glenn, S., Kohut, J., Perry, M. J., Eriksen, C., Send, U., Davis, R., Rudnick, D., Sherman, J., Jones, C., Webb, D., Lee, C. and Owens, B. (2010). 'Gliders as a component of future observing systems', *Proceedings of OceanObs'09: Sustained Ocean Observations and Information for Society*, Volume 2, Venice, Italy: ESA Publications WPP-306. doi: 10.5270/OceanObs09.cwp.89.

Thomalla, S. J., Fauchereau, N., Swart, S. and Monteiro, P. M. S. (2011). 'Regional scale characteristics of the seasonal cycle of chlorophyll in the Southern Ocean', *Biogeosciences*, 8(10), pp. 2849–2866. doi: 10.5194/bg-8-2849-2011.

Thomalla, S. J., Moutier, W., Ryan-Keogh, T. J., Gregor, L. and Schütt, J. (2018). 'An optimized method for correcting fluorescence quenching using optical backscattering on autonomous platforms', *Limnology and Oceanography: Methods*, 16(2), pp. 132–144. doi: 10.1002/lom3.10234.

Thomalla, S. J., Ogunkoya, A. G., Vichi, M. and Swart, S. (2017). 'Using Optical Sensors on Gliders to Estimate Phytoplankton Carbon Concentrations and Chlorophyll-to-Carbon Ratios in the

Southern Ocean', *Frontiers in Marine Science*, 4(February), pp. 1–19. doi: 10.3389/fmars.2017.00034.

Thomalla, S. J., Racault, M., Swart, S. and Monteiro, P. M. S. (2015). 'High-resolution view of the spring bloom initiation and net community production in the Subantarctic Southern Ocean using glider data', *ICES Journal of Marine SCience,* 72(6), pp. 1999–2020. doi.org/10.1093/icesjms/fsv105.

Thomas, H., Bozec, Y., Elkalay, K. and de Baar, H. J. W. (2004). 'Enhanced open ocean storage of CO2 from shelf sea pumping.', *Science*, 304(5673), pp. 1005–1008. doi: 10.1126/science.1095491.

Thompson, A. F., Lazar, A., Buckingham, C., Naveira Garabato, A. C., Damerell, G. M. and Heywood, K. J. (2016). 'Open-ocean submesoscale motions: A full seasonal cycle of mixed layer instabilities from gliders', *Journal of Physical Oceanography*,46, pp. 1285-1307. doi: 10.1175/JPO-D-15-0170.1.

Thomsen, S., Kanzow, T., Gerd, K., Greatbatch, R. J., Dengler, M. and Lavik, G. (2015). 'The formation of a subsurface anticyclonic eddy in the Peru-Chile Undercurrent and its impact on the near-coastal salinity, oxygen, and nutrient distributions', *Journal of Geophysical Research: Oceans*, 121(1), pp. 476–501. doi: 10.1002/2015JC010878.

Thorpe, S. A. (2007). '*An introduction to ocean turbulence*, *An Introduction to Ocean Turbulence',* Cambridge University Press. doi: 10.1017/CBO9780511801198.

Le Traon, P.-Y., Antoine, D., Bentamy, A., Bonekamp, H., Breivik, L. A., Chapron, B., Corlett, G., Dibarboure, G., DiGiacomo, P., Donlon, C., Faugère, Y., Font, J., Girard-Ardhuin, F., Gohin, F., Johannessen, J. A., Kamachi, M., Lagerloef, G., Lambin, J., Larnicol, G., Le Borgne, P., Leuliette, E., Lindstrom, E., Martin, M. J., Maturi, E., Miller, L., Mingsen, L., Morrow, R., Reul, N., Rio, M. H., Roquet, H., Santoleri, R. and Wilkin, J. (2015). 'Use of satellite observations for operational oceanography: recent achievements and future prospects', *Journal of Operational Oceanography*, 8(sup1), pp. s12–s27. doi: 10.1080/1755876X.2015.1022050.

Tsunogai, S., Watanabe, S., Sato, T., Whelan, M., Galy, V., Basile, I., Chappellaz, J., Davis, M., Delaygie, G., Delmotte, M., Kotlyakov, V., Legrand, M., Lipenkov, V., Lorius, C., Pépin, C., Ritz, C., Saltzman, E. and Stievenard, M. (1999). 'Is there a "continental shelf pump" for the absorption of atmospheric CO2?', *Tellus B: Chemical and Physical Meteorology*, 51(3), pp. 701–712. doi: 10.3402/tellusb.v51i3.16468.

Tweddle, J. F., Sharples, J., Palmer, M. R., Davidson, K. and McNeill, S. (2013). 'Enhanced nutrient fluxes at the shelf sea seasonal thermocline caused by stratified flow over a bank', *Progress in Oceanography*, 117, pp. 37–47. doi: 10.1016/j.pocean.2013.06.018.

Tweddle, J.F. (2007). 'Nutrient Fluxes into the seasonal thermocline of the Celtic sea'. Doctoral Thesis. University of Southampton. Available at: http://eprints.soton.ac.uk/158357/.

Vichi, M., Allen, J. I., Masina, S. and Mountford, N. J. H. (2011). 'The emergence of ocean biogeochemical provinces : A quantitative assessment and a diagnostic for model evaluation', *Global Biogeochemical Cycles,* 25(2), pp. 1–17. doi: 10.1029/2010GB003867.

Vincent, A. G., Pascal, R. W., Beaton, A. D., Walk, J., Hopkins, J. E., Woodward, E. M. S., Mowlem, M. and Lohan, M. C. (2018). 'Nitrate drawdown during a shelf sea spring bloom revealed using a novel micro fl uidic in situ chemical sensor deployed within an autonomous underwater glider', *Marine Chemistry*, 205(July), pp. 29–36. doi: 10.1016/j.marchem.2018.07.005.

Walsh, J. J. (1991) 'Importance of continental margins in the marine biogeochemical cycling of carbon and nitrogen', *Nature*, 350(6313), pp. 53–55. doi: 10.1038/350053a0.

Webb, D. C., Simonetti, P. J. and Jones, C. P. (2001). 'SLOCUM: An underwater glider propelled by environmental energy', *IEEE Journal of Oceanic Engineering*, 26(4), pp. 447–452. doi: 10.1109/48.972077.

Weston, K., Fernand, L., Mills, D. K., Delahunty, R. and Brown, J. (2005). 'Primary production in the deep chlorophyll maximum of the central North Sea', *Journal of Plankton Research*, 27(9), pp. 909–922. doi: 10.1093/plankt/fbi064.

Weston, K., Fernand, L., Mills, D. K., Delahunty, R. and Brown, J. (2018). 'Primary production in the deep chlorophyll maximum of the central', *Journal of Plankton Research,* 27(April), pp. 909–922. doi: 10.1093/plankt/fbi064.

Wetlabs, (2017) '*User manual ECO Fluorometers and Scattering Sensors*'. Seabird. Available at: www.seabird.com%2Fasset-get.download.jsa%3Fid%3D54712835751&usg=AOvVaw087FfKENl_ghkB_pBD9Xm_. (Accessed: 29 Aug 2018).

Widdicombe, C. E., Eloire, D. and Harbour, D. (2010). 'Long-term phytoplankton community dynamics in the Western English Channel', *Journal of Plankton Research,* 32(5), pp.643-655. doi: 10.1093/plankt/fbp127.

Wihsgott, J. U. (2018) 'A Tale of Four Seasons : Investigating the seasonality of physical structure and its biogeochemical responses in a temperate continental shelf sea by', Doctoral Thesis, University of Liverpool.

Wild-Allen, K. and Rayner, M. (2014). 'Continuous nutrient observations capture fine-scale estuarine variability simulated by a 3D biogeochemical model', *Marine Chemistry,* 167, pp. 135–149. doi: 10.1016/j.marchem.2014.06.011.

Williams, C. (2013). 'The Supply of Nutrients To the Subsurface Chlorophyll Maximum in Temperate Shelf Seas'. Doctoral Thesis, University of Liverpool.

Williams, C., Sharples, J., Green, M., Mahaffey, C. and Rippeth, T. (2013). 'The maintenance of the subsurface chlorophyll maximum in the stratified western Irish Sea', *Limnology and Oceanography: Fluids & Environments*, 3(C), pp. 61–73. doi: 10.1215/21573689-2285100.

Williams, C., Sharples, J., Mahaffey, C. and Rippeth, T. (2013). 'Wind-driven nutrient pulses to the subsurface chlorophyll maximum in seasonally stratified shelf seas', *Geophysical Research Letters*, 40(20), pp. 5467–5472. doi: 10.1002/2013GL058171.

Wojtasiewicz, B., Hardman-Mountford, N. J., Antoine, D., Dufois, F., Slawinski, D. and Trull, T. W. (2018). 'Use of bio-optical profiling float data in validation of ocean colour satellite products in a remote ocean region', *Remote Sensing of Environment*, 209(March), pp. 275–290. doi: 10.1016/j.rse.2018.02.057.

Wood, S. L. and Mierzwam, C. (2013). 'State of Technology in Autonomous Underwater Gliders', *Marine Technology Society Journal*, 47(5), pp. 84–96.

Woodward, E. M. S. and Rees, A. P. (2001). 'Nutrient distributions in an anticyclonic eddy in the northeast Atlantic ocean, with reference to nanomolar ammonium concentrations', *Deep-Sea Research Part II: Topical Studies in Oceanography*, 48(4–5), pp. 775–793. doi: 10.1016/S0967-0645(00)00097-7.

Wurl, O. (2009). '*Practical guidelines for the analysis of seawater*'. CRC Press. Available at: https://books.google.co.uk/books?id=XqRQh58gb_IC&printsec=frontcover&dq=practical+guidelines+for+seawater+oliver+wurl&hl=en&sa=X&ved=0ahUKEwj_7fWQsavbAhUH8RQKHeedDSgQ6AEIKjAA#v=onepage&q=practical guidelines for seawater oliver wurl&f=false. (Accessed: 29 May

2018).

Yamamuro, M. and Kayanne, H. (1995). ‘Rapid direct determination of organic carbon and nitrogen in carbonate-bearing sediments with a Yanaco MT-5 CHN analyzer’, *Limnology and Oceanography*, 40(5), pp. 1001–1005. doi: 10.4319/lo.1995.40.5.1001.

Yamazaki, H. and Osborn, T. (1990) ‘Dissipation Estimates for Stratified Turbulence'. *Journal of Geophysical Research: Oceans*, 95(C6), pp. 9739–9744.

Yang, J., Gong, P., Fu, R., Zhang, M., Chen, J., Liang, S., Xu, B., Shi, J. and Dickinson, R. (2013). ‘The role of satellite remote sensing in climate change studies’, *Nature Climate Change*, 3(10), pp. 875–883. doi: 10.1038/nclimate1908.

Yoder, J. A. and Kennelly, M. A. (2006). ‘What Have We Learned About Ocean Variability From Satellite Ocean Color Imagers?’, *Oceanography*, 19(1), pp. 152–171. doi: 10.5670/oceanog.2006.98.

Yücel, M., Beaton, A. D., Dengler, M., Mowlem, M. C., Sohl, F. and Sommer, S. (2015). ‘Nitrate and Nitrite Variability at the Seafloor of an Oxygen Minimum Zone Revealed by a Novel Microfluidic In-Situ Chemical Sensor’, *Plos One*, 10(7), pp. 1–16. doi: 10.1371/journal.pone.0132785.

Zhang, X., Hu, L. and He, M. (2009). ‘Scattering by pure seawater : Effect of salinity’, *Optical Express,*17(7), pp. 5698–5710.

Appendix A Published Paper

Vincent, A.G., Pascal, R.W., Beaton, A., Walk, J., Hopkins, J.E., Woodward, E.M.S., Mowlem, M. and Lohan, M. (2018), Nitrate drawdown during a shelf sea spring bloom revealed using a novel microfluidic in-situ chemical sensor deployed within an autonomous underwater glider, *Mar. Chem.* https://doi.org/10.1016/j.marchem.2018.07.005.

Appendix A

Marine Chemistry 205 (2018) 29–36

Contents lists available at ScienceDirect

Marine Chemistry

journal homepage: www.elsevier.com/locate/marchem

Nitrate drawdown during a shelf sea spring bloom revealed using a novel microfluidic *in situ* chemical sensor deployed within an autonomous underwater glider

Alexander G. Vincent[a,*], Robin W. Pascal[b], Alexander D. Beaton[b], John Walk[b], Joanne E. Hopkins[c], E. Malcolm S. Woodward[d], Matthew Mowlem[b], Maeve C. Lohan[a]

[a] Ocean and Earth Science, University of Southampton, Southampton SO14 3ZH, UK
[b] Ocean Technology and Engineering Group, National Oceanography Centre, Southampton SO14 3ZH, UK
[c] National Oceanography Centre, Joseph Proudman Building, Liverpool L3 5DA, UK
[d] Plymouth Marine Laboratory, Prospect Place, Plymouth PL1. 3DH, UK

ARTICLE INFO

Keywords:
Microfluidics
Autonomous underwater vehicles
Shelf seas
Nutrients

ABSTRACT

Here we describe, for the first time, the use of a miniaturized Lab-on-Chip (LoC) nutrient sensor deployed within an autonomous underwater vehicle (AUV; Kongsberg Seaglider) to collect high-resolution nitrate (nitrate + nitrite) data in a highly dynamic shelf sea environment. Seasonally stratified temperate shelf seas act as important carbon sinks, where primary production is controlled by the availability of nutrients such as nitrate. Spring phytoplankton blooms and sporadic mixing events can drastically modify the availability of nitrate on temporal scales from hours to days. Traditional sampling methods are unable to capture high frequency events that can be clearly observed using a wet-chemical microfluidic system deployed within a glider. We highlight firstly, an excellent agreement between the LoC and shipboard nitrate + nitrite measurements ($r^2 = 0.98$ $n = 11$). Secondly, the LoC was able to observe a decrease in nitrate within the surface mixed layer from 5.74 μM (4th) to 1.42 μM (25th) during the onset of the spring bloom, whilst bottom layer concentrations remained constant (6.86 ± 0.16 μM), with an estimated analytical uncertainty of < 0.2 μM. Thirdly, the ability of an LoC sensor deployed within an AUV to accurately capture simultaneous biogeochemical and physical parameters at an enhanced resolution, on both spatial and temporal scales, improves our understanding of biogeochemical cycles within the dynamic temperate shelf sea environments.

1. Introduction

Seasonally stratified temperate shelf seas act as important global carbon sinks through the continental shelf pump mechanism (Takahashi et al., 2009; Thomas et al., 2004; Tsunogai et al., 1999). Despite the shelf seas relatively small size (8% of global ocean area), they actually account for 15–30% of total oceanic primary production (Tweddle et al., 2013) and have an average carbon fixation rate per unit area ~ 2.5 times greater than the open ocean (Simpson and Sharples, 2012). The interplay between light, nutrients and mixing are key drivers of primary production. A well-studied temperate shelf system, the Celtic Sea, shows a clear seasonal cycle, whereby initial light and nutrient conditions are ideally suited to support the onset of the spring bloom (Fasham et al., 1983). This results in the rapid drawdown of nitrate (NO_3^-) from ~ 6–8 μM to below the limit of detection (< 0.1 μM) (e.g. Davidson et al., 2013; Hickman et al., 2012). Post-bloom, new primary production is limited to the sub-surface chlorophyll maximum (SCM) where fluxes of NO_3^- into the thermocline fuels new production (Hickman et al., 2009).

In the central Celtic Sea, shear generated turbulence (Rippeth et al., 2009; Sharples et al., 2007; 2001) and wind-driven oscillations (Rippeth, 2005) are the central mechanisms in driving diapycnal mixing of NO_3^- up into the nutrient deplete surface mixed layer. Wind-driven shear occurs in episodic short-lived spikes (0.5–1 h) and has the potential to have a large impact on NO_3^- fluxes with observations indicating that this flux can be up to 4 times greater than when no shear was observed (Palmer et al., 2008; Rippeth et al., 2009; Sharples et al., 2001).

At present, it is difficult to effectively sample nitrate at the high resolution required to observe these key short-term mixing events

* Corresponding author at: Ocean and Earth Science, National Oceanography Centre, Southampton SO14 3ZH, UK.
E-mail address: agv1e15@soton.ac.uk (A.G. Vincent).

https://doi.org/10.1016/j.marchem.2018.07.005
Received 26 March 2018; Received in revised form 27 June 2018; Accepted 14 July 2018
Available online 17 July 2018
0304-4203/

(Sharples et al., 2007; Williams et al., 2013). Combined with limited winter data, this can lead to incorrect seasonal estimates of NO_3^- fluxes that are key to primary production and carbon fixation. Chemical *in situ* sensors can provide the high-resolution data necessary to resolve biogeochemical processes occurring in shelf seas (Adornato et al., 2010; Prien, 2007). Wet-chemical analyzers, centered on microfluidic Lab-on-Chip (LoC) technology, are at the leading edge of advancements for chemical *in situ* nutrient measurements (Nightingale et al., 2015). Due to their compactness, low resource use and analytical performance comparable to laboratory-based methods, LoC nutrient sensors are well suited to high-resolution float, glider and mooring deployments. Autonomous underwater vehicles, such as gliders, have already been shown to provide an economic and efficient observation platform to resolve mesoscale and submesoscale structures allowing for high-resolution sampling of biogeochemical parameters, such as NO_3^- using an *in situ* ultraviolet spectrophotometer (Johnson et al., 2009; Sauzède et al., 2017; Rudnick, 2016).

Here we demonstrate the power of coupling the LoC nutrient sensor into a Seaglider to obtain continuous *in situ* high temporal and spatial resolution nitrate + nitrite (NO_3^- + NO_2^-; hereafter defined as ΣNO_x) measurements over the duration of the spring bloom in April 2015. This enabled short-term mixing events key to establishing the spring bloom and its subsequent decline to be observed.

2. Experimental

A single LoC ΣNO_x sensor (Ocean Technology and Engineering Group, National Oceanography Center, Southampton, UK) was integrated within the science bay of a Kongsberg Seaglider (Ogive fairing) and deployed from the *R.S.S Discovery* in the Celtic Sea, as part of the NERC funded Shelf Sea Biogeochemistry program in April 2015. In addition, a second LoC ΣNO_x sensor was mounted on a Conductivity-Temperature-Depth (CTD; Seabird 911 plus) rosette to enable direct comparison of its measurements to concentrations of ΣNO_x from seawater samples collected *in situ* at the same depth and time.

Both LoC deployments by Seaglider and discrete ship-based CTD rosette samples were collected from the Central Celtic Sea site (CCS; Fig. 1) located ~137 miles off the Cornish coast, UK (49°24.134′N, 8°36.248′W), with a water column depth of ~145 m. The Seaglider with integrated LoC ΣNO_x sensor was deployed for 21 days (4th–25th April 2015) and completed 776 dives within 10 km of the CCS station. A total of 24 CTD casts within < 22 km of CCS were also conducted allowing for comparison. The rosette package consisted of a Seabird 911 plus CTD and 24 bottle Niskin system, which was used to collected discrete seawater samples. Chlorophyll *a* (hereafter Chl-*a*) was measured on a pre-calibrated (spinach extract, Sigma Aldrich) fluorometer (Turner Design Trilogy). Water samples collected from the Niskin bottles were analyzed onboard for NO_3^- + NO_2^- using a segmented-flow auto-analyzer (Bran & Luebbe) following the colorimetric procedures of Woodward and Rees (2001).

The LoC ΣNO_x sensor is composed of a three-layer PMMA chip, which contains precision-milled microchannels (150 µm wide, 300 µm deep), mixers and optical components consisting of LEDs (525 nm, Avago Technologies, USA) and photodiodes. Syringe pump, valves and electronics are mounted on the chip, which was encased in a mineral oil-filled housing (PVC, 12 cm diameter, 30 cm height) with an internally fitted pressure-compensating bladder. The LoC ΣNO_x sensor uses colourimetric detection, using the Griess assay (Grasshoff et al., 2009) where NO_3^- is reduced to NO_2^- using an off-chip copper activated cadmium column to enable ΣNO_x to be determined. A detection limit of 20 nM and linear range of up to 350 µM have been demonstrated in laboratory settings (Beaton et al., 2012). The LoC ΣNO_x sensor relies on a standard measurement and a blank measurement to determine the concentration of the sample. All reagents (Griess, imidazole buffer), standard and blank solutions were stored in externally attached gas impermeable 150 mL Flexboy bags (Sartorius, UK) and the waste was collected into a 500 mL Flexboy bag. The LoC ΣNO_x sensor, reagents and standards used in this study have previously been described in detail by Beaton et al. (2011, 2012) where it was deployed in a dynamic estuarine environment. More recently, the LoC ΣNO_x sensor was deployed on a benthic lander in the Mauritian oxygen minimum zone to examine cross-shelf transport of NO_3^- rich waters (Yücel et al., 2015), and in glacial meltwaters rivers draining the Greenland Ice Sheet (Beaton et al., 2017).

The LoC ΣNO_x sensor was integrated into the payload bay of the Seaglider (Fig. 2) and connected by cable directly into one of the glider serial ports. The inlet tube with filter is located on the surface of the payload bay cover ~30 cm behind the CT sail (Seabird Electronics). The Seaglider software uses a CNF file that contains the configuration for each on-board instrument and a CMD file that provides mission parameters. The CNF file enables communication between the seaglider and the LoC ΣNO_x sensor. The LoC ΣNO_x sensor is set to 'logger' in the CNF file, which enables the glider to send a number of commands. These commands allow the Seaglider to send and receive data to and from the sensor. Some of the key commands are 'clock-set' used only at the start of each dive but enables the sensor to store any time offset between glider and sensor, 'Status' which sends the sensor depth every 5 s along with 3 trigger values and 'download' sent at the end of each dive requesting the sensor to send both ascent and descent data files of processed ΣNO_x values. During deployments the CMD file is typically transmitted to the Seaglider by satellite and includes three trigger values that can be passed to the LoC ΣNO_x sensor using the 'status' command. These triggers are used to modify sensor behavior at different depths. Primarily these are used to ensure the LoC ΣNO_x sensor does not take samples on the surface and risk the intake of air, and to aid with additional blank and standard measurements.

For deployments on the CTD rosette, the LoC ΣNO_x sensor was programmed in a continuous mode and performed a repeating measurement sequence of artificial seawater blank, sample, and NO_3^- standard (3 µM), until the CTD rosette was recovered to 5 m where the power was turned off. The operation of the LoC sensor was as follows; The seawater sample was drawn into the sensor through a 0.45 µm MILLEX-HP filter unit (Millipore). Both the filtered seawater sample and imidazole buffer were pushed simultaneously through a serpentine mixer (used to aid mixing) before moving through an off-chip cadmium column. Griess reagent was added to the resultant buffered reduced seawater sample and then pushed through the 25 mm absorption measurement cell, where the pink-coloured azo dye developed. Absorbance was calculated by comparing the optical intensity measured by the photodiode after a 100 s reaction wait time for each measurement. Each step involved 7 flushes prior to the measurement to minimize sample carryover. Photodiode data was recorded at 1 Hz and the average of the last 10 readings of each wait stage was used to calculate absorbance, according to the Beer-Lambert law. Concentrations were calculated by comparing the absorbance of each sample to that of the subsequent standard measurement. This results in one blank-corrected sample measurement and standard every 17 min during CTD deployments.

For the Seaglider deployments, the LoC ΣNO_x sensor was programmed to obtain a minimum of one artificial seawater blank and a standard measurement (6.5 µM NO_3^-) at the beginning and end of each dive. After the first measurement of blank and standard, continuous sample measurements took place on both the descent and ascent until the glider was at 10 m. Discrete seawater samples were drawn through a 0.45 µm MILLEX-HP filter unit (Millipore) into the sensor within the payload bay. Over the period of sampling (21 days) this resulted in 312 and 199 artificial seawater blanks and standards, which was sufficient to determine both the ΣNO_x concentration and any drift associated with either the artificial seawater blank and/or the NO_3^- standard.

The Seaglider is a buoyancy driven autonomous underwater vehicle capable of multi-month deployments collecting high-resolution profiles of physical and biogeochemical parameters to 1000 m with a maximum

Appendix A

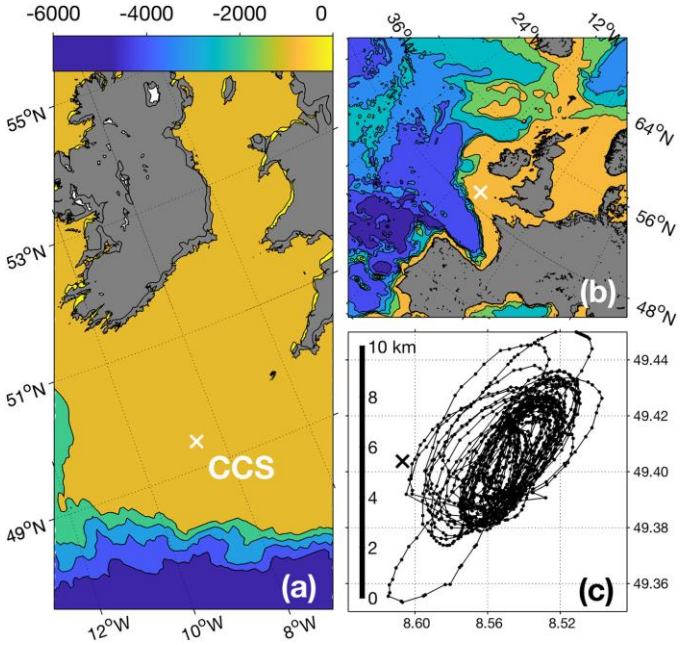

Fig. 1. (a) Location of the Central Celtic Sea (CCS) sampling site (white cross) and shelf and shelf edge bathymetry. (b) Location of the Celtic sea on the North West European Shelf. (c) Seaglider tracks (black line) and surfacing points (black dots) in relation to CCS from the 4th to 25th of April 2015.

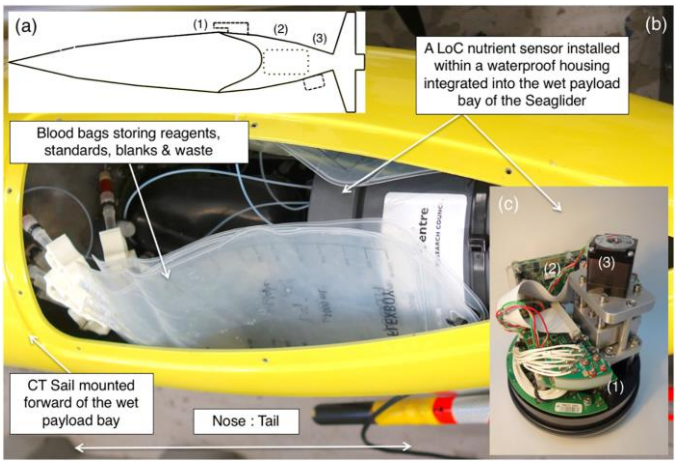

Fig. 2. (a) Diagram of the locations of sensors deployed on the Seaglider (Kongsberg; Not to scale): (1) CT sail, (2) LoC, and (3) EcoPuck. (b) A LoC ΣNOx Sensor deployed with housing within the sensor payload bay of a Seaglider (Ogive Profile). (c) A LoC ΣNOx sensor consisting of (1) microfluidic chip, (2) custom electronics, and (3) syringe pump assembly.

travel range of 4600 km (Rudnick et al., 2004). Bilateral communication between the Seaglider and base station, through an Iridium satellite connection, allowed dive configurations to be modified once deployed. Data was transmitted back to shore during deployments to assess the performance of the LoC ΣNO_x sensor. In addition to the LoC ΣNO_x sensor within the science bay, the Seaglider measured conductivity & temperature (non-pumped Sea-Bird SBE13 CT Sail, Seabird Electronics), pressure (Pain Electronics) and fluorescence, turbidity and optical backscatter (Triplet Ecopuck, Wet Labs). Conductivity, temperature and pressure were collected at a frequency of 1 Hz during deployment with all dive profiles lying within 4 km of CCS (Fig. 1). Temperature and conductivity were extracted and processed using the UEA Glider Toolbox (Queste, 2013). These routines apply manufacturer calibrations, correct for thermal inertia following the methods of Garau

et al. (2011) remove spikes and anomalous data, and draw upon a flight model similar to that described by Frajka-Williams et al. (2011). Four CTD casts, taken within 1.6 km of the glider, were used to calibrate the temperature and salinity. Manufacturer calibrations were initially applied to data from the Wetlabs Triplet for coloured dissolved organic matter (CDOM), backscatter & fluorescence by subtracting the instrument blank and applying a scaling factor. Calibration to convert fluorescence to Chl-*a* is based on the sensor's response to a cultured diatom, *Thalassiosira weissflogii* at a known Chl-*a* concentration (Hemsley et al., 2015; Sea-Bird Scientific, 2017).

3. Results and discussion

The ability of the LoC ΣNO_x sensor to accurately determine ΣNO_x was assessed in two ways: (i) by comparison of the LoC ΣNO_x sensor mounted on the stainless steel rosette with discrete water samples collected at the same time and (ii) by comparing profiles obtained from the LoC ΣNO_x sensor deployed within the glider with discrete water samples collected from the CTD on the same day at CCS. The LoC ΣNO_x sensor, along with battery and reagents, was a similar size to the 20 L Niskin bottle and was mounted in place of a single Niskin bottle on the frame. Once below 5 m, a pressure sensor on the battery activated the power to the LoC ΣNO_x sensor. The CTD rosette was held at three depths (45, 50 & 90 m) for at least 90 min to allow for triplicate LoC ΣNO_x sensor measurements at the prescribed depth, each bracketed by a blank and standard measurement. During this time period, two Niskin bottles were fired, one within 5 min of the first LoC ΣNO_x sensor measurement and the second within 5 min of the last LoC ΣNO_x sensor measurement. Water was collected from these discrete bottle firings for determination of $NO_3^- + NO_2^-$ concentrations using the segmented flow autoanlyzer in the ship-based laboratory. Fig. 3a indicates the excellent agreement between sensor measurements and analysis of discrete water samples with a correlation of $r^2 \geq 0.99$ ($n = 9$; $p \leq 0.001$). The estimated analytical uncertainty of the LoC ΣNO_x sensor was calculated from two times the standard deviation of the absorbance value of the deployed standard over the three deployments and was 0.14 μM ($n = 10$). This analytical uncertainty is higher than reported values for traditional segmented flow autoanlyzer analysis of ΣNO_x (0.03–0.07 μM) (Dafner, 2015) but lower than previous LoC ΣNO_x deployments (0.4–1 μM) (Yücel et al., 2015).

LoC ΣNO_x data, collected from within the glider, was compared with $NO_3^- + NO_2^-$ values from 24 CTD profiles collected at CCS throughout the 21 day deployment. Unlike the previous assessment of analytical uncertainty, data from the CTD profiles were not collected at the same time (1–10 h window) or depth range (± 3 m) and all samples were collected in a dynamic shelf sea system. Fig. 3b however, shows the excellent agreement the LOC ΣNO_x data and the discrete water sample measurements over the 21 day period, with a correlation of $r^2 \geq 0.98$ ($n = 51$; $p \leq 0.001$). The average estimated analytical uncertainty for the LoC ΣNO_x sensor during this period was 0.19 μM ($n = 142$) similar to the 0.14 μM ($n = 10$) for the CTD NO_3^- profiles.

Initial Seaglider dives (4th to 9th of April) were configured in a standard flight mode, whereby the Seaglider adjusts its pitch and buoyancy to maintain a uniform glide slope and descent and ascent speed (Eriksen et al., 2001). The LoC ΣNO_x sensor was switched on at the beginning of each dive and completed a blank and standard measurement followed by continuous measurements. The LoC ΣNO_x sensor acquired depth information directly from the Seaglider, and using a depth trigger at 10 m the sensor recognized the Seaglider was diving and after completing its current blank or standard measurement would undertake continuous sample measurements. Triggers were also used to take advantage of extra time at the beginning, apogee and end of dives to undertake extra blank and standard measurements.

Fig. 4a shows that when the Seaglider was operated in the standard dive mode, the LoC ΣNO_x sensor carried out 5 sample measurements per 120 m dive with a total dive time of 30 ± 8 min. Moreover, these measurements were always in the same depth ranges within the water column due to the relatively shallow water column (~145 m) and sensor operation timings. Fig. 4b shows the excellent agreement between the LoC ΣNO_x sensor and traditional CTD segmented flow

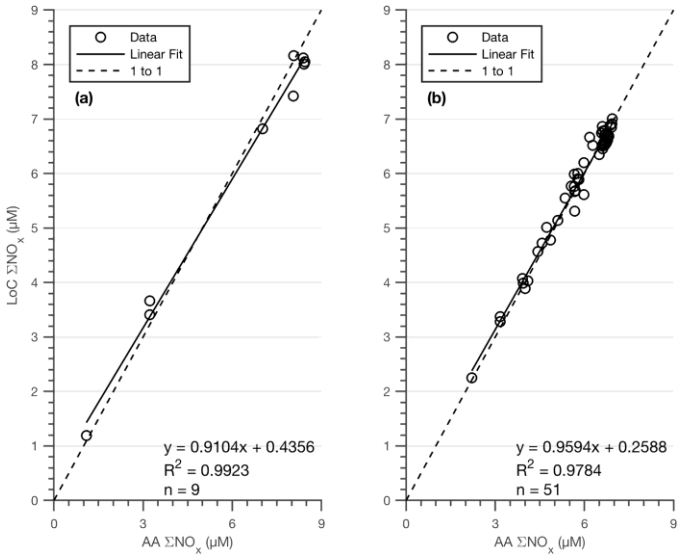

Fig. 3. Comparison of autoanalyzer (AA) and LoC ΣNO_x measurements. (a) AA and *in situ* LoC ΣNO_x measurements obtained from CTD casts. (b) AA and LoC ΣNO_x measurements obtained from separate CTD casts (3rd to 6th, 11th, 12th, 15th, 16th, 20th, 21st and 25th April) and *in situ* LoC glider profiles at CCS.

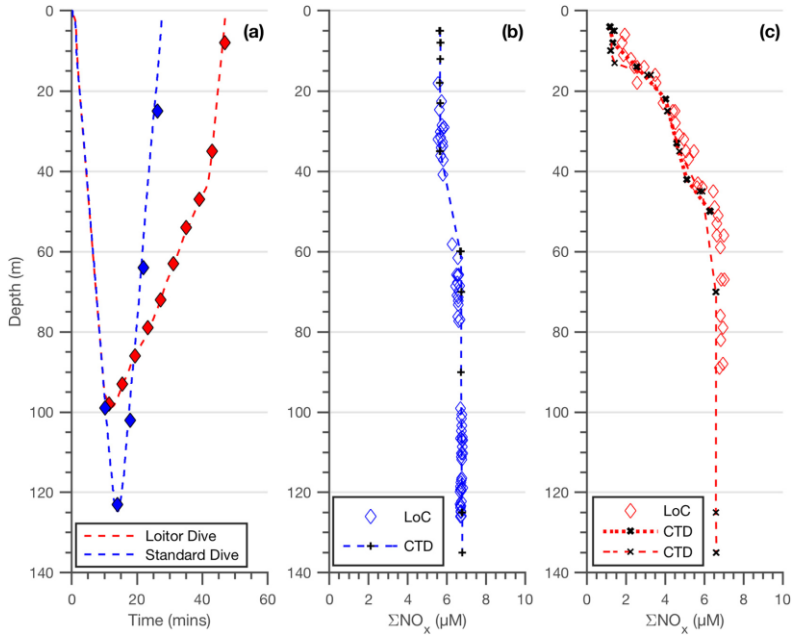

Fig. 4. (a) Comparison of the two different dives used in this study. Blue and red diamonds indicate where ΣNO_x measurements were obtained. (b) ΣNOx measurements from one CTD cast (02:06 am; dashed line) and sixteen standard dives (00:18 to 09:25 am; diamonds) from the 6th April 2015. (c) ΣNO_x measurements from two CTD cast (02:06 and 08:22 am; dashed lines) and seven 'loiter' dives (11:19 to 16:25 pm; diamonds) from the 16th April 2015. (For interpretation of the references to colour in this figure legend, the reader is referred to the web version of this article.)

autoanlyzer measurements, for one single CTD cast at 02:06 am and sixteen dives by the Seaglider from 00:18 to 09:25 am on the 6th of April 2015. However, the temporal and spatial resolution of ΣNO_x data (over the period of the day within the surface layer and across boundaries such as the nitricline) would not be sufficient to investigate the depletion of ΣNO_x as the spring bloom develops. As the glider can be controlled remotely, to increase the distribution of measurements by the LoC ΣNO_x sensor throughout the water column, (in particular across the nitricline), a second dive methodology - termed a '*loiter*' dive - was employed. After the Seaglider has reached its maximum depth for that particular dive and started its ascent, for 30 mins the ascent angle was lowered and the glider 'loitered', thus increasing the resolution of measurements within the water column (Fig. 4a). Selected maximum target depths (90, 60, 40 and 25 m) were used to control the maximum dive depth and ensured a higher number of measurements in areas of interest (Fig. 4c). Loiter dives to 90 m doubled the amount of measurements made compared to the previous standard dives. Fig. 4c shows a comparison between ΣNO_x concentrations from two CTD casts at 02:06 and 08:22 am and LoC ΣNO_x concentrations from seven 'loiter' dives from 11:19 am to 16:25 pm on the 15th of April 2015. Once more, good agreement between the LoC ΣNO_x sensor and traditional segmented flow autoanlyzer measurements of CTD discrete samples was observed throughout the whole water column during this 14-h period. To ascertain the ability of the LoC ΣNO_x sensor to make comparable measurements to the segmented flow autoanlyzer, over an extended time period (4th to 25th April 2015), we compared the measurements within the bottom layer at 60–120 m where little changes in ΣNO_x were observed. Excellent agreement between both the segmented flow autoanlyzer (6.86 ± 0.09 μM; n = 22) and LoC ΣNO_x sensor (6.86 ± 0.16 μM; n = 120) was observed. We have demonstrated the ΣNO_x concentrations measured from the LoC ΣNO_x sensor are comparable to those of the shipboard measurements analyzed on a segment flow autoanlyzer. Moreover, this shows that accurate measurements can be obtained from the LoC ΣNO_x wet chemical sensor over 21 days in a dynamic shelf environment.

On-board calibration with artificial seawater blanks and NO_3^- standard for each dive enables both the monitoring of instrument performance and stability over long-term deployments. To ensure maximum efficiency of the cadmium column, where NO_3^- is reduced to NO_2^- a flow rate of 150 μl/min was chosen (Beaton et al., 2012). However, it is important to monitor any drift in the efficiency of the cadmium column over time as this may impact on the ΣNO_x concentrations. In this study, a decrease in absorbance values was observed, likely due to the gradual reduction in efficiency of the cadmium column over time. As sample concentrations are calculated from their associated blank and standard measurements, where the ratio of the absorbance of the sample and standard are determined, any drift caused by the decreasing reduction efficiency of the cadmium column is compensated for. Our results demonstrate that any decrease in absorbance values observed did not impact on the accurate determination of ΣNO_x from the LoC as shown by the excellent agreement with traditional autoanlyzer ΣNO_x method from discrete water samples collected throughout the 21-day deployment.

The data set presented here was collected during the spring phytoplankton bloom, a period during which integrated net productivity becomes greater than integrated losses and phytoplankton biomass accumluates in surface waters (Sverdrup, 1953). Over the 21-day deployment the LoC ΣNOx sensor was able to accurately capture the large

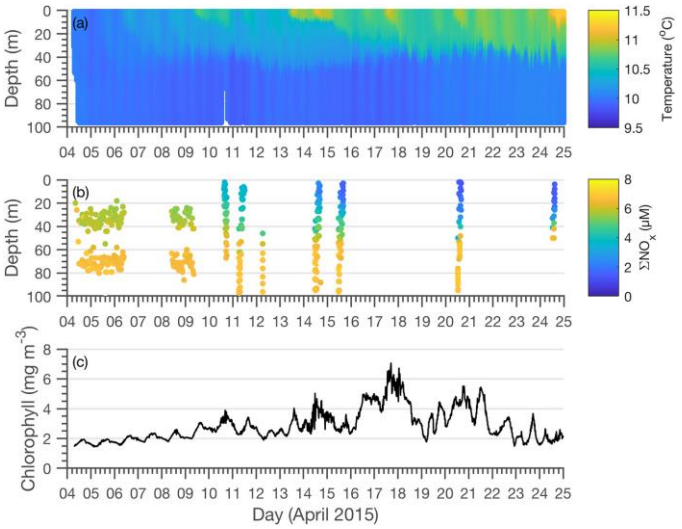

Fig. 5. (a) temperature (°C), (b) LoC ΣNO_z (μM) and (c) mean surface (< 20 m) Chlorophyll-*a* measurements obtained from one Seaglider deployment from the 4th to 25th April 2015.

drawdown of ΣNOx within the surface layer due to the onset of the spring bloom (Fig. 5). Concentrations decreased from 5.74 μM (4th) to 1.42 μM (25th), whilst bottom layer NO_3^- concentrations remained constant (6.86 ± 0.16 μM), as observed in previous studies within the Celtic Sea (Tweedle, 2007; Williams, 2013).

At the start of the deployment (4th – 6th April 2015), a small 0.8 μM difference between near surface (20–40 m) and bottom water (60-80 m) ΣNO_x concentrations was observed. During this time, surface Chl-*a* concentrations were relatively low (1.8 mg m^{-3}), but much higher (by 1.5 mg m^{-3}) than those typically observed during the winter in the area (Pingree et al., 1976; Smyth et al., 2010). This suggests that some phytoplankton growth had already occurred prior to deployment of the glider.

Between the 4th and 6th April the ΣNO_x concentration between 20 and 40 m remained constant. Any changes in the near surface (< 20 m) water however, where you might expect the largest drawdown in NO_3^-, were not resolved since the standard dive pattern used during this early period did not result in near surface LoC ΣNO_x measurements being made. Nevertheless, it is clear from Fig. 5 that a large drawdown of 3 μM ΣNO_x occurred between the 4th and 11th of April 2015 (< 40 m) as stratification of the water column initialized. This can be backed up with the observed increase in surface water Chl-*a,* from 1.8 mg m^{-3} to 3.7 mg m^{-3}, indicative of phytoplankton growth, and thus nutrient drawdown, during the onset of the spring bloom. Changing the dive configuration to 'loiter' dives on the 11th of April increased the resolution of ΣNOx surface data.

Just as the temperature sensor resolves the gradual deepening and warming of the surface mixed layer, the LoC ΣNOx sensor resolves the coincident deepening of the nitricline and drawdown of ΣNOx above it. Between the 4th and 25th April surface waters warmed by > 1 °C and a 40 m deep thermocline is established. During this time there is a 4.2 μM drawdown of ΣNOx and an increase in Chl-a from a background of 1.8 mg m^{-3} to 4–6.8 mg m^{-3}.

By the end of the Seaglider deployment (25th) a two-layer water column had developed with a warm, nutrient depleted, 40 m surface layer overlying colder, nutrient rich bottom waters. Previous studies suggest that phytoplankton growth starts to become ΣNO_x limited when concentrations fall below 1 μM (Eppley et al., 1969). The low surface water ΣNO_x concentrations (1.4 μM) measured during the end of the deployment suggest that this was close to happening. This is supported by a coinciding decrease in Chl-*a* (to < 2 mg m^{-3}) towards the end of the deployment. Ship-based observations show that it was not until the 28th that surface water concentration were below the limit of detection of 0.1 μM (Birchill et al., 2017).

This study has demonstrated for the first time that it is possible to accurately measure ΣNO_x over long-term deployments using a wet chemical nutrient sensor deployed within a glider. Our study provides a novel methodology, of differing operational characteristics to current high-resolution capable methodology (Johnson et al., 2013), enabling an increase in observations of ΣNO_x dynamics in temperate shelf seas during key transitional events (e.g. the onset of stratification and the spring bloom, convective overturning and the autumn bloom) and across fine-scale vertical and horizontal features (e.g. tidal mixing fronts, sub-surface chlorophyll maximum). At present, wet chemical biogeochemical sensors do not have the vertical resolution capabilities of the commonly used physical and optical sensors such as temperature, fluorescence or established ultraviolet spectrophotometer nitrate sensors (Johnson and Coletti, 2002). This resolution could be further improved by decreasing the time taken between measurements. By increasing flow rate, decreasing colour development time, decreasing the number of flushes and increasing N.E.D (naphthylethylenediamine dihydrochloride) concentration and reaction temperature, an increased measurement resolution could be achieved, but at the expense of measurement sensitivity (Beaton et al., 2012; Pai et al., 1990).

For long-term deployment of wet chemical sensors, reduced resource consumption (power and reagents) and compact size are the main advantages of microfluidic systems. Deployment of sensors on moorings, where solar and wind power are available, negates power constraints. However, for autonomous underwater vehicles power becomes the greatest limiting resource (Dickey et al., 2008). During the 21-day deployment, the LoC ΣNO_x sensor (version 3.2) had a low power consumption of 1.5 W. This was only marginally higher than the other standard sensor packages on the Seaglider (0.9 W and 0.25 W for the Wetlabs ECO Triplet and SBE pumped payload CTD respectively), but

Appendix A

lower than other wet chemical and UV absorption systems (e.g. ISUS V3, Satlantic, USA; NitraVis, YSI, USA; SubChemPak, SubChem Systems, USA). A single dive of the LoC ΣNO_x sensor consumed 2.5 mL of Griess reagent, 2.5 mL of buffer solution and 0.21 mL of standard and blank solution achieving 1 blank and standard measurement and ~ 10 samples on a dive to 120 m. This would enable a total of 400 dives to be made and 4000 sample measurements. During this study, the LoC was only active during periods when the *R.S.S Discovery* was also sampling at CCS to enable a direct comparison between the two types of measurements over a long-term deployment of the LoC. This resulted in accurate LoC ΣNO_x determined over 21 days. With a sampling strategy focused on achieving the maximum amount of measurements, a profile consisting of 10 sample measurements could be undertaken every ~ 40 min, allowing for increased observations of episodic and transient events unable to be observed by discrete sampling.

4. Conclusion

The temporal and spatial variability of biogeochemical processes has been successfully measured through the use of remote sensing, time series moorings and ship-based methods, but these, to an extent, fall short in resolving the dynamic temporal and spatial elements with long-term endurance in a low cost package. From this, there has been a strong call for the development of biogeochemical sensors to be deployed, on stationary and mobile platforms, to provide *in situ* measurements as part of sensor networks aimed at providing long term monitoring within a low cost package (Adornato et al., 2010; Johnson et al., 2009). The LoC ΣNO_x sensor deployed within the Seaglider in this study clearly demonstrates that nitrate & nitrite can be accurately determined over monthly timescales due to the sensor's low resource use, small size and *in situ* calibration abilities. Moreover, deployed within a glider with other physical and biochemical data (e.g. CTD and the Wetlabs Triplet sensor measurements), it provided a powerful tool for resolving dynamic biogeochemical processes within a dynamic shelf system.

Acknowledgements

The authors would like to thank the captain and crew of the R.S.S Discovery. This project was funded by UK Natural Environmental Research Council through the Sensors on Gliders program (NE/J020184/1) to MCL and (NE/K001701/1) to JEH. The field deployment took place under the Shelf Sea Biogeochemistry program with funding to MCL from NERC (NE/K001779/1). Funding from the European Union Seventh Framework Program (FP7/2007-2013) under grant agreement n°614141 (SenseOCEAN) contributed to the research leading to these results. We would also like to thank David White, Alvaro Lorenzo Lopez, Sam Ward, James Burris and Stephen Woodward of the Marine Autonomous and Robotics Systems group, and David Owsianka and Adrian Nightingale of the Ocean Technology and Engineering group at the National Oceanography Centre, UK.

References

Adornato, L., Cardenas-Valencia, A., Kaltenbacher, E., Byrne, R., Daly, K., Larkin, K., Hartman, S., Mowlem, M., Prien, R., Garcon, V., 2010. In situ nutrient sensors for ocean observing systems. In: Hall, J., Harrison, D.E., Stammer, D. (Eds.), Proceedings of OceanObs'09: Sustained Ocean Observations and Information for Society. European Space Agencey, pp. 9–18. https://doi.org/10.5270/OceanObs09.cwp.01.

Beaton, A.D., Sieben, V.J., Floquet, C.F.a., Waugh, E.M., Abi Kaed Bey, S., Ogilvie, I.R.G., Mowlem, M.C., Morgan, H., 2011. An automated microfluidic colourimetric sensor applied in situ to determine nitrite concentration. Sensors Actuators B Chem. 156, 1009–1014. https://doi.org/10.1016/j.snb.2011.02.042.

Beaton, A.D., Cardwell, C.L., Thomas, R.S., Sieben, V.J., Legiret, F.-E., Waugh, E.M., Statham, P.J., Mowlem, M.C., Morgan, H., 2012. Lab-on-chip measurement of nitrate and nitrite for in situ analysis of natural waters. Environ. Sci. Technol. 46, 9548–9556. https://doi.org/10.1021/es300419u.

Beaton, A.D., Wadham, J.L., Hawkings, J., Bagshaw, E.A., Lamarche-Gagnon, G., Mowlem, M.C., Tranter, M., 2017. High-resolution in situ measurement of nitrate in runoff from the Greenland ice sheet. Environ. Sci. Technol. 12518–12527. https://doi.org/10.1021/acs.est.7b03121.

Birchill, A.J., Milne, A.S., Woodward, E.M., Harris, C., Annett, A., Rusiecka, D., Achterberg, E.P., Gledhill, M., Ussher, S.J., Worsfold, P.J., Geibert, W., Lohan, M.C., 2017. Seasonal iron depletion in temperate shelf seas. Geophys. Res. Lett. 8987–8996. https://doi.org/10.1002/2017GL073881.

Dafner, E.V., 2015. Segmented continuous-flow analyses of nutrient in seawater: Intralaboratory comparison of Technicon AutoAnalyzer II and Bran+Luebbe Continuous Flow AutoAnalyzer III. Limnol. Oceanogr. Methods 13, 511–520. https://doi.org/10.1002/lom3.10035.

Davidson, K., Gilpin, L.C., Pete, R., Brennan, D., McNeill, S., Moschonas, G., Sharples, J., 2013. Phytoplankton and bacterial distribution and productivity on and around Jones Bank in the Celtic Sea. Prog. Oceanogr. 117, 48–63. https://doi.org/10.1016/j.pocean.2013.04.001.

Dickey, T.D., Itsweire, E.C., Moline, M., Perry, M.J., 2008. Introduction to the limnology and oceanography special issue on autonomous and Lagrangian platforms and sensors (ALPS). Limnol. Oceanogr. 53, 2057–2061. https://doi.org/10.4319/lo.2008.53.5_part_2.2057.

Eppley, R.W., Rogers, J.N., McCarthy, J.J., 1969. Half-saturation constants for uptake of nitrate and ammonium by marine phytoplankton. Limnol. Oceanogr. 14 (6), 912–920. https://doi.org/10.4319/lo.1969.14.6.0912.

Eriksen, C.C., Osse, T.J., Light, R.D., Wen, T., Lehman, T.W., Sabin, P.L., Ballard, J.W., Chiodi, A.M., 2001. Seaglider: a long-range autonomous underwater vehicle for oceanographic research. IEEE J. Ocean. Eng. 26, 424–436. https://doi.org/10.1109/48.972073.

Fasham, M.J.R., Holligan, P.M., Pugh, P.R., 1983. The spatial and temporal development of the spring phytoplankton bloom in the Celtic Sea, April 1979. Prog. Oceanogr. 12, 87–145. https://doi.org/10.1016/0079-6611(83)90007-1.

Frajka-Williams, E., Eriksen, C.C., Rhines, P.B., Harcourt, R.R., 2011. Determining vertical water velocities from Seaglider. J. Atmos. Ocean. Technol. 28, 1641–1656. https://doi.org/10.1175/2011JTECHO830.1.

Garau, B., Ruiz, S., Zhang, W.G., Pascual, A., Heslop, E., Kerfoot, J., Tintoré, J., 2011. Thermal lag correction on slocum CTD glider data. J. Atmos. Ocean. Technol. 28, 1065–1071. https://doi.org/10.1175/JTECH-D-10-05030.1.

Grasshoff, K., Kremling, K., Ehrhardt, M. (Eds.), 2009. Methods of Seawater Analysis. John Wiley & Sons.

Hemsley, V.S., Smyth, T.J., Martin, A.P., Frajka-Williams, E., Thompson, A.F., Damerell, G., Painter, S.C., 2015. Estimating oceanic primary production using vertical irradiance and chlorophyll profiles from ocean gliders in the North Atlantic. Environ. Sci. Technol. 49, 11612–11621. https://doi.org/10.1021/acs.est.5b00608.

Hickman, A.E., Holligan, P.M., Moore, C.M., Sharples, J., Krivtsov, V., Palmer, M.R., 2009. Distribution and chromatic adaptation of phytoplankton within a shelf sea thermocline. Limnol. Oceanogr. 54, 525–536.

Hickman, A., Moore, C., Sharples, J., Lucas, M., Tilstone, G., Krivtsov, V., Holligan, P., 2012. Primary production and nitrate uptake within the seasonal thermocline of a stratified shelf sea. Mar. Ecol. Prog. Ser. 463, 39–57. https://doi.org/10.3354/meps09836.

Johnson, K., Berelson, W., Boss, E., Chase, Z., Claustre, H., Emerson, S., Gruber, N., Körtzinger, A., Perry, M.J., Riser, S., 2009. Observing biogeochemical cycles at global scales with profiling floats and gliders: prospects for a global array. Oceanography 22, 216–225. https://doi.org/10.5670/oceanog.2009.81.

Johnson, K.S., Coletti, L.J., 2002. In situ ultraviolet spectro- photometry for high resolution and long term monitoring of nitrate, bromide and bisulfide in the ocean. Deep Sea Res. I 49, 1291–1305.

Johnson, K.S., Coletti, L.J., Jannasch, H.W., Sakamoto, C.M., Swift, D.D., Riser, S.C., 2013. Long-term nitrate measurements in the ocean using the in situ ultraviolet spectrophotometer: sensor integration into the APEX profiling float. J. Atmos. Ocean. Technol. 30, 1854–1866. https://doi.org/10.1175/JTECH-D-12-00221.1.

Nightingale, A.M., Beaton, A.D., Mowlem, M.C., 2015. Trends in microfluidic systems for in situ chemical analysis of natural waters. Sensors Actuators B Chem. 221, 1398–1405. https://doi.org/10.1016/j.snb.2015.07.091.

Pai, S.C., Yang, C.C.P., Riley, J., 1990. Formation kinetics of the pink azo dye in the determination of nitrite in natural waters. Anal. Chim. Acta 232, 345–349. https://doi.org/10.1016/S0003-2670(00)81252-0.

Palmer, M.R., Rippeth, T.P., Simpson, J.H., 2008. An investigation of internal mixing in a seasonally stratified shelf sea. J. Geophys. Res. 113, C12005. https://doi.org/10.1029/2007JC004531.

Pingree, R.D., Holligan, P.M., Mardell, G.T., Head, R.N., 1976. The influence of physical stability on spring, summer and autumn phytoplankton blooms in the Celtic Sea. J. Mar. Biol. Assoc. U. K. 56, 845–873. https://doi.org/10.1017/S0025315400020919.

Prien, R.D., 2007. The future of chemical in situ sensors. Mar. Chem. 107, 422–432. https://doi.org/10.1016/j.marchem.2007.01.014.

Queste, B.Y., 2013. Hydrographic Observations of Oxygen and Related Physical Variables in the North Sea and Western Ross Sea Polynya. University of East Anglia.

Rippeth, T.P., 2005. Thermocline mixing in summer stratified continental shelf seas. Geophys. Res. Lett. 32, L05602. https://doi.org/10.1029/2004GL022104.

Rippeth, T.P., Wiles, P., Palmer, M.R., Sharples, J., Tweddle, J., 2009. The diapcynal nutrient flux and shear-induced diapcynal mixing in the seasonally stratified western Irish Sea. Cont. Shelf Res. 29, 1580–1587. https://doi.org/10.1016/j.csr.2009.04.009.

Rudnick, D.L., 2016. Ocean research enabled by underwater gliders. Annu. Rev. Mar. Sci. 8, 519–541. https://doi.org/10.1146/annurev-marine-122414-033913.

Rudnick, D.L., Davis, R.E., Eriksen, C.C., Fratantoni, D.M., Perry, M.J., 2004. Underwater gliders for ocean research. Mar. Technol. Soc. J. 38, 73–84.

Sauzède, R., Bittig, H.C., Claustre, H., Pasqueron de Fommervault, O., Gattuso, J.-P., Legendre, L., Johnson, K.S., 2017. Estimates of water-column nutrient concentrations

and carbonate system parameters in the global ocean: a novel approach based on neural networks. Front. Mar. Sci. 4, 128. https://doi.org/10.3389/fmars.2017.00128.

Sea-Bird Scientific, 2017. User Manual ECO Fluorometers and Scattering Sensors. WWW Document. http://www.seabird.com/eco-triplet-fluorometer-and-backscattering-sensor (URL accessed 10.25.17).

Sharples, J., Moore, M.C., Rippeth, T.P., Holligan, P.M., Hydes, D.J., Fisher, N.R., Simpson, J.H., Moore, C.M., Rippeth, T.P., Holligan, P.M., Hydes, D.J., Fisher, N.R., Simpson, J.H., 2001. Phytoplankton distribution and survival in the thermocline. Limnol. Oceanogr. 46, 486–496. https://doi.org/10.4319/lo.2001.46.3.0486.

Sharples, J., Tweddle, J.F., Green, J.A.M., Palmer, M.R., Kim, Y., Hickman, A.E., Holligan, P.M., Moore, C.M., Rippeth, T.P., Simpson, J.H., Krivtsov, V., 2007. Spring – neap modulation of internal tide mixing and vertical nitrate fluxes at a shelf edge in summer. Limnol. Oceanogr. 52, 1735–1747.

Simpson, J.H., Sharples, J., 2012. Introduction to the Physical and Biological Oceanography of Shelf Seas. Cambridge University Presshttps://doi.org/10.1017/CBO9781139034098.

Smyth, T.J., Fishwick, J.R., Al-Moosawi, L., Cummings, D.G., Harris, C., Kitidis, V., Rees, A., Martinez-Vicente, V., Woodward, E.M.S., 2010. A broad spatio-temporal view of the western English Channel observatory. J. Plankton Res. 32, 585–601. https://doi.org/10.1093/plankt/fbp128.

Sverdrup, H.U., 1953. On conditions for the vernal blooming of phytoplankton. J. Cons. Perm. Int. Explor. Mer. 18, 287–295.

Takahashi, T., Sutherland, S.C., Wanninkhof, R., Sweeney, C., Feely, R.A., Chipman, D.W., Hales, B., Friederich, G., Chavez, F., Sabine, C., Watson, A., Bakker, D.C.E., Schuster, U., Metzl, N., Yoshikawa-Inoue, H., Ishii, M., Midorikawa, T., Nojiri, Y., Körtzinger, A., Steinhoff, T., Hoppema, M., Olafsson, J., Arnarson, T.S., Tilbrook, B., Johannessen, T., Olsen, A., Bellerby, R., Wong, C.S., Delille, B., Bates, N.R., de Baar, H.J.W., 2009. Climatological mean and decadal change in surface ocean pCO2, and net sea-air CO2 flux over the global oceans. Deep. Res. Part II Top. Stud. Oceanogr. 56, 554–577. https://doi.org/10.1016/j.dsr2.2008.12.009.

Thomas, H., Bozec, Y., Elkalay, K., de Baar, H.J.W., 2004. Enhanced open ocean storage of CO2 from shelf sea pumping. Science 304, 1005–1008. https://doi.org/10.1126/science.1095491.

Tsunogai, S., Watanabe, S., Sato, T., 1999. Is there a “continental shelf pump” for the absorption of atmospheric CO2? Tellus Ser. B Chem. Phys. Meteorol. 51, 701–712. https://doi.org/10.3402/tellusb.v51i3.16468.

Tweddle, J.F., Sharples, J., Palmer, M.R., Davidson, K., McNeill, S., 2013. Enhanced nutrient fluxes at the shelf sea seasonal thermocline caused by stratified flow over a bank. Prog. Oceanogr. 117, 37–47. https://doi.org/10.1016/j.pocean.2013.06.018.

Tweedle, J., 2007. Nutrient Fluxes into the Seasonal Thermocline of the Celtic Sea. University of Southampton.

Williams, C., 2013. The Supply of Nutrients to the Subsurface Chlorophyll Maximum in Temperate Shelf Seas. University of Liverpool.

Williams, C., Sharples, J., Mahaffey, C., Rippeth, T., 2013. Wind-driven nutrient pulses to the subsurface chlorophyll maximum in seasonally stratified shelf seas. Geophys. Res. Lett. 40, 5467–5472. https://doi.org/10.1002/2013GL058171.

Woodward, E.M.S., Rees, A.P., 2001. Nutrient distributions in an anticyclonic eddy in the Northeast Atlantic Ocean, with reference to nanomolar ammonium concentrations. Deep. Res. Part II Top. Stud. Oceanogr. 48, 775–793. https://doi.org/10.1016/S0967-0645(00)00097-7.

Yücel, M., Beaton, A.D., Dengler, M., Mowlem, M.C., Sohl, F., Sommer, S., 2015. Nitrate and nitrite variability at the seafloor of an oxygen minimum zone revealed by a novel microfluidic in-situ chemical sensor. PLoS ONE 10, 1–16. https://doi.org/10.1371/journal.pone.0132785.

Appendix B Methodology

B.1 Example of Lab-on-Chip data transmitted via Iridium

Download: profile=1: P1=10 P2=500 P3=10, max depth=94.

Glider time: 14/04/2015, 13:45:28 (at 14/04/2015, 13:42:25)

Dive number: 387

Average 0: ASM=5, DEP=33m, AV=649505.32

Average 1: ASM=9, DEP=70m, AV=592652.16

Average 2: ASM=19, DEP=94m, AV=625509.04

Average 3: ASM=19, DEP=94m, AV=605075.76

Average 4: ASM=19, DEP=94m, AV=594482.80

Average 5: ASM=19, DEP=94m, AV=592925.16

Average 6: ASM=19, DEP=94m, AV=592736.76

Average 7: ASM=19, DEP=94m, AV=592943.32

Average 8: ASM=19, DEP=94m, AV=592272.76

Average 9: ASM=19, DEP=94m, AV=592422.44

Average 10: ASM=27, DEP=33m, AV=593597.76

Average 11: ASM=27, DEP=0m, AV=599702.76

SC>

B.2 Example of Lab-on-Chip raw datafile from onboard storage

% File number: 193
% File name: Nitrate 50 Sensor 93
% File creation date: 2015/04/10 16:22:26
% Sensor name: Nitrate 50
% Glider time: 1974/05/20 00:00:00

Elapsed Time	State	Long Channel	Middle Channel	Small Channel	n/a	n/a	Reference Channel	Time from Glider	Depth from Glider	Temperature on sensor controller	Supply Voltage	Hall effect sensor 0	Hall effect sensor 1
1	0	61114118	53519336	40056393	6419193	61299444	6424300	1428682947	0	12.3	10.1	2468	3927
2	1	61113768	53478825	40080180	6448457	61290197	6452408	1428682948	0	12.3	9.9	2468	3927
3	1	61134158	53183871	40211918	6476911	61184738	6479546	1428682949	0	12.3	9.3	2690	3916
4	1	61348016	53276658	40146652	6504678	61172805	6506078	1428682950	0	12.3	9.3	2898	3904
5	1	61303279	53371772	40137590	6531894	61181582	6531974	1428682951	0	12.3	9.4	3067	3890
6	1	61249544	53433904	40123594	6558795	61186093	6557765	1428682952	0	12.3	9.3	3206	3874
7	1	61215940	53477960	40139688	6585358	61188448	6583166	1428682953	0	12.3	9.3	3322	3857
8	1	61192835	53471016	40163237	6611408	61190644	6608258	1428682954	0	12.3	9.5	3420	3840
9	1	61178303	53463924	40191682	6637501	61194088	6633307	1428682955	0	12.3	9.4	3500	3818
10	1	61158614	53471201	40200315	6662740	61193892	6657587	1428682956	0	12.3	9.5	3571	3794
11	1	61150992	53453810	40181521	6688181	61197646	6682012	1428682957	0	12.3	9.6	3630	3769
12	1	61145843	53495984	40173266	6713635	61202345	6706268	1428682958	0	12.3	9.6	3682	3739
13	1	61129355	53484471	40174143	6738652	61207731	6730636	1428682959	0	12.3	9.6	3726	3705
14	1	61122901	53493835	40225794	6763764	61211400	6754578	1428682960	0	12.3	9.6	3765	3666
15	1	61119529	53500557	40231219	6788574	61213857	6778647	1428682961	0	12.3	9.5	3799	3623
16	1	61120446	53486027	40240359	6813435	61216613	6802292	1428682962	0	12.3	9.6	3829	3573
17	1	61117509	53470799	40219716	6837957	61218186	6826146	1428682963	0	12.3	9.6	3855	3515
18	1	61110650	53473687	40258593	6862423	61216864	6849554	1428682964	133	12.3	9.6	3879	3447
19	1	61104882	53494761	40253705	6886773	61223972	6873014	1428682965	133	12.3	9.6	3900	3369
20	1	61102573	53472802	40258695	6911104	61221804	6896273	1428682966	133	12.3	9.6	3918	3276
21	1	61099260	53466079	40270384	6935290	61222832	6919702	1428682967	133	12.3	9.6	3935	3167
22	1	61098597	53468820	40216949	6959287	61205830	6942909	1428682968	133	12.3	9.6	3943	3100